

UNIVERSITÀ DEGLI STUDI DI NAPOLI
FEDERICO II

**Synthesis of New Ligands of Urokinase
Receptor and New Urotensin-II
Derivatives**

Ph.D. Dissertation

Submitted by

ALI MUNAIM YOUSIF

DIPARTIMENTO DI FARMACIA
Dottorato di Ricerca in Scienza Del Farmaco
XXVII Ciclo

Coordinatore:
Chiar.ma Prof.ssa
MARIA VALERIA D'AURIA

Tutor:
Chiar.mo Prof.
PAOLO GRIECO

Supervisor:
Chiar.mo Prof.
WILLIAM D. LUBELL

2014/2015

To Daddy, Mammy, Zainab, Alyaa, and Yousra.

TABLE OF CONTENTS

Acknowledgements.....	6
List of abbreviations.....	7
Abstract.....	13
Unit 1: Synthesis of new urokinase receptor peptide ligands.....	14
Introduction.....	15
Urokinase system in cell migration.....	16
Structure, ligands binding and regulation of uPAR.....	17
uPAR: a surface signaling receptor.....	20
uPAR signaling through fMLP receptors or FPRs.....	21
uPAR signaling through integrins.....	22
Structure-Activity relationship studies.....	25
suPAR crystal structure and uPAR conformations.....	26
S ⁸⁸ RSRY ⁹²	29
New S ⁸⁸ RSRY ⁹² analogues.....	33
Phosphorylated S ⁸⁸ RSRY ⁹² analogues.....	34
Linear S ⁸⁸ RSRY ⁹² analogues.....	35
Cyclic S ⁸⁸ RSRY ⁹² analogues.....	36
Synthetic strategies.....	39
Linear peptide synthesis.....	40
Cyclic peptide synthesis.....	41
Results and discussions.....	46
Linear analogues.....	47
Results: Biological data.....	47
Discussion.....	50
Cyclic analogues.....	51
Results: Biological, stability and conformational Data.....	51
Discussion.....	56
Conclusions.....	58
Experimental section.....	60
Characterization.....	66
References.....	71
Unit 2: Synthesis of new urotensin-II analogues.....	78
Introduction.....	79
Urotensin-II.....	80
Human Urotensin-II receptor.....	81
Structure-Activity relationship studies.....	85
New Urotensin-II analogues.....	96
Peptoids of Urotensin-II.....	97
Azasulfurylpeptides analogues of urotensin-II.....	98
Synthetic strategies.....	101
Peptoids of U-II analogues synthesis.....	102
Peptoids 7 and 9.....	102

Peptoids 5, 6, 8 and 10.....	104
Azasulfurylpeptides of U-II synthesis.....	108
Hydrazide of tryptophan synthesis.....	108
Sulfamidate of tyrosine synthesis.....	109
Synthesis of protected azasulfuryl protected tripeptide.....	110
Solid phase synthesis.....	111
Conclusions.....	114
Characterization.....	116
Experimental section.....	118
Solution synthesis.....	119
Solid phase synthesis	128
References.....	132
Spectra section.....	138

ACKNOWLEDGEMENTS

Infinite appreciation and deepest gratitude for all people contribute in way or another in making this dissertation possible.

Professor Paolo Grieco, I would like to express my deepest gratitude to my supervisor for his constant support and guidance. Without his help, this would not have been possible.

Professor William D. Lubell, my sincere gratitude to my second supervisor and I am glad for being part of his group. His passion for science, energy and optimism always amazed me.

Salvatore Di Maro and **Francesco Merlino**, as my colleagues and friends. Their valuable comments and suggestions helped me in the success of this study.

Stephane Turcotte, Mariam Traore, Antoine Douchez and all Lubell's group members, as my Canadian colleagues, my sincere acknowledgments to them for helping me. My experience in Lubell's group led me to meet wonderful people and to establish friendships which will remain all my lifetime.

Also let me express my gratitude towards all people who have been involved in my research, especially, **Dr. Maria Vincenza Carriero** for the biological tests in Italy, **Etienne Bilard** from Pr. Chatenet's group for the biological tests in Canada and **Marie-Christine Tang** for HRMS spectrums from the University of Montreal, Canada.

Finally, I can't express in words my gratitude to my family and my love, Yousra. "Thank you" and I am indebted to you for a lifetime.

LIST OF ABBREVIATIONS

δ	chemical shift in NMR spectroscopy
λ	wavelength
Alloc	Allyloxycarbonyl group
APC	activated protein C
ATF	amino-terminal fragment
ATN615	anti-urokinase receptor antibody
Boc	<i>tert</i> -butyloxycarbonyl
br	broad singlet
BTTP	<i>tert</i> -Butylimino-tri(pyrrolidino)-phosphorane
Btz	Benzothiazolylalanine
Cin	(4-Cl)-(<i>trans</i>)-cinnamoyl
CNS	Central Nervous System
Dab	2,4-Diaminobutyric acid
d	doublet
DBU	1,8-diazabicyclo[5.4.0]undec-7-ene
DCC	dicyclohexylcarbodiimide
DCE	dichloroethane
DCM	dichloromethane
dd	doublet of doublets
DIPEA	diisopropylethyl amine

DMAP	4-dimethylamino pyridine
DMF	<i>N,N</i> -dimethylformamide
DMSO	dimethyl sulfoxide
EGF	epidermal growth factor
EI	electron ionization
Equiv	equivalents
ERK	extracellular-signal-regulated kinase
ESI	electrospray ionization
Fab	fragment antigen binding
FAK	focal adhesion kinase
FBS	fetal bovine serum
Fmoc	9-fluorenylmethoxycarbonyl
FPRs	Formyl Peptide Receptors
G-protein	guanine nucleotide-binding protein
GFD	growth factor-like domain
GPCR	G protein coupled receptor
GPI	glycosyl-phosphatidylinositol
HATU	<i>O</i> -(7-azabenzotriazol-1-yl)- <i>N,N,N',N'</i> -tetramethyluronium hexafluorophosphate
HIV	human immunodeficiency virus
HOAt	1-hydroxy-7-azabenzotriazole
HOBt	1-hydroxybenzotriazol
HPLC	high performance liquid chromatography

hr(s)	hour(s)
HRMS	high resolution mass spectrometry
<i>hU-II</i>	human urotensin-II
Hz	Hertz
IC50	median inhibition concentration (concentration that reduces the effect by 50%)
<i>J</i>	coupling constant in NMR spectroscopy
JAK	Janus kinase
K	Kelvin
LACI	lipoprotein-associated coagulation inhibitor
Ly6	lymphocyte 6 protein
m	multiplet
M	molar
<i>m/z</i>	mass-charge relation
mAb	monoclonal antibody
MAPK	mitogen-activated protein kinase
MeCN	acetonitrile
MEK	MAPK/ERK kinase
min	minute
mL	milliliter
mmol	millimole
MMP	matrix metalloproteinase
mp	melting point

MS	mass spectrometry
MW	molecular weight
N	normal
Nal	naphthyl alanine
NDMBA	1,3-Dimethylbarbituric acid
NMR	nuclear magnetic resonance
NBS	Nitrobenzenesulfonyl
NSG	<i>N</i> -Substituted glycine oligomers
Orn	Ornithine
Pen	Penicillamine
PAI	plasminogen activator inhibitor
Pbf	2,2,4,6,7-pentamethyldihydrobenzofuran-5-sulfonyl
PBS	phosphate-buffered saline
PC	protein C
PI3K	phosphatidylinositol 3-kinase
PKA	protein kinase A
PKC	protein kinase C
q	quartet
quant.	quantitative
rf	reflux
<i>R</i> f	retention factor
RP	reverse phase

rpm	rotations per minute
rt	room temperature
<i>Rt</i>	retention time
s	singulet
SAR	structure-activity relationships
SPPS	solid-phase peptide synthesis
sst	somatostatin
STAT	signal transducer and activator of transcription
suPAR	soluble urokinase-type plasminogen activator receptor
t	triplet
TBTU	<i>O</i> -(benzotriazol-1-yl)- <i>N,N,N,N</i> -tetramethyluronium tetrafluoroborate
<i>t</i> -Bu	tertiary butyl
TFA	trifluoroacetic acid
TGF	transforming growth factor
THF	tetrahydrofurane
TIS	triisopropylsilane
TLC	thin layer chromatography
tPA	Tissue plasminogen activator
Trt	trityl
uPA	urokinase-type plasminogen activator
uPAR	urokinase-type plasminogen activator receptor
UV/Vis	ultraviolet/visible

U-II	Urotensin-II
URP	Urotensin Related Peptide
UTR	Urotensin-II receptor
v/v	volume by volume
Vn	vitronectin

ABSTRACT

Unit 1: The urokinase-type plasminogen activator receptor (uPAR) is involved in the regulation of cell migration. The uPAR is formed by three domains connected by short linker region. The Ser⁸⁸-Arg-Ser-Arg-Tyr⁹² is the minimum chemotactic sequence of uPAR required to induce the same intracellular signaling as result of its binding with formyl peptide receptor (FPRs). With aim to perform a SAR study on this sequence we have synthesized a large peptide library using phosphorylated amino acids, non-coded amino acids, D-amino acid scan and cyclic analogues. A new two potent inhibitors of cell migration, uPAR2 and uPAR18, have been identified represented, respectively, by the analogue with phosphorylated Ser⁹⁰ and the analogue with cyclic conformation.

Unit 2: Urotensin II (U-II) is a cyclic peptid has been described as the most potent vasoconstrictor documented. The vasoconstriction effect of U-II is a result of the binding with its receptor UT receptor. The cyclic region of U-II, [Cys-Phe-Trp-Lys-Tyr-Cys], plays an essential role in terms of affinity for UT receptor. We developed new two different libraries of U-II analogues carried structure modification on the peptide bond to explore new SARs on the cyclic region of U-II. Peptoids analogues represent the first library whose the side chain are appended to *N*-atom rather than the α -Carbon. The second library represented by *N*-aminosulfamide analogues (azasulfurylpeptides), a class of peptidomimetics, in which the C _{α} H and the carbonyl are respectively replaced by a nitrogen atom and a sulfonyl group.

UNIT 1

***SYNTHESIS OF NEW UROKINASE RECEPTOR
PEPTIDE LIGANDS***

1. INTRODUCTION

1.1. Urokinase system in cell migration

Cell migration is a central process in the development and tissue repair by which cells move from one location to another by adopting different motility modes, such as mesenchymal, amoeboid or collective migration, and the dysregulation of this process contribute to numerous disorders. The harmonized movement of cells in particular directions to specific locations is a crucial requirement for the tissue formation. The ungoverned and often rapid proliferation of cells can lead to an initially benign tumour but it may carry a risk of turning malignant cancer and metastasis. To counteract the invasive tumour cells migration, an understanding of mechanism by which cells migrate may lead to the development of novel therapeutic strategies. Cells often migrate in response to specific external signals, including chemical signals and mechanical signals. The extracellular matrix (ECM) is a complex of extracellular proteins and polysaccharides secreted by cells that provides structural and biochemical support to the surrounding tissues. The intricate network of cell–ECM interactions is crucial during development as well as for normal function, remodelling and repair of tissues during adult life [1]. Many proteins are involved in cell migration, including chemoattractants and their receptors, cell adhesion molecules, proteinases, regulators of the cytoskeleton and several signalling enzymes. The urokinase system is one of the important networks involved in the regulation of cell migration for the presence of the urokinase-type plasminogen activator receptor (uPAR) [2, 3]. The binding of the urokinase-type plasminogen activator (uPA) with uPAR convert the zymogen plasminogen to serine proteinase plasmin, the latter is responsible of fibrinolysis, facilitating cell migration and to regulate ECM proteolysis [4]. uPAR harmonizes the initiation of several intracellular signal-transduction pathways that involve cytosolic and transmembrane kinases and cytoskeletal components with other molecules (include vitronectin, members of the integrin adhesion receptor superfamily, caveolin and G-protein-coupled receptor (GPCR)).

The receptor of urokinase is expressed during the ECM remodelling, for example in gestational tissue during embryo implantation and placental development [5], and in keratinocytes during epidermal wound healing [6]. uPAR expression also induced by stress, injury and inflammation. uPAR is expressed in many human cancers including solid tumours, leukaemias and lymphomas [7]. Importantly, uPAR expression in tumours can occur in

tumour cells and/or tumour-associated stroma cells [8], such as fibroblasts and macrophages [9]. There is increasing evidence that the urokinase-type plasminogen activator receptor (uPAR) which is expressed by a wide variety of hematologic cells, including monocytes and macrophages, plays an important role in leukocyte recruitment following inflammation [10].

1.2. Structure, ligands binding and regulation of uPAR

The receptor for the urokinase-type plasminogen activator (uPAR) is a widely recognized master regulator of cell migration and uPAR₈₈₋₉₂ is the minimal sequence required to induce cell motility. uPAR is a member of the lymphocyte 6 (Ly-6) superfamily of proteins that are characterized by the Ly-6 and uPAR domain, also called three-finger fold [11]. The uPAR domain folds into a globular structure with 5-6 antiparallel β -strands linked by 4-5 disulphide bonds [12]. The uPAR consists of a single polypeptide chain of 313 amino acids, with a molecular weight of about 55 kDa, highly glycosylated and organized into three domains D_I (amino acids 1–77), D_{II} (amino acids 93–177) and D_{III} (amino acids 193–272) which is a GPI-linked membrane, are characterized by the presence of phylogenetically conserved cysteine residues that form intramolecular disulfide bridges (Figure 1A). The N-terminal D_I contains the primary binding site with high affinity for the domain growth factor-like of uPA (GFD) (Figure 1B).

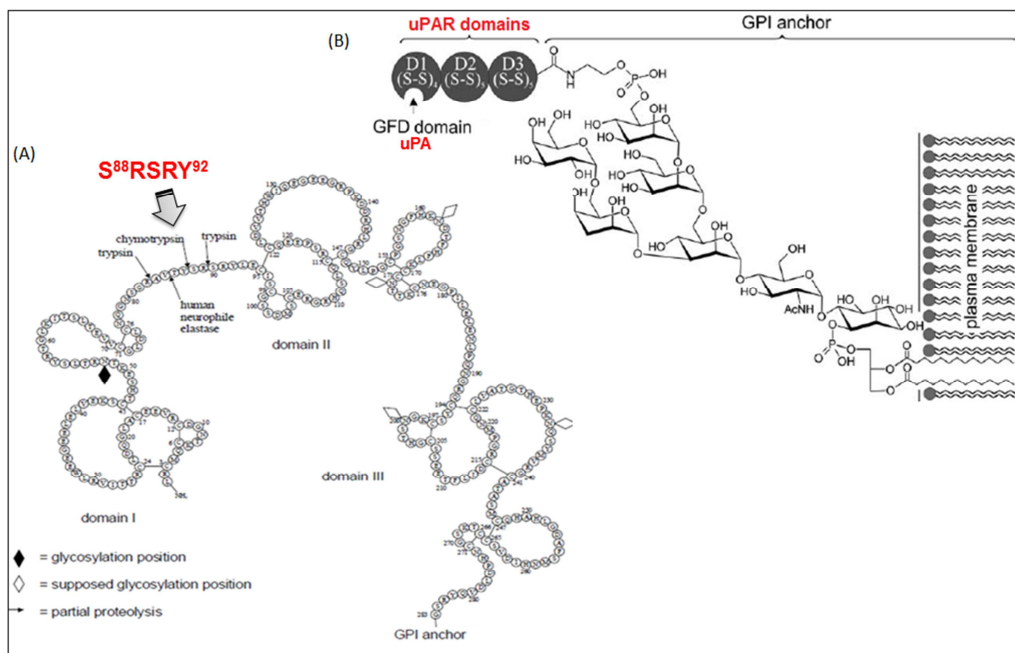


Figure 1. (A) Amino acid sequence of uPAR: between D_I and D_{II} there is a chemotactic sequence S⁸⁸RSRY⁹² which is a target of many proteases. (B) Structure of uPAR: consists of three domains connected to plasma membrane by GPI-anchor. D_I contains the uPA-uPAR binding site.

The domains D_{II} and D_{III} participate in the formation of the pocket that accommodates the uPA, increasing the affinity for the ligand, probably by stabilizing the tertiary structure of the D_I and appear to be involved in the binding to vitronectin (Vn) (Figure 2) [13]. Between domains D_I and D_{II} exists a chemotactic sequence *Ser*⁸⁸-*Arg-Ser-Arg-Tyr*⁹², active also in form of synthetic peptide. This sequence promotes cell migration and formation of protrusions of F-actin in uPAR-independent, FPR-dependent and $\alpha v\beta 5$ -dependent.

The vitronectin-binding site of uPAR is found in D_I and the D_I-D_{II} linker. Trp³², Arg⁵⁸, Ile⁶³ (in D_I), Arg⁹¹ and Tyr⁹² (in the D_I-D_{II} linker) are crucial residues for binding to vitronectin in its N-terminal somatomedin B (SMB) domain [14]. As shown in Figure 2, the binding sites of uPA and vitronectin are distinct, therefore, uPAR can simultaneously bind both ligands, allowing coordinated regulation of proteolysis, cell adhesion and signalling. Importantly, in terms of crosstalk between ligands, binding of uPA to uPAR enhances vitronectin binding by uPAR [15].

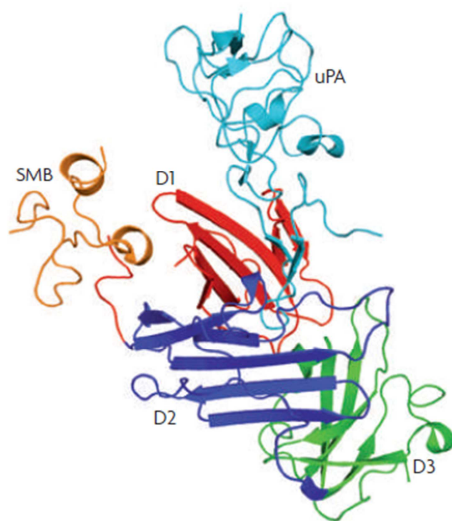


Figure 2. Urokinase-type plasminogen activator receptor (uPAR) binding sites. The binding of the ligand urokinase-type plasminogen activator (uPA; also known as urokinase) and the somatomedin B (SMB) domain of vitronectin. The three-dimensional structure of uPAR, with domains coloured. The uPA-binding site is located in the central cavity formed by the concave arrangement of the three domains and the vitronectin (SMB) binding site [13].

Cleavage sites. Soluble uPAR (suPAR) originates from cleavage and release of the membrane-bound uPAR, and is present in plasma, urine, blood, serum and cerebrospinal fluid

[16]. suPAR is the soluble form of the urokinase-type plasminogen activator receptor (uPAR) released from the cell membrane by cleavage between this membrane-anchoring GPI-molecule and D_{III} (Figure 3). This cleaved receptor with two domains will be referred as suPAR_{II-III} [17].

On the other hand, cleavage in the D_I-D_{II} linker uPAR₈₈₋₉₂ by proteases (Figure 3), such as uPA, plasmin and MMPs, creates a soluble D_I fragment and a D_{II}-D_{III} fragment that can be membrane associated or shed. uPA-uPAR bound can cleave neighbouring uPAR molecules, therefore, clustering of uPA-uPAR complexes through GPI-anchorage and lipid raft partitioning accelerates this process. Overturning of uPA and vitronectin binding and integrin interactions [18] suggest that cleavage inhibits uPAR signaling. Indeed, association of uPAR with the mannose-6-phosphate receptor (M6PR; also known as IGF2R) enhances uPA-mediated cleavage of uPAR and inhibits uPAR-induced tumour cell migration and invasion [19]. Cleavage also inhibits endothelial cell migration in vitro. However, cleaved uPAR might signal through pathways independently of uPA, vitronectin and integrins. The peptide sequence Ser⁸⁸-Arg-Ser-Arg-Tyr⁹², near the N-terminus of the D_{II}-D_{III} fragment, interacts with the G protein-coupled receptor (GPCR) formyl peptide receptor-like 1 (FPRL1; also known as FPR2), inducing cell migration [20]. An uncleavable uPAR mutant has been used to discriminate pathways that are activated by full length uPAR and D_{II}-D_{III} fragments. However, the mutated residues lie in the vitronectin-binding site. It is therefore unlikely that this mutant signals in the same way as wild-type uPAR.

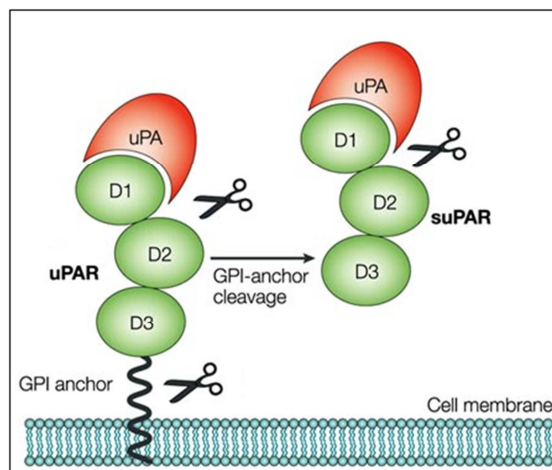


Figure 3. Schematic representation of cleavage sites of urokinase receptor. The GPI-anchor links uPAR to the cell membrane making it available for uPA binding. When the receptor is cleaved between the GPI-anchor and D_{III}, it becomes soluble [21].

1.3. uPAR: a surface signaling receptor

The urokinase system consisting of the serine proteases urokinase-type plasminogen activator, the membrane-bound receptor uPAR (also known CD87) and the inhibitors of plasminogen-activator type 1 and 2 which belong to the superfamily of the serpins (serine protease inhibitors) [22]. Plasmin, a serine protease, is involved in the dissolution of ECM and basement membrane during tissue degradation. This protease is generated via the action of plasminogen activators such as uPA or tPA (tissue Plasminogen Activator) and can influence tissue remodelling either directly or through activation of latent collagenases. uPAR regulates the activity of plasminogen system by binding the serine protease uPA and its zymogen form pro-uPA. uPAR localizes uPA and pro-uPA to the cell surface. Activated uPA cleaves the zymogen plasminogen, generating the protease plasmin, which cleaves and activates pro-uPA [23].

Being GPI-anchored means lacking transmembrane and intracellular domains, uPAR must cooperate with transmembrane receptors to activate intracellular signalling such as Formyl Peptide Receptors (FPRs) and integrins, the latter represent a major family of ECM receptors involved in the signalling co-receptors of uPAR as demonstrated by Aguire et. al., in 2002 [24].

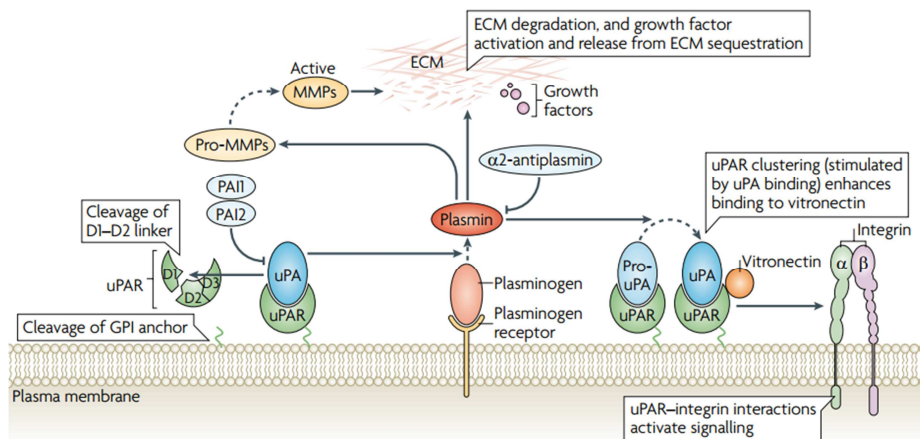


Figure 4. uPAR role in the plasminogen activation system. uPA binding to its receptor uPAR cleaves plasminogen, generating the active protease plasmin. Plasmin can reciprocally activate pro-uPA. The serine protease inhibitors (serpins) antagonize the proteolytic activities of uPA and plasmin. uPAR and its ligands interact with integrin co-receptors for intracellular signal transduction. uPA also cleaves uPAR in the linker between its first and second domains (D_I and D_{II}), generating a soluble D_I fragment and a membrane-associated D_{II}-D_{III} fragment [13].

1.3.1. uPAR signaling through fMLP receptors or FPRs

The D_{II}-D_{III(88-274)} uPAR fragment has been identified as an endogenous ligand for FPR like-1 that is necessary and sufficient to mediate D_{II}-D_{III(88-274)}-dependent chemotaxis [20]. Binding of S⁸⁸RSRY⁹² sequence to the seven-membrane-spanning domain FPRL1 receptor for fMLP has been reported as responsible of cell motility via the high affinity FPR [18]. The ATF (urokinase amino terminal fragment) engagement with its receptor further the 'open' conformation of the linker S⁸⁸RSRY⁹² even though the previously reported ATF/suPAR/ATN615 ternary complex structure suggests that fair degree of flexibility of the linker is retained [25]. This sequence promotes cell migration tying the higher affinity than fMLP (*N*-formyl-Methionyl-Leucyl-Phenylalanine, a peptide derived from bacterial to chemotactic action) for FPR and FPRL-1 receptors (Figure 5) [18]. In 2005 Gargiulo et al., provided evidence for specific binding of to FPR and showed not only that FPR is a mediator of uPAR signalling but also that SRSRY-triggered signalling requires changes in $\alpha\beta 5$ function. The FPR activates a broad spectrum of fMLP-dependent sequence cellular signalling events, including changes cytoskeleton, motility, and PKC activity [26]. Accordingly, S⁸⁸RSRY⁹² triggers FPR signalling by activating both PKC and $\alpha\beta 5$ integrin, the latter leads to ERK1/2 phosphorylation. As a result of the interaction with the sequence chemotactic uPAR, the receptor FPR is internalized and active, with a mechanism "inside out", the vitronectin receptor. The latter interacts with the uPAR, giving rise to a series of cascade reactions that culminate with the cytoskeletal reorganization and cell motility (Figure 5).

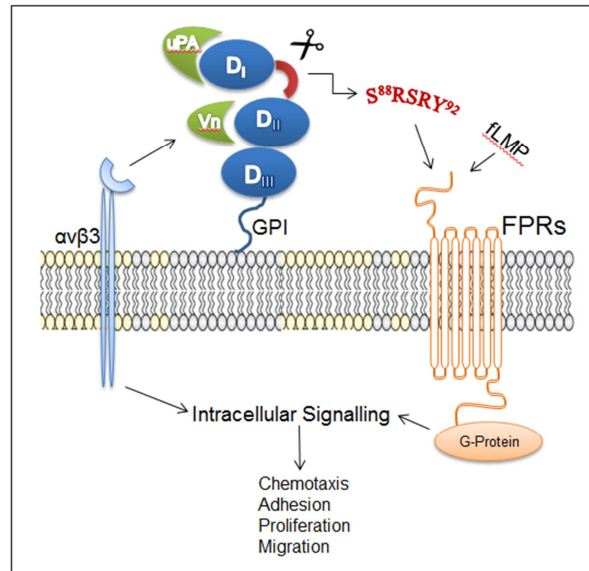


Figure 5. uPAR structure and signalling. The N-terminal domain D_I contains the binding site with high affinity for urokinase. A short sequence of five amino acids, Ser-Arg-Ser-Arg-Tyr (SRSRY), with a strong chemotactic activity, connects the domains D_I and D_{II}. The uPAR focuses on the cell surface proteolytic activity uPA. Both forms of membrane-soluble ones can expose, after proteolytic removal of the D_I, chemotactic a sequence capable of activating the receptors for fMLP (FPRs). As a result of the interaction with the sequence chemotactic uPAR, the receptor FPR is internalized and active, with a mechanism "inside out", the vitronectin receptor. The latter interacts with the uPAR, giving rise to a series of cascade reactions that culminate with the cytoskeletal reorganization and cell motility. Such signals may be inhibited by specific inhibitors of the sequence chemotactic [27].

1.3.2. uPAR signaling through integrins

Being a membrane surface receptor, many studies shown that uPAR signalling requires interaction with others co-receptors such as integrins. Interestingly, integrins seem to confer specificity to the signalling output of uPAR. Peptides can inhibit uPAR-integrine co-immunoprecipitation and cell signalling if correspond to the integrin sequences. Regions in the uPAR D_{III} might form a corresponding binding site for $\alpha 3\beta 1$ and $\alpha 5\beta 1$ [28, 29], and the D_{II} might be involved in the uPAR binding to $\alpha 5\beta 3$ integrin [30].

uPAR- $\beta 1$ integrin signalling. $\alpha 5\beta 1$ integrin is a fibronectin receptor and $\alpha 3\beta 1$ integrin is a laminin receptor. uPAR- $\beta 1$ integrin interactions promote Tyr phosphorylation of FAK, leading to activation of the Ras-ERK pathway[31]. uPAR- $\beta 1$ integrin signalling to ERK and Src increases the expression of uPA and MMPs through AP1 transcription factors (Figure 6A, B) [32]. This suggests that uPAR signalling through $\beta 1$ integrins can contribute to invasion by increasing pericellular proteolysis.

uPAR- β 3 integrin signalling. $\alpha\beta$ 3 integrin has been demonstrated to be crucial in uPAR signalling and can be co-immunoprecipitated with uPAR [33]. Both uPAR and β 3 integrin bind vitronectin, with uPAR recognizing the SMB domain and β 3 integrins the Arg-Gly-Asp sequence of vitronectin. The uPAR- β 3 integrin interaction has an important role in the signalling for cell migration through activation of the Rho family small GTPase Rac (Figure 6C). Interestingly, Wei et al., in 2007 has suggested a direct pathway linking uPAR- β 1 integrin interactions to Rac activation in some cell lines[34]. This pathway was activated by cell adhesion to fibronectin through α 5 β 1 integrin. However, several other studies have found that uPAR-driven Rac activation and cell morphology changes do not occur on fibronectin [35]. The reasons for this discrepancy are unclear, and the potential for multiple pathways mediating Rac activation by uPAR remains a possibility that is under investigation.

uPAR- β 5 vitronectin receptor. The involvement of α v β 5 integrin in the uPAR signaling SRSRY-dependent migration on Vitronectin (Vn) coated surfaces. In 2005 Gargiulo et. al., shown the important role of the synthetic form of SRSRY in the integrin activation. The important role of α v β 5 in mediating SRSRY-dependent signaling is indicated by several lines of evidence: (a) the SRSRY-dependent mitogen effect occurs on vitronectin-coated filters, but not on filters that are uncoated or coated with collagen, laminin, or fibronectin; (b) anti- α v β 5 antibodies block SRSRY-dependent migration and cytoskeletal rearrangements; (c) exposure to the synthetic form of SRSRY inhibit cell adhesion to vitronectin; and (d) treatment of cells with the synthetic form of SRSRY results in increased physical association between uPAR and α v β 5 [27].

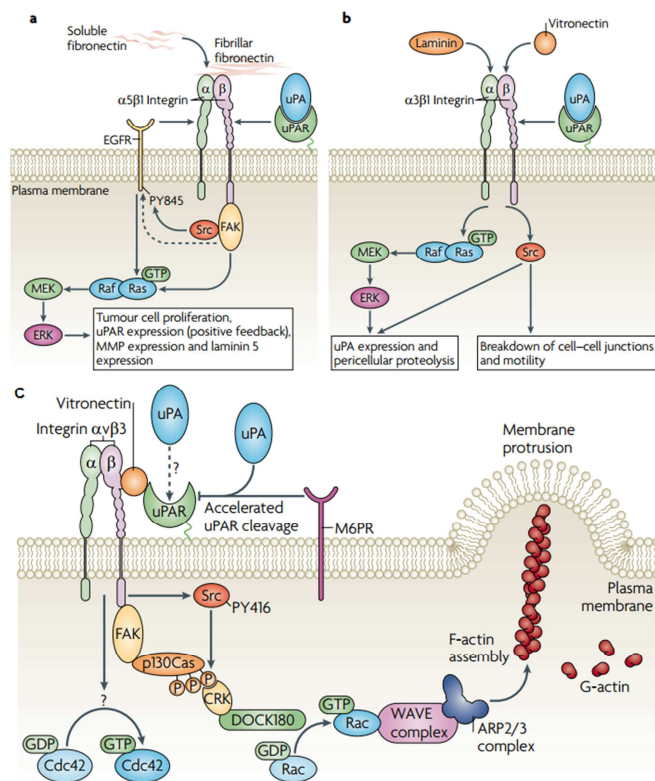


Figure 6. uPAR–integrin signalling. A) B) Urokinase-type plasminogen activator receptor (uPAR) signals through $\alpha 5 \beta 1$ and $\alpha 3 \beta 1$ integrins in fibroblasts, kidney epithelial cell lines and some carcinoma cells. uPA binding to uPAR is required for signalling through $\beta 1$ integrins. C) The uPAR– $\beta 3$ integrin interaction has an important role in the signalling for cell migration through activation of the Rho family small GTPase Rac [35].

2. STRUCTURE-ACTIVITY RELATIONSHIP STUDIES

2.1. suPAR crystal structure and uPAR conformations

In the last decade has been provided significant advancements in perception of the structure-function relationships in the urokinase plasminogen activator receptor. This progress has primarily been fuelled by the advent of an increasing number of crystal structures of uPAR in order to further SARs. suPAR is the soluble form of the urokinase-type plasminogen activator receptor which is a GPI-linked membrane protein (Figure 7). The soluble form (suPAR) is released from the cell membrane by cleavage between this membrane-anchoring GPI-molecule and the attached D_{III} (Figure 7). As already reported, suPAR consists of three homologues domains (D_I, D_{II}, and D_{III}), while the secondary structure consists of 17 antiparallel β -strands with three short α -helices. Furthermore, the linker region connecting D_I and D_{II}-D_{III} (Ser⁸⁸-Arg-Ser-Arg-Tyr⁹²) is protease sensitive and thus an important sequence in suPAR's molecular regulation. The domains of suPAR are assembled in a right-handed orientation generating a concave shaped receptor with a space between D_I and D_{III}. In 2006 Huai et al., found that the D_I domain showed a rotation of 20.5°, while the D_{II}-D_{III} remained in the same orientation suggesting high flexibility of suPAR inter-domain organization [36]. suPAR and uPAR have slightly different conformations and that this might affect the cleavage of the linker region S⁸⁸RSRY⁹² [37]. The conformational change does not occur within the three domains but rather in the linker region S⁸⁸RSRY⁹² connecting the D_I with D_{II}-D_{III}. However, an antibody raised to a peptide comprising residues 84-94, which constitutes a part of the linker-region, recognizes uPAR but not suPAR [37]. Cleavage of uPAR does not only occur at the GPI-anchor portion of the protein, but also within the actual receptor. The linker region connecting D_I with D_{II}-III contains uPA-cleavage site (see Figure 3), but in 2001 Høyer-Hansen et al., demonstrated that the soluble form, in contrast to the membrane-bound form, was not cleaved by uPA. This finding confirms the hypothesis that suPAR_{I-III} can act as uPA scavenger. The same authors, have also demonstrated that D_I is required for efficient binding of vitronectin. The five residues identified as "hot spots" for vitronectin binding forms an epitope consisting of two loops connecting the central four stranded β -sheet in uPAR D_I (Trp³², Arg⁵⁸, and Ile⁶³) as well as a region of the flexible linker-region connecting uPAR D_I and D_{II} (Arg⁹¹ and Tyr⁹²) [38]. To further investigate the chemotactic properties of suPAR, Fazioli et al., have constructed truncated suPAR_{II-III} mutants by cleavage of recombinant suPAR with chymotrypsin to identify the chemotactically active region. Fragments which

containing the SRSRY sequence (residues 88–92) showed a chemotactic effect and this sequence promoted chemotactic properties both when present on the C-terminus, as in suPAR_I, and when present in the N-terminus, as in suPAR_{II-III} (Figure 7) [39].

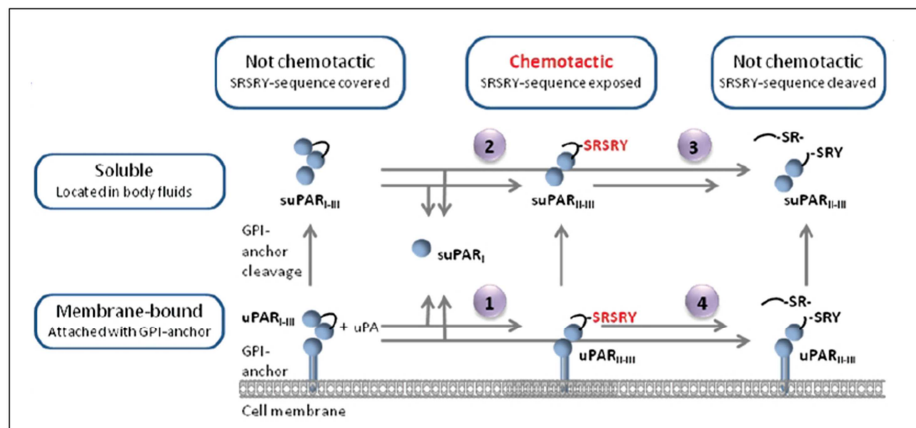


Figure 7. suPAR release and cleavage and SRSRY role. The top-horizontal line of molecules represents the three variants of suPAR that are soluble, while the bottom-horizontal line of receptors is the membrane-bound uPAR-variants. Only the cleaved uPAR/suPAR illustrated with intact SRSRY-sequence are believed to have chemotactic properties

According to the model proposed by Gårdsvoll, the multi-domain uPAR reversibly populates discrete conformational states “open” and “closed” that differ in their capacity to induce lamellipodia on vitronectin-coated surfaces (Figure 8) [40]. In the absence of uPA, a sizable fraction of the glycolipid-anchored uPAR adopts an “open conformation”, which is unable to induce lamellipodia. uPA binding to the central cavity drives the receptor into a closed conformation with an accompanying increase in its vitronectin-dependent signalling (see Figure 8). Obviously, any perturbation of this equilibrium, shifting it towards the open uPAR conformation.

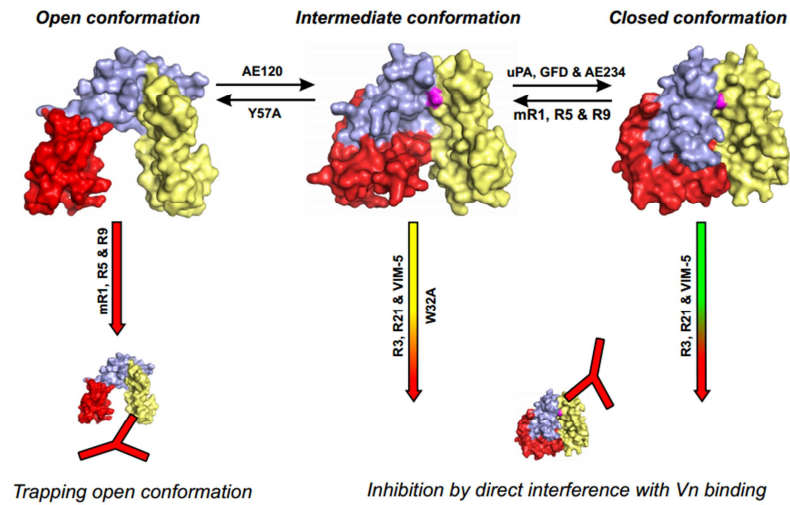


Figure 8. uPAR conformational switch. The equilibrium between these states “open” and “closed” is sensitive to engagement of different ligands.

Crystallographic studies have shown greater flexibility of the complex $D_I D_{II}$ than $D_{II} D_{III}$, uPAR activated by its ligand, undergoes a conformational change that sees the domain D_I rotate on the axis of the domains $D_{II}-D_{III}$ (Figure 9A) [40]. The main protagonists of the conformational change are: the interaction between domains D_I and D_{III} and the loop130-140 in the domain D_{II} . While the portion ATF uPAR binds the central portion formed by all three domains, SMB binds the outer side, at the interface between D_I and D_{II} , not perturbing the structure of the binary complex uPAR-ATF.

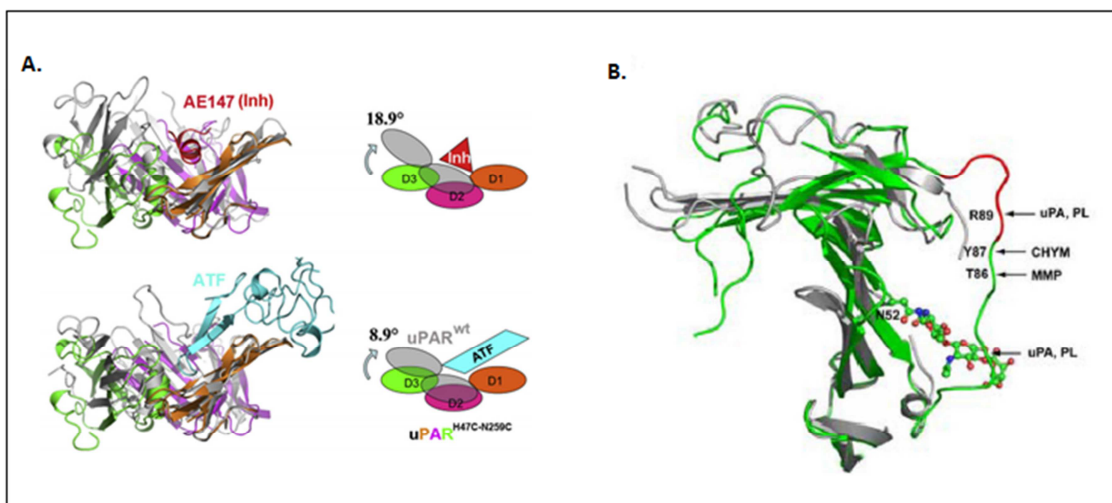


Figure 9. Structural flexibility of uPAR. (A) The engagement of uPA with its uPAR see D_I rotate on the axis of D_{II} and D_{III}. The crystalline structure in the form of uPAR has free length of about 2.4Å°, while in a bound form to the amino-terminal fragment of uPA, a length of 3.2Å°. (B) Displacement of the linker region (amino acid residues Gln⁷⁸-Tyr⁹²), connecting domains D_I and D_{II} of suPAR upon ATF binding. The epitope with chemotactic attributes (amino acids Ser⁸⁸-Tyr⁹²) is show in red and positions susceptible to hydrolysis by various proteases are indicated with arrows [41].

2.2. S⁸⁸RSRY⁹²

One of the most noticeable aspects in the conformational change by the engagement of uPAR-ATF is a readjustment of highly mobile amino acid segment (Gln⁷⁸- Tyr⁹²) connecting D_I and D_{II}. In 2006 Barinka et al., has demonstrated that the spatial rearrangement makes the linker more susceptible to the hydrolysis by various proteases (Figure 9B) (including plasmin, uPA or matrix metalloproteases) and as well it converts the strong chemotactic epitope Ser⁸⁸-Arg-Ser-Arg-Tyr⁹² from its cryptic form to the form easily accessible to interactions with an fMLP receptors [41]. Although the ‘open’ conformation of the Gln⁷⁸-Tyr⁹² linker observed in structure results from the crystallographic contacts between different molecules of receptor, it likely represents a preferred conformation of the linker in the complex between suPAR and ATF.

Previously, by Ala-scan study, as a first approach in a SAR study, has been shown that the last four residues of the sequence chemotactic uPAR, Ser⁸⁸-Arg-Ser-Arg-Tyr⁹² are essential for chemotactic activity [27]. In 2008 Bifulco et al., five Glu-scanned SRSRY peptide analogues were synthesized and tested for their ability to promote or to prevent directional cell migration in Boyden chambers. Interestingly, the addition of Ser-Arg-Glu-Arg-Tyr (Figure 10A) and SRSRY caused 31% of inhibition of HEK 29 cell migration. This finding suggest that the central core Arg-Glu-Arg may be relevant to the inhibition of cell migration. While the control peptide H-Ala-Arg-Ala-Arg-Tyr-OH did not exert any effect, pGlu-Arg-Glu-Arg-Tyr-OH and H-Glu-Arg-Glu-Arg-Tyr-OH caused 100pM concentration, at 45% and 30% inhibition, respectively. Furthermore the C-terminal amidate peptide pERERY-NH₂ triggered 70% inhibition at 100pM concentration. It is known that D_{II}(88–183) uPAR fragment binds to FPR or FPRL1 through the SRSRY sequence [42]. pERERY-NH₂ shares the same binding site with SRSRY on the FPR and prevents: (a) binding of a fluorescent fMLF analogue to RBL-2H3/ETFR cell surfaces; (b) fMLF-directed cell migration of RBL-2H3/ETFR cells stably

expressing FPR; (c) agonist-dependent FPR internalization and ERK1/2 phosphorylation. These remarkable effects are due to its binding to the FPR. It has been assessed whether pERERY-NH₂ interferes with the ability of fMLF to evoke an increase in intracellular Ca²⁺ concentration.

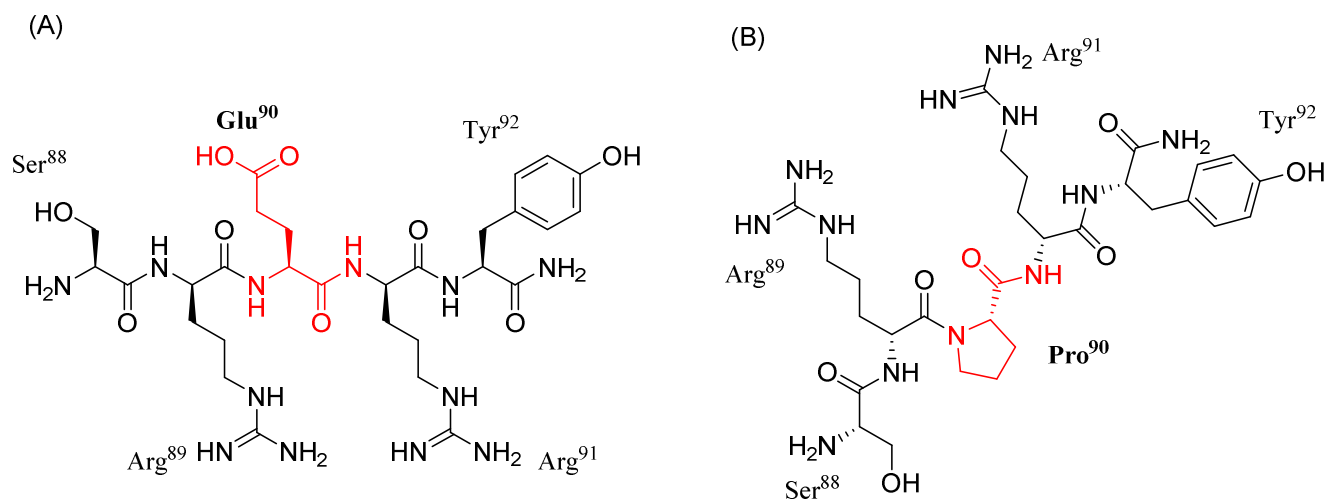


Figure 10. Peptide structures derived by the substitution of Ser⁹⁰ with Glu (A) and Pro(B).

To investigate the structural requirements for this inhibitory effect, in 2009 Carriero et al., has investigated about the conformation preference of the Arg-X₁-Arg-X₂ sequence (X₂: any amino acid; X₁: Tyr, Phe, Trp) [43]. The conformations of the sequence Arg-X₁-Arg-X₂ have been investigated using the Protein Data Bank (PDB). Figure 11A shows the percentage of Arg-X₁-Arg-X₂ sequences with α -turn or β -extended conformation for each amino acid at the X₁ position. Ser⁹⁰ is present in 26 structures with an about equal distribution among the three different classes of conformations. This suggests that Arg-Ser-Arg-Tyr could be accommodated either in an α -turned or β -extended conformation. On the other hand, Glu is observed 26 times in an α -turn conformation. Cys is observed in α -turn conformation in two of three structures only. These findings allowed us to conclude that the Arg-Glu-Arg-X₂ sequence might be the best candidate to obtain compact turned structure. Figure 11D depicts the superposition of the α -turned structure in Arg-Glu-Arg-Tyr sequences. The α -turned structure has the following characteristics: an aromatic residue is spatially flanked by two basic residues (Arg), and a Glu residue is opposite to the aromatic residue. Overall, these theoretical findings prompted us to examine the biological properties of RERX₂ peptides (X₂:

Tyr, Phe, Trp). Furthermore, to avoid the perturbing effects of the end charges on the conformational preferences, has been synthesized N-terminal acetylated and C-terminal amidated RERW, RERY, and RERF peptides. RERF exerted the strongest inhibition and was further characterized for its conformational preferences and biological activity. The conformational preferences of RERF were investigated by circular dichroism and nuclear magnetic resonance spectroscopy. RERF with femtomolar concentration interferes with FPR biological activity either by inducing FPR internalization or by blocking agonist-FPR interaction and migration. In addition, RERF display some conformational flexibility, preferentially adopts an α -turn (Figure 11E).

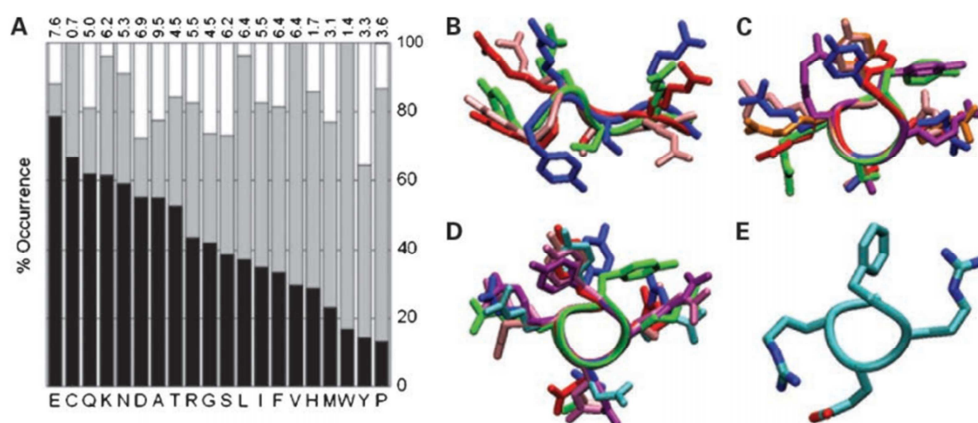


Figure 11. Structural analysis. Analysis of the conformational preferences of Arg-X1-Arg-X2 sequences (X1= any amino acid, X2= Phe, Tyr, Trp) as found in our subset of the PDB. Columns, percentage of occurrence of α -turned (black columns), β -extended (grey columns), and all the other structures (white columns) for each amino acid (single-letter codes) at the X1 position. The occurrence of each amino acid at the X1 position is also indicated on the top as percentage of the total.

In 2012 Bifulco et al., has presented significant advancement that the substitution of Ser⁹⁰ in the uPAR chemotactic sequence with Pro enhance agonist triggered FPR activation and internalization, increases cell adhesion onto Vn and favours uPAR/Vn association (Figure 10B). In contrast, the substitution of Ser⁹⁰ with Glu residue prevents agonist-triggered FPR activation and internalization, decreases binding to and cell adhesion onto Vn and inhibits uPAR/VnR association (Figure 10A). These findings uncover an inherent switch localized on Ser⁹⁰ that potently affects uPAR activity [44]. The analysis of the conformational preferences adopted by uPAR chemotactic sequence shows that residue Ser⁹⁰ is positioned in a critical

“hinge”, which possibly influences the conformation of nearest residues (Figure 12A). This study confirms that Ser⁹⁰ with its surrounding chemotactic sequence is crucial to uPAR function and provides further support to the generation of uPAR₈₈₋₉₂-derived peptides, as drugs targeting uPAR function.

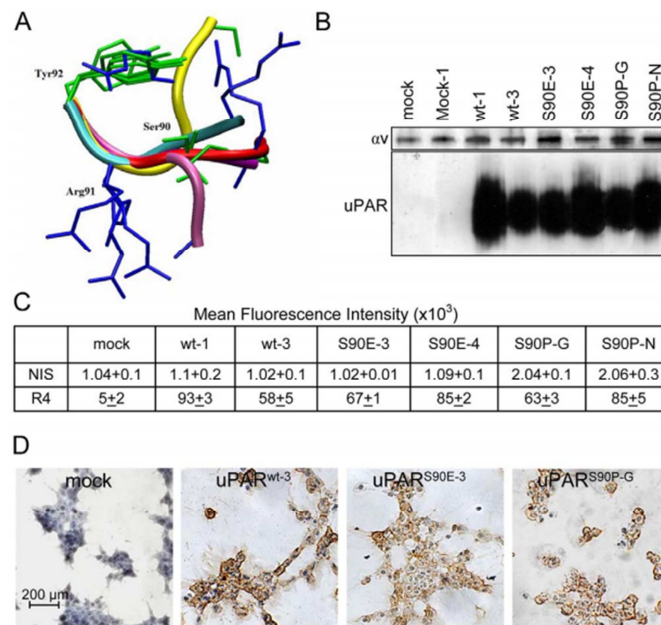


Figure 12. uPAR carrying S90E and S90P substitutions. A: Arg⁹¹ and Tyr⁹² superposition of the backbone atoms of the various 88–92 segments of SuPAR from x-ray structures. Residue 89 is not visible in the electron density map of 1YWH. Side chains are reported as stick, Arg residues are in blue. Backbones are reported as ribbon drawing: Yellow, 2I9B, chain E and F, residues 88–92; Red, 3BT2, chain U, residues 88–92; Mauve, 1YWH, chain E, residues 89–92; Cyan, 1YWH chain M, residues 89–92; Purple, 1YWH chain A, residues 89–92. B. Lysates (25 mg/sample) from 293 stably transfected either with pcDNA3 empty vector (293/mock) or pcDNA3 coding for human uPAR (293/uPARwt, uPAR S⁹⁰E, uPAR S⁹⁰P), were resolved on a 10% SDS-PAGE followed by Western blotting with R4 anti-uPAR or anti-av mAbs. C. Cytofluorimetric analysis of the indicated stably transfected 293 clones with R4 anti-uPAR mAb or nonimmune immunoglobulins. D. Representative images of the indicated stably transfected 293 clones immuno-stained with anti-uPAR R4 mAb.

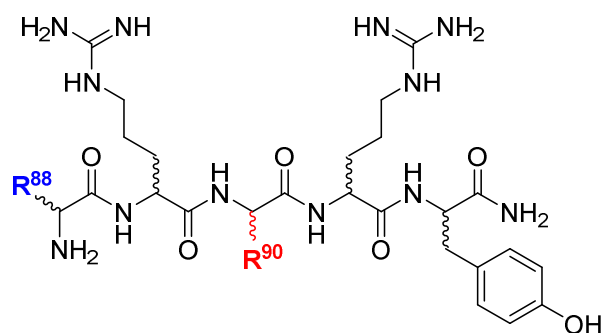
3. *NEW S⁸⁸RSRY⁹² ANALOGUES*

Peptides are, however, often ill-suited for use as drugs, because of physicochemical and pharmacological properties, including limited stability and short half-life, conformational flexibility, which may carry interactions with multiple receptors leading to undesired side effects. In the last decade the role of the chemotactic sequence S⁸⁸RSRY⁹² became more clear in pathways of urokinase receptor (see paragraph 2.2.). In the first part of the present thesis, I developed new analogues of the chemotactic sequence S⁸⁸RSRY⁹² for acquiring information on structure-activity relationship, to stabilize specific conformations, constricting into macrocyclic conformation and to improve to improve pharmacokinetic aspects of peptides such as low stability, and short half-life.

3.1. Phosphorylated S⁸⁸RSRY⁹² Analogues

The role of Ser⁹⁰ in the chemotactic activity of S⁸⁸RSRY⁹² sequence is crucial for the pathways of uPAR. Protein phosphorylation plays a central role in neural and hormonal control of cellular activity [45-47]. Phosphorylation and dephosphorylation of proteins represents one of the most widespread and important reactions in the regulation of cellular process. Specific Serine residues in the substrate become phosphorylated by the action of a protein kinase which catalyses the transfer of phosphate group. Multiple basic amino acids, particularly arginine, at the phosphorylation site are prerequisites for an appreciable rate of the phosphorylation by cyclic AMP-dependent protein kinase [48]. Significantly, arginine forms stable complexes with orthophosphate esters due to the combined influence of electrostatic interaction and hydrogen-bonding [49, 50]. Therefore it is plausible that such interactions could occur on the phosphorylated peptides, the newly phosphorylated serine residue forming interaction with one or more adjacent arginine residues, thus inducing a conformation change in the product. Such interactions would be more weaker with lysine and histidine. The first library of peptides of the present thesis which I synthesized hold the phosphorylated serine one time in position 90 and another in 88 (Table 1). The preparation of phosphorylated peptide analogues has been accomplished by solid phase method.

Table 1. Phosphorylated Peptide Library:

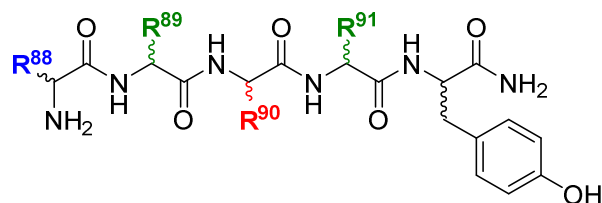


Name	Sequence
uPAR1	H-Ser-Arg-Ser _p -Arg-Tyr-NH ₂
uPAR2	H-Ser _p -Arg-Ser-Arg-Tyr-NH ₂
uPAR3	H-Ser-Arg-Ser _p -Tyr-Arg-NH ₂

3.2. Linear S⁸⁸RSRY⁹² Analogues

To develop effective ligands of the uPAR, it is necessary to know the structure-activity relationships (SARs) of the natural molecule in detail. In the case of a short peptide like the S⁸⁸RSRY⁹², D-amino acid scan can be a useful strategy to increase our knowledge about the SARs for this peptide. Replacement of each residue by its optical isomer provides useful information regarding the stereochemical requirements at each position in the sequence and the location of possible turn conformations as only certain turn types can accommodate both L- and D- residues and still place the amino acid side chains in the same relative position in three-dimensional space [51]. Retro-synthesis tool represent another of the most important tools for developing SARs, and following this criteria, have been synthesised retro-peptide analogues. In addition, the role of Arg⁸⁹ and Arg⁹¹ has been investigated by providing analogues with Orn residue in position 89, position 91 and both. In Table 2, I reported the library of peptide analogues described in the present paragraph which were synthesized by standard Fmoc chemistry in solid phase.

Table 2. Linear Peptide Library:



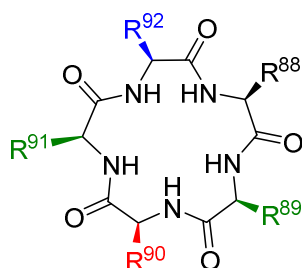
Peptide	Sequence
uPAR4	H-DSer-Arg-Ser-Arg-Tyr-NH ₂
uPAR5	H-Ser-DArg-Ser-Arg-Tyr-NH ₂
uPAR6	H-Ser-Arg-DSer-Arg-Tyr-NH ₂
uPAR7	H-Ser-Arg-Ser-DArg-Tyr-NH ₂
uPAR8	H-Ser-Arg-Ser-Arg-DTyr-NH ₂
uPAR9	H-DSer-DArg-DSer-DArg-DTyr-NH ₂
uPAR10	H-DTyr-DArg-DSer-DArg-DSer-NH ₂
uPAR11	H-Tyr-Arg-Ser-Arg-Ser-NH ₂
uPAR12	H-Ser-Orn-Ser-Arg-Tyr-NH ₂
uPAR13	H-Ser-Arg-Ser-Orn-Tyr-NH ₂
uPAR14	H-Ser-Orn-Ser-Orn-Tyr-NH ₂
uPAR15	H-Ser-Orn-Glu-Arg-Tyr-NH ₂
uPAR16	H-Ser-Arg-Glu-Orn-Tyr-NH ₂
uPAR17	H-Ser-Orn-Glu-Orn-Tyr-NH ₂

3.3. Cyclic S⁸⁸RSRY⁹² Analogues

Cyclic peptides have been used in medicine for centuries and constitute a class of compounds that have made significant contributions to the treatment of several diseases, including cancer. Cyclic peptides present several advantages as therapeutic agents, such as: low toxicity resulting from peptide degradation, minimized accumulation of peptides in tissues, and low cost of manufacturing [52]. Additionally, linear peptides possess many conformations in solution and this flexibility often relates to poor selectivity for biological targets. One strategy to limit a peptide's flexibility is the cyclization, typically preserves biological properties of peptides and increases their resistance to degradation and elimination [53]. Cyclizing a linear peptide is an useful technique to reduce their conformational freedom, and potentially improve binding affinity towards a target. Thus, I have synthesized a library containing cyclic peptides (Table 3) of the S⁸⁸RSRY⁹² peptide, changing also the order of amino acid sequence. This

library of cyclic peptide was performed to investigate the role of Ser⁹⁰ in the constricted conformation by the cyclization of analogues with phosphorylated serine and glutamic residue to have a clear comparison with RERF analogue (see paragraph 2.2.). It has been investigated also the role of the aromatic moiety by the replacement of Tyr⁹² with Phe, Trp, Nal(1) and Nal(2). Finally, have been synthesized cyclic analogues with Orn instead of Arg residue in position 89, position 91 and in both positions.

Table 3. Cyclic S⁸⁸RSRY⁹² Analogues:

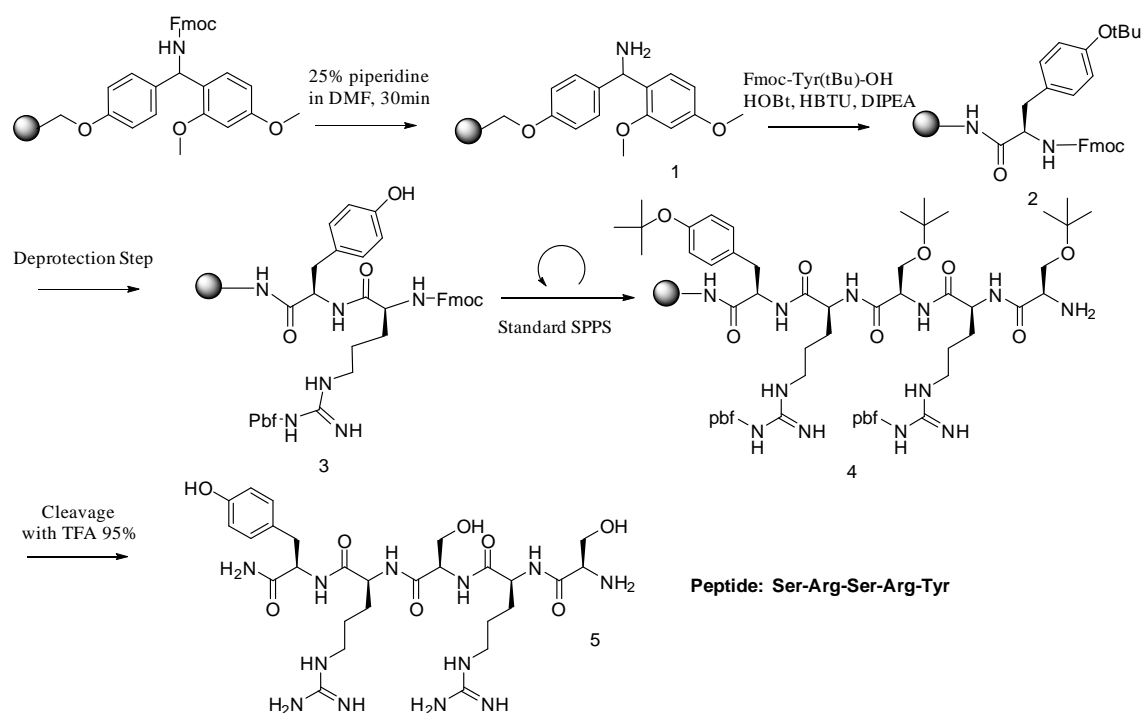


Peptide	Sequence
uPAR18	[Ser-Arg-Ser-Arg-Tyr]
uPAR19	[Ser-Arg-Ala-Arg-Tyr]
uPAR20	[Ser-Arg-Arg-Ser-Tyr]
uPAR21	[Arg-Ser-Ser-Tyr-Arg]
uPAR22	[Ser-Arg-Ser _p -Arg-Tyr]
uPAR23	[Ser _p -Arg-Ser-Arg-Tyr]
uPAR24	[Ser-Arg-Ser _p -Tyr-Arg]
uPAR25	[Ser-Arg-Glu-Arg-Tyr]
uPAR26	[Glu-Arg-Ser-Arg-Tyr]
uPAR27	[Glu-Arg-Glu-Arg-Tyr]
uPAR28	[Ser-Arg-Ser-Arg-Phe]
uPAR29	[Ser-Arg-Ser-Arg-Trp]
uPAR30	[Ser-Arg-Ser-Arg-Nal(1)]
uPAR31	[Ser-Arg-Ser-Arg-Nal(2)]
uPAR32	[Ser-Arg-Glu-Arg-Phe]
uPAR33	[Ser-Arg-Glu-Arg-Trp]
uPAR34	[Ser-Arg-Glu-Arg-Nal(1)]
uPAR35	[Ser-Arg-Glu-Arg-Nal(2)]
uPAR36	[Ser-Orn-Ser-Arg-Tyr]
uPAR37	[Ser-Arg-Ser-Orn-Tyr]
uPAR38	[Ser-Orn-Ser-Orn-Tyr]
uPAR39	[Ser-Orn-Glu-Arg-Tyr]
uPAR40	[Ser-Arg-Glu-Orn-Tyr]

4. SYNTHETIC STRATEGIES

4.1. Linear peptide synthesis

The synthesis of S⁸⁸RSRY⁹² linear analogues was accomplished on solid-phase, Fmoc/*t*Bu strategy, using Fmoc-Rink amide linker resin as solid support (Scheme 1). The first step was to remove Fmoc protecting group with piperidine (25% in DMF; 1 x 5 min and 1 x 25 min) and the first amino acid N^α-Fmoc-Tyr(*t*Bu)-OH (3 equiv) was coupled to the resin in the presence of HBTU (3 equiv), HOBT (3 equiv), DIEA (6 equiv) in DMF for 2h at room temperature. The resin was washed with DMF (3x) and DCM (3x). The N^α-Fmoc protecting group was removed from the Tyr residue as above reported, then the resin was washed with DMF (3x). A positive Kaiser ninhydrin test was observed. The following protected amino acids were added stepwise to synthesize the desired sequences for peptide **uPAR1-17**: N^α-Fmoc-Zaa-OH, (Zaa = Arg(Pbf), Ser(*t*Bu), Ser(HPO₃Bz), D-Ser(*t*Bu), D-Arg(Pbf), D-Tyr(*t*Bu), Orn(Boc), Glu(O*t*Bu)). Each coupling reaction was accomplished using a 3-fold excess of amino acid with HBTU (3 equiv) and HOBT (3 equiv) in the presence of DIEA (6 equiv). After the coupling, the peptide-resin was washed with DCM (3x) and DMF (3x). The Fmoc deprotection protocol described above was repeated and the next coupling step was initiated in a stepwise manner. The Kaiser test was used as colorimetric test to confirm every coupling/deprotection step occurred in the peptide sequence elongation. Analytical HPLC and MS spectrometry monitored the achievement of linear sequences for the compounds uPAR1-17. The N-terminal Fmoc group was removed as described above. The resin was washed with DMF (3x) and DCM (3x) and dried *in vacuo*. The peptide was released from the solid support and all protecting groups were cleaved using a cocktail of TFA/TIS/H₂O (95:2.5:2.5, v/v/v) for 3 h. The resin was removed by filtration and the crude peptide was recovered by precipitation from the filtrate using chilled diethyl-ether to give a white powder, which was purified by RP-HPLC using a semi-preparative C18-bonded silica column (Phenomenex, Jupiter 4μ Proteo 90Å, 1.0 x 25 cm) with a gradient of methanol and water containing 0.1% TFA (from 0 to 90% over 40 min) at a flow rate of 5.0 mL/min. The product was obtained by lyophilization of the appropriate fractions after removal of the Methanol by rotary evaporation under reduced pressure. Analytical RP-HPLC indicated >95% purity and the correct molecular ions were confirmed by LC/ESI-MS.



Scheme 1. Linear peptide synthesis in solid phase.

4.2. Cyclic peptide synthesis

Cyclic peptides were synthesized by a combination of solution synthesis and Fmoc chemistry solid-phase approach. There are four ways to constrain a peptide into macrocyclic conformation: *side chain to side chain*, *side chain*, *head to tail* and *head to side chain to tail* (Figure 13) [54].

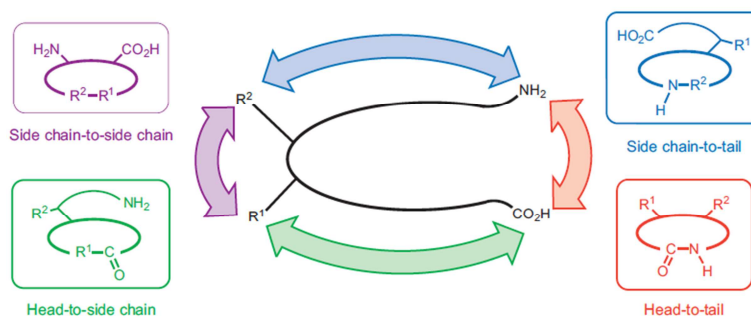
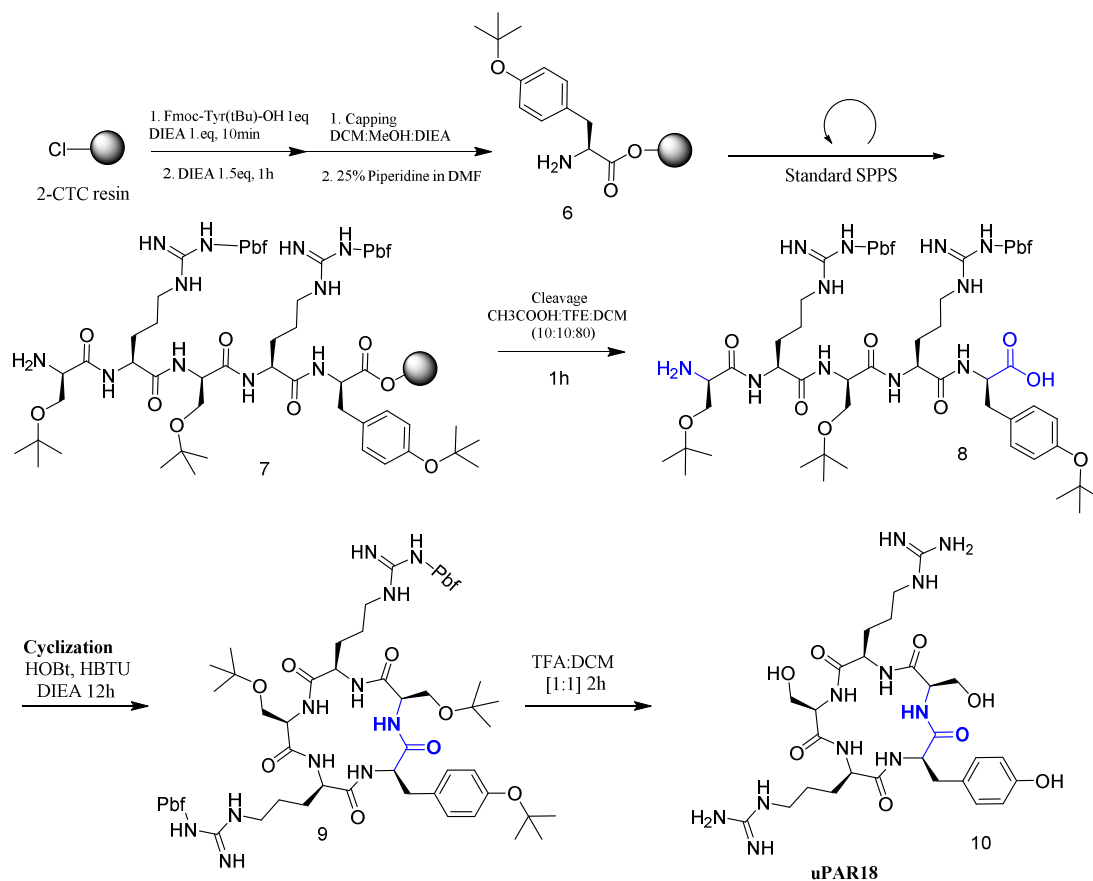


Figure 13. Strategies for peptide macrocyclization.

In the present thesis we reported two types of these macrocyclizations. *Head to tail* cyclization (Scheme 2) was carried out using a 2-chlorotrityl Resin (0.312g, 0.8mmol/g), swelled for 30 minutes in dichloromethane (DCM). The first coupling was carried out using 1.0 equivalent of N^α-Fmoc-Tyr(tBu)-OH, dissolved in 5mL of DCM. The amino acid solution was added to 2-chlorotrityl Resin. To this mixture was added 1.0 equivalent of DIPEA, agitated in the shaker for 10 minutes then 1.5 equivalents of DIPEA were added. The mixture was agitated vigorously for 60 minutes. To endcap any remaining reactive 2-chlorotrityl groups, a mixture of DCM/MeOH/DIPEA (80:15:5, v/v/v) was added and mixed for 30 minutes. For removing the Fmoc protecting group from the first amino acid, the resin was suspended in 25% solution of piperidine in dimethylformamide (DMF) (1x5 minutes and 1x20 minutes). The following protected amino acids were then added stepwise, N^α-Fmoc-Ser(tBu)-OH and N^α-Fmoc-Arg(Pbf)-OH. Each coupling reaction was accomplished using a 3-fold excess of amino acid with HBTU (3eq) and HOBt (3eq) in the presence of (6eq) of DIPEA. The N^α-Fmoc protecting groups were removed by treating the protected peptide resin with a 20% solution of piperidine in DMF, (1x5 minutes and 1x20 minutes). The peptide resin was washed three times with DCM and the next coupling step was initiated in a stepwise manner. The peptide resin was washed with DCM (3x), DMF (3x) and the deprotection protocol was repeated after each coupling step. The N-terminal Fmoc group was removed as described above. The peptide was released from the resin with a mixture of DCM/AcOH/Trifluoroethanol (TFE) (80:10:10, v/v/v) for 1 hour, keeping all the side-chains protecting groups intact. The resin was removed by filtration and the crude linear peptide was recovered by precipitation with cold anhydrous diethyl-ether to give a pale yellow powder. The linear peptide was dissolved in 10 mL of DCM/DMF 1:1 under stirring, 2.4 equivalents of DIPEA was added and allowed to preactive for 15 minutes, then HOAt (1.2 equiv.) and HATU (1.2 equiv.) were added and the resulting reaction mixture was stirred until the completion of reaction (determined by thin layer chromatography) for 12 hours (Scheme 2). At this point the side-chains protecting groups were removed using a solution of TFA 50% in DCM (20 mL) to afford the crude peptide. Crude peptide was recovered by precipitation from the filtrate using chilled ether to give a powder, which was purified by RP-HPLC using a semi-preparative C18-bonded silica column (Phenomenex, Jupiter 4μ Proteo 90Å, 1.0 x 25 cm) with a gradient of MeOH and water containing 0.1% TFA (from 0 to 90% over 40 min) at a flow rate of 5.0 mL/min. The product

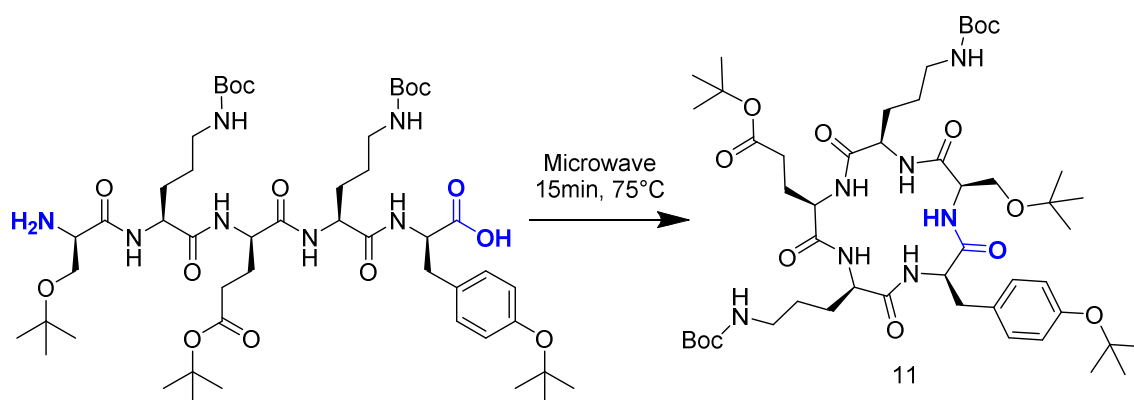
was obtained by lyophilization of the appropriate fractions after removal of the MeOH by rotary evaporation under reduced pressure. Analytical RP-HPLC indicated >95% purity and the correct molecular ions were confirmed by LC/ESI-MS.



Scheme 2. Synthesis of uPAR18: *head to tail* cyclization.

Cyclization *head to tail* was also accomplished using microwave irradiation (Scheme 3). After the elongation of the peptide on resin with same protocol reported above. The peptide was cleaved from the resin with a mixture of DCM/AcOH/TFE (80:10:10, v/v/v) for 1 hour, keeping all the side-chains protecting groups intact. The linear peptide was dissolved in 10mL of DCM/DMF (1:1) in microwave vessel 20mL under stirring, 2.4 equivalents of DIPEA was added and HOAt (1.2 equiv.) and HATU (1.2 equiv.) were added and the resulting reaction mixture was stirred under microwave irradiation for 15 minute at 75 °C (Scheme 3). The cyclization was monitored by LC-MS. At this point the side-chains protecting groups were removed using a solution of TFA 50% in DCM (20mL) to afford the crude peptide. Crude

peptide was recovered by precipitation from the filtrate using chilled ether to give a powder, which was purified by RP-HPLC using a semi-preparative C18-bonded silica column (Phenomenex, Jupiter 4 μ Proteo 90Å, 1.0 x 25 cm) with a gradient of MeOH and water containing 0.1% TFA (from 0 to 90% over 40 min) at a flow rate of 5.0 mL/min. The product was obtained by lyophilization of the appropriate fractions after removal of the MeOH by rotary evaporation under reduced pressure. Analytical RP-HPLC indicated >95% purity and the correct molecular ions were confirmed by LC/ESI-MS.



Scheme 3. Cyclization head to tail in microwave irradiation

The second way of macrocyclization carried out in the present thesis is *side chain to tail* (Scheme 4). The building block N^α-Fmoc-Orn-OAll was synthesized in solution. Then was insert in solid phase using 2-chlorotrityl Resin (0.312g, 0.8mmol/g) and the same protocol for the first coupling above. After the elongation of the peptide on the resin, the Allyl protecting group was removed using Pd(PPh₃)₄/DMBA in DCM:DMF (1:1) for 2 hours per two times. The N-terminal Fmoc group was removed as described above. The cyclization was carried out by HOBt (3eq), HBTU (3eq) and DIEA (6eq) for 12 hours (Scheme 4). The cyclization was monitored by LC-MS. At this point the side-chains protecting groups were removed using a solution of TFA 50% in DCM (20mL) to afford the crude peptide. Crude peptide was recovered by precipitation from the filtrate using chilled ether to give a powder, which was purified by RP-HPLC using a semi-preparative C18-bonded silica column (Phenomenex, Jupiter 4 μ Proteo 90Å, 1.0 x 25 cm) with a gradient of MeOH and water containing 0.1% TFA (from 0 to 90% over 40 min) at a flow rate of 5.0 mL/min. The product was obtained by lyophilization of the appropriate fractions after removal of the MeOH by rotary evaporation

under reduced pressure. Analytical RP-HPLC indicated >95% purity and the correct molecular ions were confirmed by LC/ESI-MS.

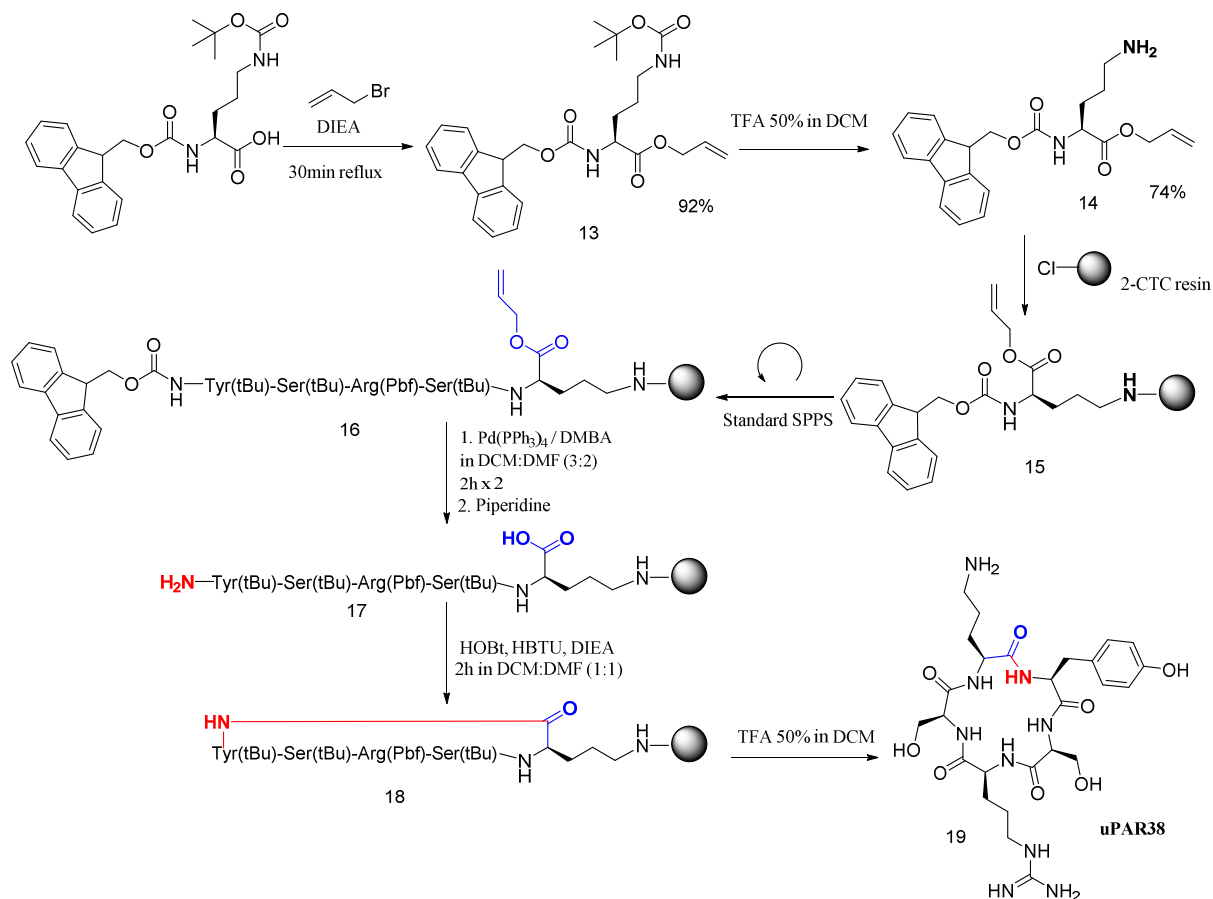


Figure 4. Synthesis of uPAR38: *side-chain to tail* cyclization.

5. RESULTS AND DISCUSSION

5.1. Linear analogues: results

5.1.1. Biological Data

HEK293 Cells Migration/uPAR. The ability of phosphorylated peptides was tested for the motility basal cell embryonic kidney HEK-293 transfected with the cDNA/uPAR [55]. As shown in Figure 14A (blue bars), none of the peptides tested, when used as a chemo-attractant, has shown to have chemotactic itself. Therefore, we investigated the ability of peptides uPAR1, uPAR2 or peptide control uPAR3 to modify the response of HEK-293 cells/uPAR to a gradient consisting of 10 nM or 10 nM fMLP SRSRY. In this case, the peptides were tested at a concentration of 10 nM, and the results expressed as percentage of cells that had migrated in the absence of chemotactic gradient (basal migration, considered to be 100%). uPAR1 reduced cell migration induced by fMLP SRSRY and, respectively, 41% and 55%, while the peptides uPAR2 and uPAR3 results are incapable of producing any effect (Figure 14A). The inhibition of cell migration induced by fMLP peptide uPAR1 is dose-dependent, starting already in the range femtomolare and reaches the maximum effect (56% inhibition) at 1nM (Figure 14B). The set of results confirms the role of Ser⁹⁰ in regulating cell motility and identifies the peptide uPAR1 as a possible inhibitor of cell migration regulated by uPAR.

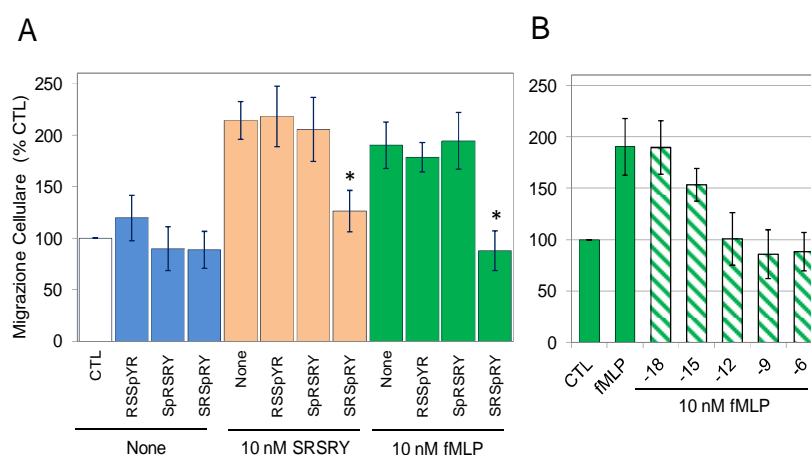


Figure 14. (A) Effect of peptides derived from the sequence chemotactic uPAR88-92, containing the phosphorylated serine, on the cell migration of HEK-293 / uPAR. (B) The inhibition of cell migration induced by fMLP peptide uPAR1 is dose-dependent, starting already in the range femtomolare and reaches the maximum effect (56% inhibition) at 1nM

uPAR expression in human osteosarcoma cells and chondrosarcoma. Before testing the effect of the peptides in question on the motility of human chondrosarcoma cells, we assessed the levels of expression of uPAR on the same and on two control lines Saos-2 and U2OS. The cells examined were grown on glass coverslips until the semi-confluence, fixed, exposed to monoclonal anti-uPAR R4 and finally incubated with anti-mouse immunoglobulin conjugated with fluorescein isothiocyanate. The fluorescence associated with the cells was visualized by a microscope equipped with UV. Cells Saos-2 and U2OS SARC express uPAR mainly localized on the cell surface (Figure 15A). Although this type of analysis is only qualitative it should be noted that the cells express SARC greater amount of uPAR on the surface. To confirm the expression of uPAR and analyze the different levels, was carried out an experiment in Western Blot. For this purpose, 50 mg/sample of cell lysates were separated by SDS-PAGE, transferred to a filter and analyzed for the levels of uPAR Western Blot. The data confirm that the cells expressing uPAR SARC greater extent than the levels observed in lysates of U2OS and Saos-2 cells (Figure 15B).

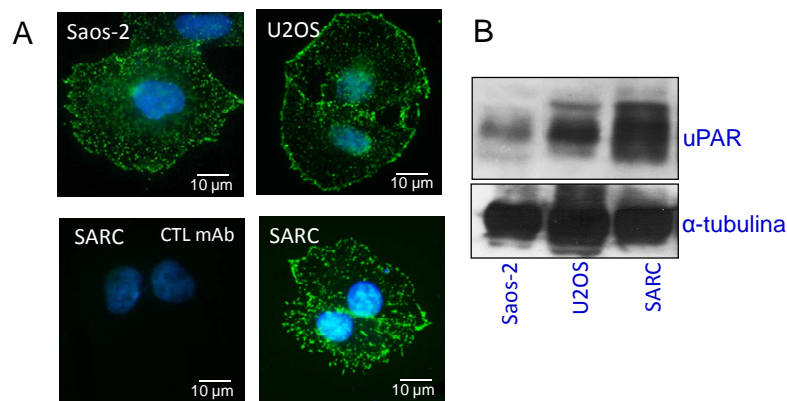


Figure 15. uPAR expression in human osteosarcoma cells and chondrosarcoma.

Effect on the migration in human osteosarcoma and chondrosarcoma cells. The ability of phosphorylated peptides was tested to inhibit the motility induced by the chemotactic peptide SRSRY or FBS, the latter used as a source of various chemoattractants. For each line, the migration of cells exposed to DMEM alone, in the absence of chemoattractant, was considered 100% (basal migration) and cell migration versus SRSRY or FBS, with or without peptides

was calculated as a percentage of 100%. As shown in Figure 16A, the Saos-2 cells that express lower levels of uPAR have reduced ability to respond to a gradient SRSRY. In contrast, cells SARC respond very well to the stimulus of SRSRY (300% of basal migration). uPAR3 have no effect. On the other hand, uPAR1 and uPAR2 produce a reduction in motility SRSRY-dependent cell U2OS, Saos-2 and SARC. However, while the peptide uPAR2 reduces migration of U2OS cells, Saos-2 and SARC vs SRSRY in a non-statistically significant, that induced by the peptide uPAR1 is significant at $p < 0.001$ for all three lines tested (Figure 16A).

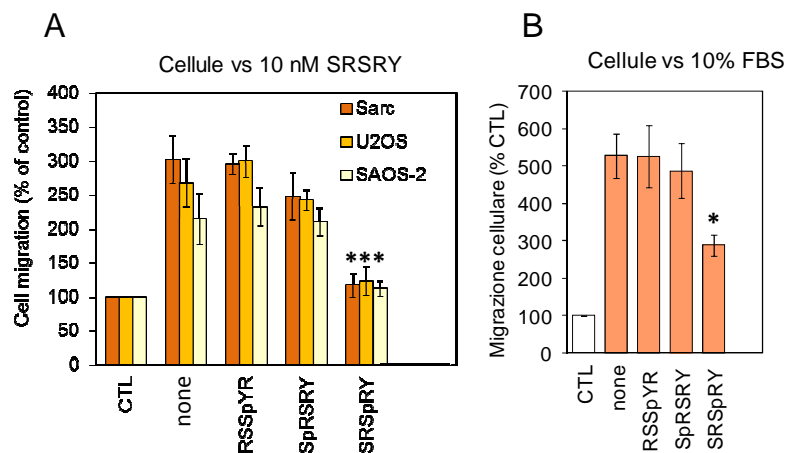


Figure 16. Effect of peptides derived from the sequence chemotactic uPAR88-92, containing the serine phosphorylated on cell migration of human osteosarcoma and chondrosarcoma.

The ability of cells to invade chondrosarcoma a monolayer of endothelial cells. We created a monolayer of endothelial cells following with the instrument it reached 100% confluence (Figure 17A). To this point (after ~ 22 hours), cells SARC were filed on endothelial monolayer and added peptides uPAR1, uPAR2 or control peptide uPAR3 (all tested at a concentration 10 nM), or DMEM. The impedance variations were recorded for further 5-6 hours. Already after 2 hours of cell SARC, the impedance values recorded have appeared reduced. This indicates that the cells have produced SARC discontinuity (invasion) in the endothelial monolayer (Figure 17B). In the presence of the peptide uPAR1 such variations are significantly lower than those recorded in the absence of peptides, in the presence of the peptide uPAR2 and control uPAR3, indicating that, indeed, the peptide uPAR1 reduces the ability of cells to invade SARC (break) the monolayer of endothelial cells (Figure 17B).

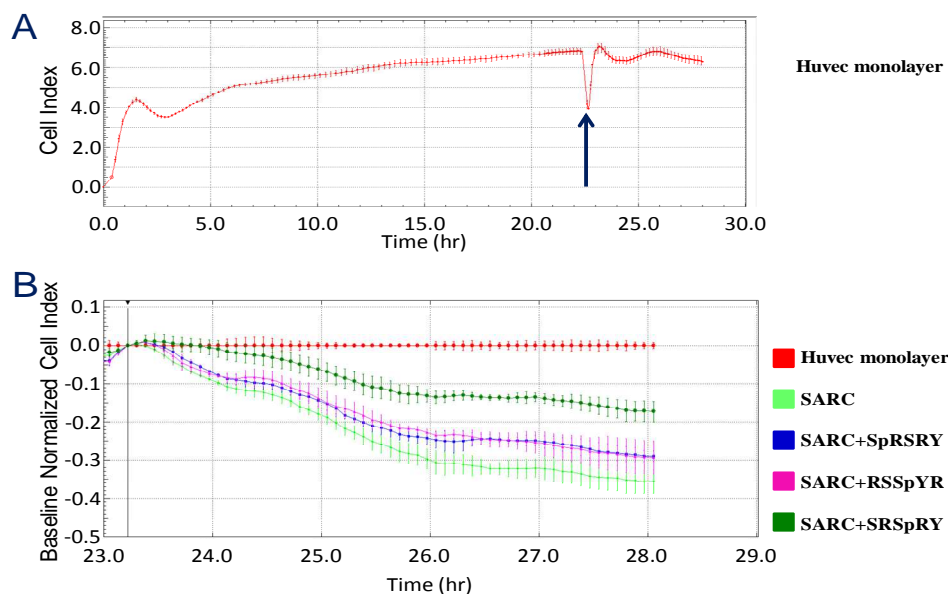


Figure 17. Effect of peptides derived from the sequence chemotactic uPAR88-92, containing the phosphorylated serine, on the ability of the human chondrosarcoma cells to invade a monolayer of endothelial cells.

5.1.2. Discussion

All chondrosarcomas may recur locally, but only some show high propensity to produce metastasis. To date, the lack of valid parameters with prognostic significance does not allow to predict the evolution of the disease, or the responsiveness to treatment. This can cause delays in diagnosis or diagnostic errors with dramatic consequences on the natural history of the disease. Chondrosarcoma generally metastasizes by blood. So there is the real possibility that drugs that reduce the motility of tumour cells and their ability to pass into the blood stream, may be usefully employed in the treatment of aggressive chondrosarcoma.

In the lab where my compounds are tested a primary culture of human chondrosarcoma whose cells express high levels of uPAR surface had been generated by enzymatic digestion of a tissue biopsy from a patient with high-grade chondrosarcoma. These cells secrete soluble forms of uPAR containing the sequence chemotactic Ser⁸⁸-Arg-Ser-Arg-Tyr⁹² [56].

It is well known that Ser⁹⁰ is critical to the regulation of the functions of uPAR [44], and when this residue is replaced by a glutamic acid the resulting peptide acquires a structure to α -helix and inhibits dramatically uPAR cell migration, invasion and angiogenesis [57].

Based on these considerations, we hypothesized that phosphorylation of Ser⁹⁰ could "force" the conformation of chemotactic sequence in a compact, for α -helix, unable to promote cell migration. Phosphorylated Ser⁹⁰ could mime Glu residue by suitable synthetic strategy that consists in the phosphorylation of Serine in position 88 and in position 90. These peptides were tested in order to evaluate its effect on migration, proliferation and invasive ability of cells of human chondrosarcoma. We have identified the peptide uPAR1 as potent inhibitor of cell motility SARC. These inhibitory effects are dose-dependent, are already beginning to femtomolare concentrations and the concentration 1 nM reduced by 56% cell motility induced by the chemotactic peptide fMLP. In addition, the peptide uPAR1 significantly reduces the ability of cells to invade a human chondrosarcoma vascular endothelium.

Chondrosarcoma is radio-resistant and is not sensitive to chemotherapy (Staals EL et al., D. Heymann, 2010). In treatment of high-grade chondrosarcoma with worse prognosis for the frequency of local recurrence and metastases, were introduced chemo- and radio-adjuvant therapies but, to date, have not been shown to have a significant impact on morbidity and mortality of patients with advanced disease. Hence the need to develop, especially for cases of chondrosarcoma that at onset presenting with malignancy grade intermediate and / or high, new drugs directed against specific molecular targets, able to control local recurrence and the development of metastases.

The dataset allows us to consider the sequence uPAR⁸⁸⁻⁹² as possible molecular target for designing molecules that are able to inhibit the biological activity, prove to be antagonists of neoplastic progression. Moreover, in light of the data obtained, we can consider the peptide uPAR1 as valid prototype for the development of new compounds able to counteract the progression of chondrosarcoma.

5.2. Cyclic analogues: results

5.2.1. Biological, stability and conformational Data

uPAR18 is a ligand of FPR1 in THP-1 cells and inhibits their migration in a dose dependent manner. Once documented that uPAR18 counteracts the fMLF-induced and FPR1-mediated

signaling, we investigated its effect on the motility of monocytes. We found that THP-1 cells exposed to 10nM fluorescent FPR-agonist at 4°C, revealed an appreciable binding which was dramatically reduced by an excess of unlabeled fMLF, SRSRY or uPAR18, but not by the control peptide uPAR21 (Figure 18A).

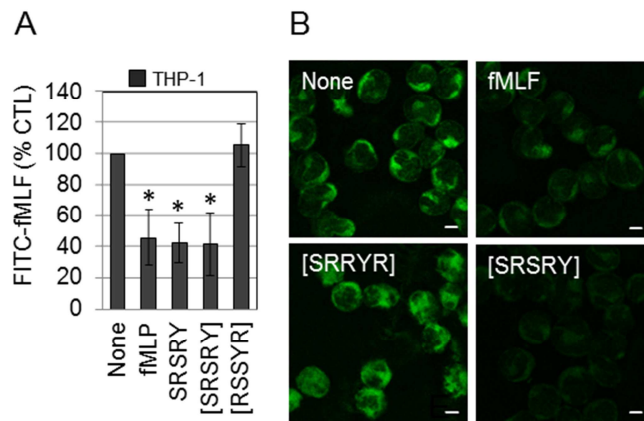


Figure 18. Cyclic SRSRY peptide binding to FPR1.

When binding experiments were performed at 37°C, FPR1 appeared mainly localized within the cytoplasm, adjacent but outside the nucleus of THP-1 cells. Internalization of fluorescent agonist was dramatically reduced in all cell population when THP-1 cells have been exposed to an excess of unlabelled fMLF, or uPAR18 whereas the control uPAR21 peptide did not exert such effect (Figure 18B). Although we did not determine the binding affinity of uPAR18 for FPR1, our findings indicate that, uPAR18 peptide inhibits fMLF/FPR1 interaction and prevents agonist-induced FPR1 internalization in THP-1 cells.

The ability of uPAR18 to affect THP-1 cell migration was analyzed in Boyden chambers using 10 nM fMLF or 10nM SRSRY as chemoattractants. Not surprisingly, 10 nM fMLF and SRSRY elicited a considerable cell migration, reaching 211% and 172% of the basal cell migration, respectively. uPAR18 reduced monocyte migration toward 10 nM fMLF or 10 nM SRSRY by 58% and 68%, respectively, whereas the uPAR21 did not exert any effect (Figure 19A). Inhibitory effect of uPAR18 was dose-dependent, it starts in the high fM range, it seems to level off in the μ M range and reaches an overall 50% reduction at 10 pM (Figure 19B). Interestingly, a dose-dependent inhibition is exerted by uPAR18 also on cell migration of THP-1 monocytes differentiated into macrophages with IC_{50} value 10 pM (Figure 19C). The

mechanisms by which monocytes move when subjected to a chemoattractant gradient, involve changes in cytoskeletal organization, which provide both protrusive and contractile forces necessary for cell migration. To gain some insights into the cellular effects exerted by uPAR18, PMA-differentiated THP-1 cells were grown adherent onto a glass slide, exposed to diluents, 10 nM fMLF gradient plus/minus 10 nM uPAR18 or 10 nM uPAR21 in a DUNN chamber for 6 hours as described [58], and then stained with rhodamine-phalloidin. Cells subjected to the fMLF gradient alone (None) or mixed to uPAR22 control peptide exhibited an elongated morphology and recognizable aligned protrusions associated to locomotion in the 70% cell population. Vice versa, the addition of uPAR18 to the fMLF gradient reduced cell elongation and alignment with the appearance of F-actin linear distribution along the plasma membranes in the 60% of cell population (Figure 19D). These findings indicate that unlike linear SRSRY, the cyclic form of the chemotactic sequence of uPAR inhibits monocyte motility in a dose dependent manner.

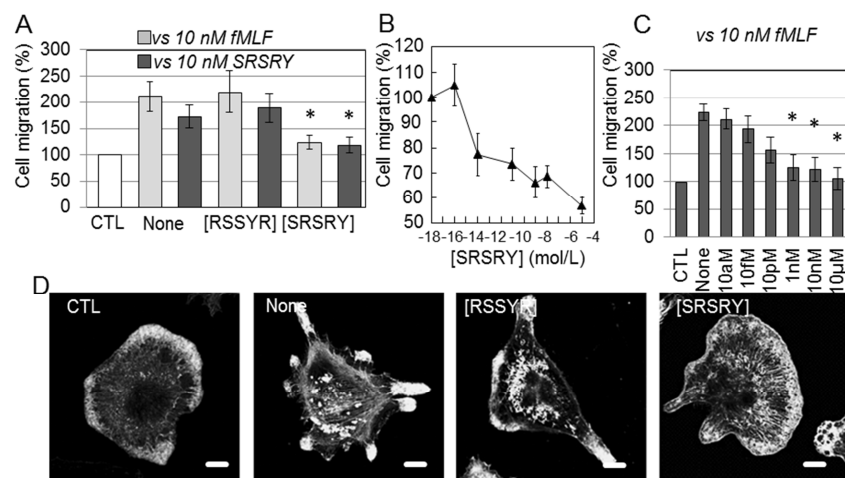


Figure 19. uPAR18 inhibits monocyte and macrophage cell migration in a dose-dependent manner causing a marked inhibition of fMLF-dependent cytoskeletal re-organization .

Effect of the uPAR18 peptide on trans-endothelial migration by THP-1 cells. Diapedesis of leukocytes plays a key role in the pathogenesis of inflammatory diseases and migration of monocytes from the blood into the sub-endothelial space is one of the earliest events [59]. Since THP-1 cells are considered a good model for analyzing molecular events during monocyte diapedesis, we investigated the effects of uPAR18 on the number and morphology of THP-1 adhered to an endothelial monolayer. Phase-contrast images revealed numerous

THP-1 cells interacting with HUVECs, that decreased upon addition of uPAR18 (Figure 20A). THP-1 cells normally extend long pseudopodia and lamellipodia once they are spread on top of the endothelium. To examine the changes in morphology in more detail and quantify monocytes interacting with endothelial monolayer, we performed a subset of experiments using GFP-tagged THP-1, labeling co-cultures for F-actin and recording images by a confocal microscope. In the presence of diluents, or uPAR21, GFP-tagged THP-1 cells formed F-actin rich lamellipodia and pseudopodia (arrows) which disappeared when GFP-tagged THP-1 were exposed to 10 nM uPAR18 (Figure 23B). Z-stack analysis of confocal images revealed transmigration of THP-1 cells underneath the endothelium (Figure 23B). In contrast, when uPAR18 was added to the co-culture, the majority of THP-1 were seen to rest on top of endothelial cells (Figure 20B). Also, in the presence of uPAR18, the number of GFP-THP-1 cells interacting with endothelial monolayer was reduced by a 40%, (Figure 20C). These findings indicate that uPAR18 not only prevents monocyte interaction with endothelium but also reduces their trans-endothelial monocyte migration. To further ascertain if the observed uPAR18-dependent impairment in migration may affect trans-endothelial migration by monocytes, the ability of THP-1 cells to cross an endothelial monolayer was analyzed using the xCELLigence RTCA technology in which impedance changes are caused by the presence of cells as described. HUVECs were allowed to grow until they formed a monolayer for 24 hours prior to seeding THP-1 cells in the presence of 10% FBS plus/minus uPAR18. At this time, reduction of impedance values, due to invading cells that interrupt monolayers were monitored in real-time for 10 hours. As shown in Figure 20D, THP-1 cells were able to cross endothelial monolayers. A 35% reduction of endothelial monolayer integrity was achieved by the addition of 10 nM uPAR18. Taken together, these data indicate that FPR1-mediated uPAR18 inhibitory effect involves a marked inhibition of cytoskeletal re-organization occurring during locomotion and trans-endothelial migration of monocytes.

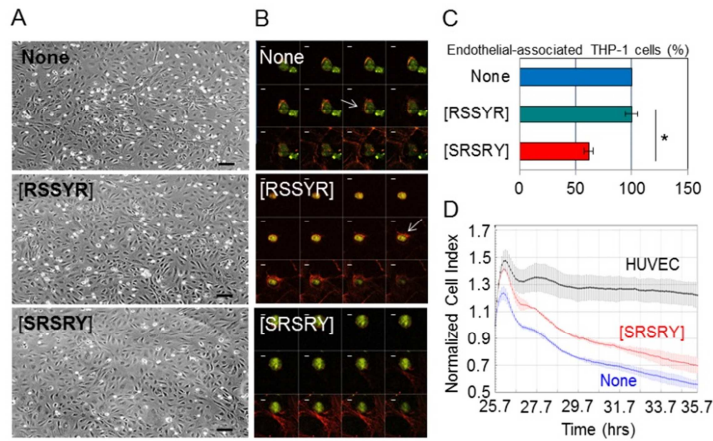


Figure 20. The [SRSRY] peptide prevents diapedesis and trans-endothelial migration of THP-1 cells.

Peptide Stability. The stability of SRSRY and uPAR18 was investigated in human serum. As shown in Figure 21, already after one hour of exposure to serum, SRSRY and uPAR18 peptides had a residual concentration lower than 75% and 85%, respectively. After 24 hours, uPAR18 showed a residual concentration higher than 80% while for compound SRSRY the concentration was lower 50% (Figure 21).

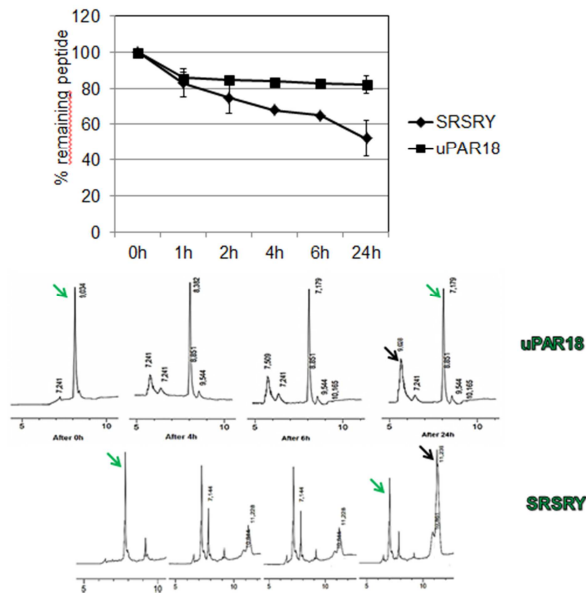


Figure 21. Stability of SRSRY and uPAR18 peptides in human serum. The green arrow represent the peptide and the black one represent the degradation.

CD Analysis. We investigated the conformational preferences of the cyclic peptide uPAR18 using circular dichroism in different solvents with different temperature. However, uPAR18 has demonstrated to be unstructured peptide in solution (Figure 22). Thus, one of the our priority is NMR studies to explore the conformational preferences of our peptides.

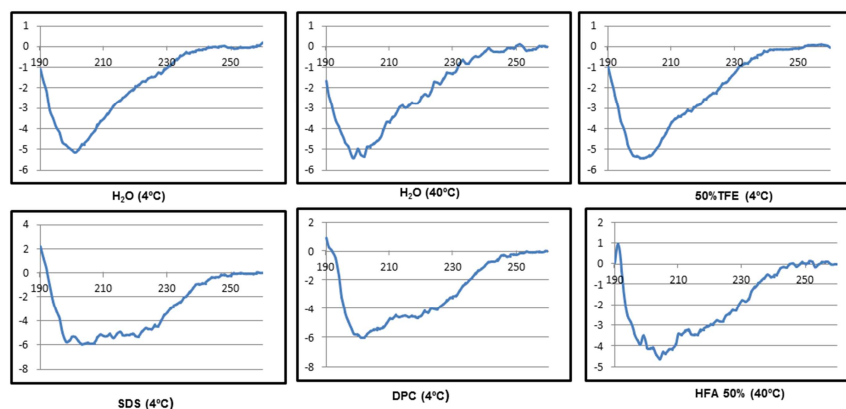


Figure 22. CD analysis of cyclic peptide. The spectra data demonstrated ton be unstructured peptides

5.2.2. Discussion

As reported previously, uPAR plays an important role in the regulation of leukocyte trafficking [60]. We and others have shown that the capability of uPAR to trigger cell migration depends on its $^{88}\text{Ser-Arg-Ser-Arg-Tyr}^{92}$ chemotactic sequence even in the form of a synthetic, linear peptide (SRSRY). Herein we provide evidence that the cyclization of the $\text{Ser}^{88}\text{-Arg-Ser-Arg-Tyr}^{92}$ chemotactic sequence of uPAR generates a new peptide uPAR18 exerting opposite effect on cell migration, as compared to its linear form. uPAR18 is a new potent inhibitor of monocyte locomotion with IC_{50} value of 0.01 nM. Moreover, uPAR18 displays higher resistance to enzymatic digestion as compared to RERF [61]. We have previously reported that, similarly to fMLF, SRSRY promotes cell migration upon interaction with the G protein-coupled FPR1. SRSRY triggers FPR1 activation by inducing its internalization [62]. Now, by competition experiments with a fluorescent fMLF structures analogue we show that an excess of uPAR18 competes with fMLF and SRSRY for binding to FPR1, and prevents agonist-induced FPR1 internalization. Our findings suggest that the linear and cyclic structures of the uPAR chemotactic sequence could share the same binding site on FPR1, although they exert opposite effects on cell motility. Alternatively, as the ligand binding pocket of FPRs consists of several key residues located in different trans-membrane

helices, it is possible that uPAR18/FPR association may affect SRSRY and/or fMLF adjacent binding. Regarding the specific affinity of uPAR18 for its target, labeled uPAR18 is unavailable to us, and therefore we could not determine the affinity of uPAR18 for FPR1. How uPAR18 interacts with FPR1 remains to be investigated. In this respect, uPAR18 could act as an inverse agonist by shifting, upon binding to FPR1, the active state of the receptor toward the inactive one. This issue is relevant *in vivo* for potential therapeutic applications, since inverse agonist effects are associated with receptor activation and inactivation, whereas neutral antagonism produces no effect when administered alone, but blocks the effects of agonists and inverse agonist [59].

Activation of FPRs results in increased cell migration, phagocytosis, release of pro-inflammatory mediators, and the signaling cascade culminates in heterologous desensitization of other receptors including chemokine receptors CCR5 and CXCR4. uPAR expression regulates the adhesive and migratory ability of CXCR4-expressing cells through a mechanism involving FPR1 [63]. Thus, by interacting with a variety of exogenous and host-derived agonists, FPRs constitute a novel group of pharmacological targets.

6. CONCLUSIONS

The urokinase-type plasminogen activator receptor (uPAR) is the master regulator of cell migration. The uPAR is formed by three domains connected by short linker region. The Ser⁸⁸-Arg-Ser-Arg-Tyr⁹² is the minimum chemotactic sequence of uPAR required to induce the same intracellular signaling as result of its binding with formyl peptide receptor (FPRs). With aim to perform new structure-activity relationship studies of the chemotactic sequence S⁸⁸RSRY⁹², I synthesized a peptide library using phosphorylated amino acids, non-coded amino acids, D-amino acid scan and cyclic analogues. Herein I summarized all goals achieved by the first part of the present thesis:

- Phosphorylated peptides have been demonstrated to have an efficient binding with FPRs binding and significant activity. **uPAR1** represent a potent inhibitor of the migration of HEK-293 cells/uPAR-induced chemotactic peptide fMLP SRSRY and in a dose-dependent, inhibits the migration of human chondrosarcoma cells expressing high levels of uPAR and reduces the ability of human chondrosarcoma cells to invade a monolayer of human endothelial cells. These findings confirm the phosphorylation of Ser⁹⁰ could mime the Glu⁹⁰. In addition, **uPAR1** represent a new analogue with higher affinity and potency in comparison with RERF analogue.
- Depending on its functional groups, a peptide can be cyclized in four different ways: *head-to-tail* (C-terminus to N-terminus), *head-to-side chain*, *side chain-to-tail* or *side-chain-to-side-chain*. In the present thesis we reported *head to tail* and *side chain to tail* cyclization. Since this cyclic peptide **uPAR18** inhibits cell migration by antagonizing FPR1 biologic activity, it may be considered as a new potent and stable FPR1 inhibitor which may suggest the generation of new pharmacological treatments for diseases sustained by a chronic excess of cell migration, such as chronic inflammatory and cancer.

7. EXPERIMENTAL SECTION

6.1. Material and Methods

N^α-Fmoc-L-Orn-OAll was synthesized according to literature methods [64]. Allyl bromide, and 1,3-dimethylbarbituric acid (NDMBA), all were purchased from Aldrich. Tetrakis(triphenylphosphine)palladium, was purchased from Aldrich and washed with ethanol prior to use. Amino acids, Fmoc-Ser(tBu), Fmoc-Tyr(tBu), Fmoc-Trp(Boc), Fmoc-Orn(Boc), Fmoc-1Nal, Fmoc-2Nal, Fmoc-Arg(pbf), Fmoc-Phe, Fmoc-D-Ser(tBu), Fmoc-D-Tyr(tBu), Fmoc-D-Arg(pbf) and coupling reagents such as HBTU and HOBt, all were purchased from GL Biochem, and used as received. The rest of *N*^α-Fmoc-protected amino acids, HBTU and HOBt were purchased from GL Biochem (China), and used as received. *N,N'*-Diisopropylcarbodiimide (DIC) was purchased from Aldrich and used as received. 2-Chlorotrityl chloride resin and Rink amide resin were purchased from GL-Biochem™, and the manufacturer's reported loading of the resin was used in the calculation of final product yields. Microwave irradiation was performed on a 300 MW Biotage apparatus on the high absorption level; temperature was monitored automatically. Flash chromatography was on 230-400 mesh silica gel. Thin layer chromatography was performed on silica gel 60 F₂₅₄ plates from Merck™. Accurate mass measurements were performed on a LC-MSD instrument from Agilent technologies in positive electrospray ionisation (ESI) mode at the University of Naples Federico II Mass Spectrometry facility or by 6110 Quadrupole, Agilent Technologies. Sodium adducts [M+Na]⁺ were used for empirical formula confirmation.

6.2. Peptide Stability

The stability of SRSRY and [SRSRY] was investigated in human serum. The peptides were incubated at 37°C in human serum at a concentration of 10⁻²mol/L. Aliquots (100mL) of serum were removed at time points varying from 0, 1, 2, 4, 6, and 24 hours and acetonitrile (300mL) was added to each aliquot before centrifuging (13000 rpm, 15 min). Aliquots (100 mL) of the supernatant were then analyzed by RP-HPLC after passing through Phenomenex Luna 100A C18 5μ, linear gradient from 0–100% acetonitrile over 25 minutes.

6.3. CD experiments

CD spectra were obtained at room temperature on a Jasco J-815 dichrograph. Data were collected at 0.2nm intervals with a 10nm/min scan speed, a 2 nm bandwidth and a 16 s

response, from 250 to 190 nm; quartz cells of 0.2 cm path length were used. Samples were prepared in 2.0 mM (pH = 7.2) at 0 and 40% trifluoroethanol (TFE), at 10-40% HFA, in DPC and SDS. Peptide concentrations were in the range 0.117 - 0.129 mM, as determined by the absorbance at 265 nm ($\epsilon = 103 \text{ M}^{-1} \text{ cm}^{-1}$) for uPAR18. CD intensities are expressed as mean residue molar ellipticities ($\text{deg cm}^2 \text{ dmol}^{-1} \text{ res}^{-1}$).

6.4. Cell lines

Rat basophilic leukaemia RBL-2H3, and RBL-2H3/ETFR cells [25] were grown in DMEM-10% FBS. Human monocytic leukemia THP-1 cell line (purchased from the American Type Culture Collection) was cultured in RPMI 1640 medium, supplemented with 10% heat-inactivated fetal bovine serum (FBS), penicillin (100 $\mu\text{g}/\text{mL}$) and streptomycin (100 U/mL). Human umbilical vein endothelial cells (HUVECs), obtained from Lonza (C2519A, Lot # 0000115425), which provided a certificate of analysis for each cell lot, were grown in Eagle Basal Medium (EBM) supplemented with 4% FBS, 0.1% gentamicin, 1 $\mu\text{g}/\text{mL}$ hydrocortisone, 10 $\mu\text{g}/\text{mL}$ epidermal growth factor and 12 $\mu\text{g}/\text{mL}$ bovine brain extract (Cambrex) [26]. All cells were maintained in an atmosphere of humidified air with 5% CO_2 at 37°C.

6.5. Differentiation and generation of GFP-transfected THP-1 cells

THP-1 differentiation into macrophages was induced using 160 nM phorbol-12-myristate acetate (PMA) purchased by Sigma Aldrich for 72 hours. To generate Green Fluorescent Protein (GFP)-tagged THP-1 cells, 2×10^7 cells were resuspended in 300 μl complete RPMI 1640 medium containing 20 mM HEPES and incubated with 5 μg pEGFP-N1 vector (Clontech) for 5 minutes on ice before being electroporated at 320 V, 1500 μF . Following electroporation, cells were kept on ice for 5 minutes then grown in 20 mL media for 24 hours. Then, G418-resistant cells expressing the highest levels of GFP were isolated and amplified.

6.6. Fluorescence microscopy

THP-1 cells (2×10^6 cells/sample) were incubated with the indicated unlabeled peptides for 30 minutes at 37°C and then exposed to 10 nM FITC-fMLF diluted in PBS for 30 minutes at 37°C as described [25]. To analyse cytoskeletal organization, PMA-differentiated THP-1 cells

were fixed and permeabilized with 2.5% formaldehyde-0.1% Triton X-100 in PBS for 10 minutes at 4°C, washed in PBS and then incubated with 0.1 µg/mL rhodamine-conjugated phalloidin (Invitrogen) at 23°C for 45 minutes. In all cases, slides were mounted using 20% (w/v) mowiol, cells were visualized with an Axiovert 200M Inverted Fluorescent Microscope (Carl Zeiss) and images were taken with a videocamera.

6.7. Western blot

Cells (1×10^6 /sample) were exposed to diluents or 10 nM fMLF plus/minus 10 nM [SRSRY] at 37°C for the indicate times and then lysed in RIPA buffer (10 mM Tris pH 7.5, 140 mM NaCl, 0.1 %SDS, 1% Triton X-100, 0.5% NP40) containing protease inhibitor mixture. Protein content of cell lysates was measured by a colorimetric assay (BioRad). Thirty-nanograms of proteins were separated on 10% SDS-PAGE and transferred onto a polyvinylidene fluoride membrane. The membranes were blocked with 5% non-fat dry milk and probed with 2 µg/ml anti-phospho-ERK1/2 monoclonal antibody. Total ERK1/2 was assessed by re-probing filters with 2 µg/ml rabbit anti-ERK1/2 monoclonal antibodies, all purchased by Cell Signaling. In all cases, washed filters were incubated with horseradish peroxidase-conjugated anti-rabbit antibody and detected by ECL (Amersham).

6.8. Chemotaxis Assay

Migration of THP-1 or PMA-stimulated THP-1 cells was assessed in Boyden chambers (Neuroprobe) as described [15]. Cell suspension (2×10^5 viable cells per mL serum-free RPMI 1640 medium) was seeded in each upper chamber. Lower chambers were filled with RPMI 1640 medium containing 10 nM fMLF (Sigma-Aldrich) or 10 nM linear SRSRY peptide, as chemoattractants with/without [SRSRY] or [RSSYR] peptides, the last used as a scramble, control peptide. The two compartments were separated by an uncoated 5 µm pore size filter, in the case of THP-1 cells, or by a collagen-coated (50 µg/mL for 2 hours at 37°C) 8 µm pore size polycarbonate filter (Neuroprobe) for PMA-stimulated THP-1 cells. Incubation, carried out at 37°C in humidified air with 5% CO₂ was 90 minutes for THP-1 cells, and 3 hours for PMA-stimulated THP-1 cells. At the end of the assay, cells on the lower filter surface were fixed with ethanol, stained with haematoxylin and 10 random fields/filter were counted at 200x magnification.

6.9. Dunn-chamber assay

PMA-stimulated THP-1 cells were seeded on 20x20 mm coverslips for 24 hours. Before inverting the cover slip on top of a double concentric chamber, cells on the cover slip covering the outer chamber were carefully scraped away as previously described [25]. A gradient of a chemoattractant was created by placing serum-free medium in the inner chamber and 10 nM fMLF with/without [SRSRY] or [RSSYR] peptides in the outer chamber. The ring separating the inner and outer chambers permits slow diffusion between the chambers. For control experiments both wells were filled with serum-free medium. After 6 hours, the coverslip was removed from the chamber and the cytoskeleton was visualized by staining with rhodamine conjugated phalloidin. A total of 100 cells/sample that translocated to the area corresponding to the outer well were examined with a fluorescence-inverted microscope and images were taken with a videocamera.

6.10. Monocyte diapedesis

Analysis of monocyte diapedesis was performed by seeding GFP-tagged THP-1 cells on an endothelial monolayer according to Ronald et al. [31]. To provide a substrate for monocyte migration, sterile round glass coverslips (12 mm in diameter) were coated with matrigel (Becton Dickinson) at a dilution of 1:8. The matrigel was air-dried at room temperature for 1 hour, followed by rehydration in EBM. HUVEC (5×10^4 cells in 200 μ l/well) were seeded onto matrigel and allowed to attach for 3 hours at 37°C, 5% CO₂. Coverslips were then flooded with endothelial growth medium and incubated for at least 24 hours before the experiments. Then, GFP-THP-1 cells (1×10^4 cells/well) were exposed to diluents, or the indicated peptides in complete endothelial medium and added to endothelial monolayer at 37°C. After 30 minutes, slides were fixed, stained with rhodamine conjugated phalloidin and finally analyzed using an inverted fluorescence microscope (Axiovert 200,) or a confocal microscope (LSM510), both purchased by Carl Zeiss.

6.11. Trans-endothelial migration assay

These assays were performed using E-16-well plates and the xCELLigence RTCA technology (Acea Bioscience) as described [12]. Microelectrodes placed on the bottom of plates, detect

impedance changes which are proportional to the number of adherent cells. The impedance value of each well was automatically monitored by the xCELLigence system and expressed as a Cell Index value. HUVECs (1×10^4 cells/well) suspended in growth medium, were seeded in E-16-well plates and allowed to grow for ~24 hours until they form a confluent monolayer, prior to seeding THP-1 cells (1×10^4 cells/well) in growth medium plus/minus 10 nM [SRSRY]. When HUVECs are challenged with invading cells, there is a drop in electrical resistance within 2-10 hours which is monitored in real-time as the Cell Index changes due to invasion of the endothelial monolayer. The experiments were performed twice in quadruplicate.

6.12. Statistical analysis

The results are expressed as the means \pm SD of the number of the indicated determinations. Data were analyzed by one-way analysis of variance and post hoc Bonferonni's modified t-test for multiple comparisons. $p < 0.01$ was accepted as significant.

8. CHARACTERIZATION

uPAR1: Purified purity >95%; LC-MS analysis (gradient 0 to 90% MeOH in water (0.1% TFA) over 15 min, flow rate of 1.0 mL/min, t_R : 7.99 min); LRMS chemical formula: $C_{27}H_{47}N_{12}O_{11}P$, calculated mass $[M+H]^+$ 746.72, found: 747.98.

uPAR2: Purified purity >95%; LC-MS analysis (gradient 0 to 90% MeOH in water (0.1% TFA) over 15 min, flow rate of 1.0 mL/min, t_R : 7.60 min); LRMS chemical formula: $C_{27}H_{47}N_{12}O_{11}P$, calculated mass $[M+H]^+$ 746.72, found: 747.94.

uPAR3: Purified purity >95%; LC-MS analysis (gradient 0 to 90% MeOH in water (0.1% TFA) over 15 min, flow rate of 1.0 mL/min, t_R : 7.57 min); LRMS chemical formula: $C_{27}H_{47}N_{12}O_{11}P$, calculated mass $[M+H]^+$ 746.72, found: 747.96.

uPAR4: Purified purity >95%; LC-MS analysis (gradient 0 to 90% MeOH in water (0.1% TFA) over 15 min, flow rate of 1.0 mL/min, t_R : 7.90 min); LRMS chemical formula: $C_{27}H_{46}N_{12}O_8$, calculated mass $[M+H]^+$ 666.44, found: 667.79.

uPAR5: Purified purity >95%; LC-MS analysis (gradient 0 to 90% MeOH in water (0.1% TFA) over 15 min, flow rate of 1.0 mL/min, t_R : 7.30 min); LRMS chemical formula: $C_{27}H_{46}N_{12}O_8$, calculated mass $[M+H]^+$ 666.44, found: 667.79.

uPAR6: Purified purity >95%; LC-MS analysis (gradient 0 to 90% MeOH in water (0.1% TFA) over 15 min, flow rate of 1.0 mL/min, t_R : 6.99 min); LRMS chemical formula: $C_{27}H_{46}N_{12}O_8$, calculated mass $[M+H]^+$ 666.44, found: 667.79.

uPAR7: Purified purity >95%; LC-MS analysis (gradient 0 to 90% MeOH in water (0.1% TFA) over 15 min, flow rate of 1.0 mL/min, t_R : 7.99 min); LRMS chemical formula: $C_{27}H_{46}N_{12}O_8$, calculated mass $[M+H]^+$ 666.44, found: 667.90.

uPAR8: Purified purity >95%; LC-MS analysis (gradient 0 to 90% MeOH in water (0.1% TFA) over 15 min, flow rate of 1.0 mL/min, t_R : 7.80 min); LRMS chemical formula: $C_{27}H_{46}N_{12}O_8$, calculated mass $[M+H]^+$ 666.44, found: 667.80.

uPAR9: Purified purity >95%; LC-MS analysis (gradient 0 to 90% MeOH in water (0.1% TFA) over 15 min, flow rate of 1.0 mL/min, t_R : 6.98 min); LRMS for chemical formula: $C_{27}H_{46}N_{12}O_8$, calculated mass $[M+H]^+$ 666.44, found: 667.79.

uPAR10: Purified purity >95%; LC-MS analysis (gradient 0 to 90% MeOH in water (0.1% TFA) over 15 min, flow rate of 1.0 mL/min, t_R : 6.98 min); LRMS for chemical formula: $C_{27}H_{46}N_{12}O_8$, calculated mass $[M+H]^+$ 666.44, found: 667.79.

uPAR11: Purified purity >95%; LC-MS analysis (gradient 0 to 90% MeOH in water (0.1% TFA) over 15 min, flow rate of 1.0 mL/min, t_R : 7.29 min); LRMS chemical formula: $C_{27}H_{46}N_{12}O_8$, calculated mass $[M+H]^+$ 666.44, found: 667.79.

uPAR12: Purified purity >95%; LC-MS analysis (gradient 0 to 90% MeOH in water (0.1% TFA) over 25 min, flow rate of 1.0 mL/min, t_R : 7.32 min); LRMS for chemical formula: $C_{26}H_{44}N_{10}O_8$, calculated mass $[M+H]^+$ 624.70, found: 625.77.

uPAR13: Purified purity >95%; LC-MS analysis (gradient 0 to 90% MeOH in water (0.1% TFA) over 15 min, flow rate of 1.0 mL/min, t_R : 7.80 min); LRMS for chemical formula: $C_{26}H_{44}N_{10}O_8$, calculated mass $[M+H]^+$ 624.70, found: 625.77.

uPAR14: Purified purity >95%; LC-MS analysis (gradient 0 to 90% MeOH in water (0.1% TFA) over 15 min, flow rate of 1.0 mL/min, t_R : 7.40 min); LRMS for chemical formula: $C_{25}H_{42}N_8O_8$, calculated mass $[M+H]^+$ 582.66, found: 583.86.

uPAR15: Purified purity >95%; LC-MS analysis (gradient 0 to 90% MeOH in water (0.1% TFA) over 15 min, flow rate of 1.0 mL/min, t_R : 6.99min); LRMS for chemical formula: $C_{28}H_{46}N_{10}O_9$, calculated mass $[M+H]^+$ 666.74, found: 667.84.

uPAR16: Purified purity >95%; LC-MS analysis (gradient 0 to 90% MeOH in water (0.1% TFA) over 15 min, flow rate of 1.0 mL/min, t_R : 7.10 min); LRMS for chemical formula: $C_{28}H_{46}N_{10}O_9$, calculated mass $[M+H]^+$ 666.74, found: 667.84.

uPAR17: Purified purity >95%; LC-MS analysis (gradient 0 to 90% MeOH in water (0.1% TFA) over 15 min, flow rate of 1.0 mL/min, t_R : 7.31 min); LRMS for molecular formula: $C_{27}H_{44}N_8O_9$, calculated mass $[M+H]^+$ 624.70, found: 625.79.

uPAR18: Purified purity >95%; LC-MS analysis (gradient 0 to 90% MeOH in water (0.1% TFA) over 15 min, flow rate of 1.0 mL/min, t_R : 8.22 min); LRMS for chemical formula: $C_{27}H_{43}N_{11}O_8$, calculated mass $[M+H]^+$ 649.71, found: 650.68.

uPAR19: Purified purity >95%; LC-MS analysis (gradient 0 to 90% MeOH in water (0.1% TFA) over 15 min, flow rate of 1.0 mL/min, t_R : 8.30 min); LRMS for chemical formula: $C_{27}H_{43}N_{11}O_7$, calculated mass $[M+H]^+$ 633.71, found: 634.74.

uPAR20: Purified purity >95%; LC-MS analysis (gradient 0 to 90% MeOH in water (0.1% TFA) over 15 min, flow rate of 1.0 mL/min, t_R : 8.50min); LRMS for chemical formula: $C_{27}H_{43}N_{11}O_8$, calculated mass $[M+H]^+$ 649.71, found: 650.78.

uPAR21: Purified purity >95%; LC-MS analysis (gradient 0 to 90% MeOH in water (0.1% TFA) over 15 min, flow rate of 1.0 mL/min, t_R : 11.4 min); LRMS for chemical formula: $C_{27}H_{43}N_{11}O_8$, calculated mass $[M+H]^+$ 649.71, found: 650.78.

uPAR22: Purified purity >95%; LC-MS analysis (gradient 0 to 90% MeOH in water (0.1% TFA) over 15 min, flow rate of 1.0 mL/min, t_R : 8.60 min); LRMS for chemical formula: $C_{27}H_{44}N_{11}O_{11}P$, calculated mass $[M+H]^+$ 729.69, found: 730.79.

uPAR23: Purified purity >95%; LC-MS analysis (gradient 0 to 90% MeOH in water (0.1% TFA) over 15 min, flow rate of 1.0 mL/min, t_R : 8.61 min); LRMS for chemical formula: $C_{27}H_{44}N_{11}O_{11}P$, calculated mass $[M+H]^+$ 729.69, found: 730.79.

uPAR24: Purified purity >95%; LC-MS analysis (gradient 0 to 90% MeOH in water (0.1% TFA) over 15 min, flow rate of 1.0 mL/min, t_R : 8.44 min); LRMS for chemical formula: $C_{27}H_{44}N_{11}O_{11}P$, calculated mass $[M+H]^+$ 729.69, found: 730.79.

uPAR25: Purified purity >95%; LC-MS analysis (gradient 0 to 90% MeOH in water (0.1% TFA) over 15 min, flow rate of 1.0 mL/min, t_R : 8.45 min); LRMS for chemical formula: $C_{29}H_{45}N_{11}O_9$, calculated mass; 691.75, found: 692.76.

uPAR26: Purified purity >95%; LC-MS analysis (gradient 0 to 90% MeOH in water (0.1% TFA) over 15 min, flow rate of 1.0 mL/min); LRMS for chemical formula: $C_{29}H_{45}N_{11}O_9$, calculated mass $[M+H]^+$ 691.75, found: 692.86.

uPAR27: Purified purity >95%; LC-MS analysis (gradient 0 to 90% MeOH in water (0.1% TFA) over 15 min, flow rate of 1.0 mL/min, t_R : 8.99 min); LRMS for chemical formula: $C_{31}H_{47}N_{11}O_{10}$, calculated mass $[M+H]^+$ 733.78, found: 734.78.

uPAR28: Purified purity >95%; LC-MS analysis (gradient 0 to 90% MeOH in water (0.1% TFA) over 15 min, flow rate of 1.0 mL/min, t_R : 8.10 min); LRMS for chemical formula: $C_{27}H_{43}N_{11}O_7$, calculated mass $[M+H]^+$ 633.71, found: 634.71.

uPAR29: Purified purity >95%; LC-MS analysis (gradient 0 to 90% MeOH in water (0.1% TFA) over 15 min, flow rate of 1.0 mL/min, t_R : 11.0 min); LRMS for chemical formula: $C_{29}H_{44}N_{12}O_7$, calculated mass $[M+H]^+$ 672.75, found: 673.78.

uPAR30: Purified purity >95%; LC-MS analysis (gradient 0 to 90% MeOH in water (0.1% TFA) over 15 min, flow rate of 1.0 mL/min, t_R : 14.1 min); LRMS for chemical formula: $C_{31}H_{45}N_{11}O_7$, calculated mass $[M+H]^+$ 683.77, found: 684.79.

uPAR31: Purified purity >95%; LC-MS analysis (gradient 0 to 90% MeOH in water (0.1% TFA) over 15 min, flow rate of 1.0 mL/min, t_R : 9.6 min); LRMS for chemical formula: $C_{31}H_{45}N_{11}O_7$, calculated mass; 683.77, found: 684.79.

uPAR32: Purified purity >95%; LC-MS analysis (gradient 0 to 90% MeOH in water (0.1% TFA) over 15 min, flow rate of 1.0 mL/min, t_R : 14.2 min); LRMS for chemical formula: $C_{29}H_{45}N_{11}O_8$, calculated mass $[M+H]^+$ 675.75, found: 676.75.

uPAR33: Purified purity >95%; LC-MS analysis (gradient 0 to 90% MeOH in water (0.1% TFA) over 15 min, flow rate of 1.0 mL/min, t_R : 11.0 min); LRMS for chemical formula: $C_{31}H_{46}N_{12}O_8$, calculated mass $[M+H]^+$ 714.79, found: 715.79.

uPAR34: Purified purity >95%; LC-MS analysis (gradient 0 to 90% MeOH in water (0.1% TFA) over 15 min, flow rate of 1.0 mL/min, t_R : 11.4 min), LRMS for chemical formula: $C_{33}H_{47}N_{11}O_8$, calculated mass $[M+H]^+$ 725.81, found: 726.87.

uPAR35: Purified purity >95%; LC-MS analysis (gradient 0 to 90% MeOH in water (0.1% TFA) over 15 min, flow rate of 1.0 mL/min, t_R : 15.6 min), LRMS for chemical formula: $C_{33}H_{47}N_{11}O_8$, calculated mass $[M+H]^+$ 725.81, found: 726.91.

uPAR36: Purified purity >95%; LC-MS analysis (gradient 0 to 90% MeOH in water (0.1% TFA) over 15 min, flow rate of 1.0 mL/min), LRMS for chemical formula: $C_{26}H_{41}N_9O_8$, calculated mass $[M+H]^+$ 607.67, found: 608.77.

uPAR37: Purified purity >95%; LC-MS analysis (gradient 0 to 90% MeOH in water (0.1% TFA) over 15 min, flow rate of 1.0 mL/min, t_R : 14.4 min), LRMS for chemical formula: $C_{26}H_{41}N_9O_8$, calculated mass $[M+H]^+$ 607.67, found: 608.77.

uPAR38: Purified purity >95%; LC-MS analysis (gradient 0 to 90% MeOH in water (0.1% TFA) over 15 min, flow rate of 1.0 mL/min, t_R : 13.8 min), LRMS for chemical formula: $C_{25}H_{39}N_7O_8$, calculated mass $[M+H]^+$ 565.63, found: 566.67.

uPAR39: Purified purity >95%; LC-MS analysis (gradient 0 to 90% MeOH in water (0.1% TFA) over 15 min, flow rate of 1.0 mL/min, t_R : 14.4 min), LRMS for chemical formula: $C_{28}H_{43}N_9O_9$, calculated mass $[M+H]^+$ 649.71, found: 650.79.

uPAR40: Purified purity >95%; LC-MS analysis (gradient 0 to 90% MeOH in water (0.1% TFA) over 15 min, flow rate of 1.0 mL/min, t_R : 13.8 min), LRMS for chemical formula: $C_{28}H_{43}N_9O_9$, calculated mass $[M+H]^+$ 649.71, found: 650.82.

9. REFERENCES

- [1] Abedin M, King N, “Diverse evolutionary paths to cell adhesion” *Trends Cell Biology*, 2010, 20(12), 734-42.
- [2] Alfano M, Sidenius NB, Panzeri F, Blasi F, Poli G, “Urokinase-urokinase receptor interaction mediates an inhibitory signal for HIV-1 replication” *Proc. Natl. Acad. Sci. USA.*, 2002, 99:8862–8867.
- [3] Blasi F, Carmeliet P, “uPAR: a versatile signalling orchestrator” *Nat. Rev. Mol. Cell Biol.*, 2002, 3:932–943.
- [4] Madsen DC, Ferraris GM, Andolfo A, Cunningham O, Sidenius N, “uPAR-induced cell adhesion and migration: vitronectin provides the key” *J Cell Biol*, 2007; 177(5):927-39).
- [5] Floridon C, “Localization and significance of urokinase plasminogen activator and its receptor in placental tissue from intrauterine, ectopic and molar pregnancies” *Placenta*, 1999, 20, 711–721 (1999).
- [6] Solberg H, Ploug M, Hoyer-Hansen G, Nielsen BS, Lund LR, “The murine receptor for urokinase-type plasminogen activator is primarily expressed in tissues actively undergoing remodelling” *J. Histochem. Cytochem.* 49, 2001, 237–246.
- [7] Bene MC, “CD87 urokinase-type plasminogen activator receptor, function and pathology in hematological disorders” *Leukemia*, 18, 2004, 394–400.
- [8] Dublin E, Hanby A, Patel NK, Liebman R, Barnes D, “Immunohistochemical expression of uPA, uPAR, and PAI-1 in breast carcinoma. Fibroblastic expression has strong associations with tumor pathology” *Am. J. Pathol.*, 2000, 157, 1219–1227.
- [9] Pyke C, “Immunohistochemical detection of the receptor for urokinase plasminogen activator in human colon cancer” *Histopathology*, 24, 1994, 131–138.
- [10] Plesner T, Behrendt N, Ploug M, “Structure, function and expression on blood and bone marrow cells of the urokinase-type plasminogen activator receptor uPAR” *Stem Cells*, 1997 15:398-408. - Mondino A, Blasi F “uPA and uPAR in fibrinolysis, immunity and pathology” *Trends Immunol*, 2004, 25, 450-5.
- [11] Smith HW, Marshall CJ, “Regulation of cell signalling by uPAR” *Nature reviews*, 11, 2010, 23.
- [12] Kjaergaard, M, Hansen LV, Jacobsen B, Gardsvoll H, Ploug M, “Structure and ligand interactions of the urokinase receptor (uPAR)” *Front. Biosci.*, 2008, 13, 5441–5461.
- [13] Harvey W, Smith C, Marshall J, “Regulation of cell signalling by uPAR” *Nature reviews*, 2010, 11, 23.
- [14] Deng G, Curriden S, Wang S, Rosenberg S, Loskutoff D, “Is plasminogen activator inhibitor-1 the molecular switch that governs urokinase receptor mediated cell adhesion and release?” *J. Cell Biol.* 134, 1996, 1563–15711.

- [15] Gardsvoll H, Ploug M, “Mapping of the vitronectin-binding site on the urokinase receptor: involvement of a coherent receptor interface consisting of residues from both domain I and the flanking interdomain linker region” *J. Biol. Chem.* 282, 2007, 13561–13572.
- [16] Thunø M, Macho B, Eugen-Olsen J, “suPAR the molecular crystal ball” *Dis Markers*, 2009, 27:157-72.
- [17] Wahlberg K, Høyer-Hansen G, Casslen B, “Soluble Receptor for Urokinase Plasminogen Activator in Both Full-Length and a Cleaved Form Is Present in High Concentration in Cystic Fluid from Ovarian Cancer” *Cancer Res* 58, 1998, 3294–3298.
- [18] Montuori N, Carriero, MV, Salzano S, Rossi G, Ragno P, “The cleavage of the urokinase receptor regulates its multiple functions” *J. Biol. Chem.* **277**, 2002, 46932–9.
- [19] Schiller HB, Zekeres A, Binder BR, Stockinger H, Leksa V, “Mannose 6-phosphate/insulin-like growth factor 2 receptor limits cell invasion by controlling $\alpha V\beta 3$ integrin expression and proteolytic processing of urokinase-type plasminogen activator receptor” *Mol. Biol. Cell*, 2009, 20, 745–756.
- [20] Resnati M, “The fibrinolytic receptor for urokinase activates the G protein-coupled chemotactic receptor FPRL1/LXA4R” *Proc. Natl Acad. Sci. USA*, 2002, **99**, 1359–1364.
- [21] Blasi F, Carmeliet P, “uPAR: A versatile signalling orchestrator” *Nature*, 2002, Vol 3, 932-43.
- [22] Ye S, Goldsmith EJ, “Serpins and other covalent protease inhibitors” *Curr. Opin. Struct. Biol.*, 2001, 11, 740–745.
- [23] Nielsen LS, “Purification of zymogen to plasminogen activator from human glioblastoma cells by affinity chromatography with monoclonal antibody” *Biochemistry*, 1982, 21, 6410–6415.
- [24] Aguirre Ghiso JA, “Inhibition of FAK signaling activated by urokinase receptor induces dormancy in human carcinoma cells in vivo” *Oncogene*, 2002, 21, 2513–2524 (2002).
- [25] Sidenius N, Sier CF, Blasi F, “Shedding and cleavage of the urokinase receptor (uPAR): identification and characterisation of uPAR fragments in vitro and in vivo” *FEBS Lett.*, 2000, 475,52–56.
- [26] Bae YS, Song JY, Kim Y, He R, Ye RD, Kwak JY, Suh PG, Ryu SH, “Differential Activation of Formyl Peptide Receptor Signaling by Peptide Ligands” *Mol. Pharmacol.*, 2003 64, 841–847.
- [27] Gargiulo L, Longanesi-Cattani I, Bifulco K, Franco P, Raiola R, Campiglia P, Grieco P, Peluso G, Stoppelli MP, Carriero MV “Cross-talk between fMLP and Vitronectin Receptors Triggered by Urokinase Receptor-derived SRSRY Peptide *Journal of Biological Chemistry*” 2005, vol 280, No. 26, 25225–25232.

- [28] Chaurasia, P, Aguirre-Ghiso JA, Liang OD, Gårdsvoll H, Ploug M, Ossowski “A region in urokinase plasminogen receptor domain III controlling a functional association with $\alpha 5\beta 1$ integrin and tumor growth” *J. Biol. Chem.* 281, 14852–14863 (2006).
- [29] Tang, C. H., Hill, M. L., Brumwell, A. N., Chapman, H. A. & Wei, Y. Signaling through urokinase and urokinase receptor in lung cancer cells requires interactions with $\beta 1$ integrins. *J. Cell Sci.* 121, 3747–3756 (2008).
- [30] Degryse, B., Resnati, M., Czekay, R.-P., Loskutoff, D. J. & Blasi, F. Domain 2 of the urokinase receptor contains an integrin-interacting epitope with intrinsic signaling activity: generation of a new integrin inhibitor. *J. Biol. Chem.* 280, 24792–24803 (2005).
- [31] Aguirre-Ghiso JA, “Inhibition of FAK signaling activated by urokinase receptor induces dormancy in human carcinoma cells in vivo” *Oncogene* 21, 2513–2524 (2002).
- [32] Wei, Y, “Urokinase receptors are required for $\alpha 5\beta 1$ integrin-mediated signaling in tumor cells” *J. Biol. Chem.* 282, 3929–3939 (2007).
- [33] Wei C, “Modification of kidney barrier function by the urokinase receptor” *Nature Med.* 14, 55–63 (2008).
- [34] Wei Y, “Urokinase receptors are required for $\alpha 5\beta 1$ integrin-mediated signaling in tumor cells” *J. Biol. Chem.* 282, 3929–3939 (2007).
- [35] Kjoller L, Hall A, “Rac mediates cytoskeletal rearrangements and increased cell motility induced by urokinase-type plasminogen activator receptor binding to vitronectin” *J. Cell Biol.* 152, 1145–1158 (2001).
- [36] Q. Huai, A.P. Mazar, A. Kuo, G.C. Parry, D.E. Shaw, J. Callahan, Y. Li, C. Yuan, C. Bian, L. Chen, B. Furie, B.C. Furie, D.B. Cines and M. Huang, “Structure of Human Urokinase plasminogen Activator in Complex with Its Receptor” *Science* 311(2006), 656–659.
- [37] Høyer-Hansen G, Pessara U, Holm U, Pass J, Weidle U, Danø K, Behrendt N, *Biochem J* 358, 2001, 673–679.
- [38] Gårdsvoll H, Ploug M, “Mapping of the Vitronectin-binding Site on the Urokinase Receptor” *Journal of Biological Chemistry* 282(2007), 13561–13572.[39] Fazioli F, Resnati M, Sidenius N, Higashimoto Y, Appella E, Blasi F, “A urokinase-sensitive region of the human urokinase receptor is responsible for its chemotactic activity” *EMBO J* , 1997, 16, 7279–7286.
- [40] Xu X, Gårdsvoll H, Yuan C, Lin L, Ploug M, Huang M, “Crystal structure of the urokinase receptor in a ligand-free form” *J. Mol. Biol.*, 416: 629-41, 2012.
- [41] Barinka C, Parry G, Callahan J, Shaw D.E, Kuo A, Bdeir K, Cines D. B, Mazar, Lubkowski J, “Structural Basis of interaction between uPA and its receptor” *J Mol Biol.* 2006 October 20; 363(2): 482–495.

- [42] Ossowski L, Aguirre-Ghiso JA, "Urokinase receptor and integrin partnership: coordination of signaling for cell adhesion, migration and growth" *Curr Opin Cell Biol* 2000; 12: 613–20.
- [43] Carriero MV, Longanesi-Cattani I, Bifulco K "Structure-based design of an urokinase-type plasminogen activator receptor-derived peptide inhibiting cell migration and lung metastasis" *Mol Cancer Ther* 2009, 8, 2708-2717.
- [44] Bifulco K, Longanesi-Cattani I, Franco P, Pavone V, Mugione P, Di Carluccio G, Masucci MT, Arra C, Pirozzi G, Stoppelli MP, Carriero MV, "Single amino Acid substitutions in the chemotactic sequence of urokinase receptor modulate cell migration and invasion". *PLoSOne*, 7(9):e44806, 2012.
- [45] Engstrom, L. (1978) *Regul. Mech. Carbohydr. Metab.: Proc. FEBS Meet.* 42, 53-60
- [46] Cohen, P. (1982) *Nature (London)* 296, 613-620.
- [47] Krebs, E. G. & Beavo, J. A. (1979) *Annu. Rev. Biochem.* 48, 923-959.
- [48] Zetterqvist O, Ragnarsson U, (1982) *FEBS Lett.* 139, 287-290.
- [49] Springs B, Haake P, (1977) *Tetrahedron Lett.* 3223-3226.
- [50] Williams RJP, (1979) *Biol. Rev. Cambridge Philos.Soc.* 54, 389-437.
- [51] Grieco P, "D-Amino Acid Scan of γ -Melanocyte-Stimulating Hormone: Importance of Trp8 on Human MC3 Receptor Selectivity" *J. Med. Chem.* 2000, 43, 4998-5002.
- [52] VanderMolen KM, McCulloch W, Pearce CJ, Oberlies NH, "Romidepsin: a natural product recently approved for cutaneous T-cell lymphoma" *J Antibiot* 2011, 64, 525-531.
- [53] Dell'Aversana C, Lepore I, Altucci L, "HDAC modulation and cell death in the clinic" *Experimental Cell Research*, 2012, 11, 1229-44.
- [54] White CJ, Yudin AK, "Contemporary strategies for peptide macrocyclization" *Nature chemistry*, 2011, 3, 509-24.
- [55] Franco P, Vocca I, Carriero MV, Alfano D, Cito L, Longanesi-Cattani I, Grieco P, Ossowski L, Stoppelli MP, "Activation of urokinase receptor by a novel interaction between the connecting peptide region of urokinase and $\alpha\beta$ 5 integrin" *Journal of Cell Science*, 119: 3424-3434, 2006.
- [56] Bifulco K, Longanesi-Cattani I, Masucci MT, De Chiara A, Fazioli F, Di Carluccio G, Pirozzi G, Gallo M, La Rocca A, Apice G, Rocco G, Carriero MV, "Involvement of the soluble urokinase receptor in chondrosarcoma cell mobilization" *Sarcoma*, 2011:842842,2011.

- [57] Carriero MV, Longanesi-Cattani I, Bifulco K, Maglio O, Lista L, Barbieri A, Votta G, Masucci MT, Arra C, Franco R, De Rosa M, Stoppelli MP, Pavone V. "Structure-based design of an urokinase-type plasminogen activator receptor-derived peptide inhibiting cell migration and lung metastasis". *Mol. Cancer Ther.*, 9, 2708-17, 2009.
- [58] Bifulco K, Longanesi-Cattani I, Liguori E, Arra C, Rea D, Masucci MT, De Rosa M, Pavone V, Stoppelli MP, Carriero MV, "An urokinase receptor-derived peptide inhibiting VEGF-dependent directional migration and vascular sprouting", *Mol. Cancer Ther.* 12(10):1981-93, 2013.
- [59] Tsubota Y, Frey JM, Tai PW, Welikson RE, Raines EW, "Monocyte ADAM17 promotes diapedesis during transendothelial migration: identification of steps and substrates targeted by metalloproteinases" *J Immunol*, (2013), 190:4236-44.
- [60] Blasi F, "uPA, uPAR, PAI-1: key intersection of proteolytic, adhesive and chemotactic highways" *Immunology Today* (1997): 18: 415-17.
- [61] Carriero MV, Longanesi-Cattani I, Bifulco K, Maglio O, Lista L, Barbieri A, Votta G, Masucci MT, Arra C, Franco R, De Rosa M, Stoppelli MP, Pavone V (2009) Structure-based design of an urokinase-type plasminogen activator receptor-derived peptide inhibiting cell migration and lung metastasis. *Mol Cancer Ther* 8:2708-17.
- [62] Bifulco K, Longanesi-Cattani I, Gala M, Di Carluccio G, Masucci MT, Pavone V, Lista L, Arra C, Stoppelli MP, Carriero MV "The soluble form of urokinase receptor promotes angiogenesis through its Ser⁸⁸-Arg-Ser-Arg-Tyr⁹² chemotactic sequence" *J Thromb Haemost*(2010): 8:2789-99.
- [63] Montuori N, Bifulco K, Carriero MV, La Penna C, Visconte V, Alfano D, Pesapane A, Rossi FW, Salzano S, Rossi G, Ragno P (2011) The cross-talk between the urokinase receptor and fMLP receptors regulates the activity of the CXCR4 chemokine receptor. *Cell Mol Life Sci* 68:2453-67.
- [64] Garrido-Hernandez H, Moon KD, Geahlen RL, Borch RF, "Design and Synthesis of Phosphotyrosine Peptidomimetic Prodrugs" *J. Med. Chem.* 2006, 49, 3368-3376.

UNIT 2

SYNTHESIS OF NEW UROTENSIN-II ANALOGUES

1. INTRODUCTION

1.1. Urotensin-II

Urotensin II (U-II), has been described as the most potent vasoconstrictor documented, with an EC_{50} value of less than 1nM, ten times more potent than endothelin-1 [1]. U-II has been recognized as teleost hormone provided with smooth muscle contracting activity and significant biological actions in mammals and in humans. U-II is primarily involved in the cardio-renal system where evidences indicates that blood pressure might be regulated by direct effects on heart, kidney, and peripheral vasculature and by indirect central mechanisms and secondary endocrine actions (Figure 1) [2]. Patients with Heart failure, congestive heart failure, carotid atherosclerosis, renal failure, renal dysfunction, portal hypertension-cirrhosis, diabetes mellitus, and essential hypertension, have been demonstrated elevated plasma levels of U-II and its receptor. Based on these considerations, U-II, in the last ten years became a major target of medicinal chemistry research.

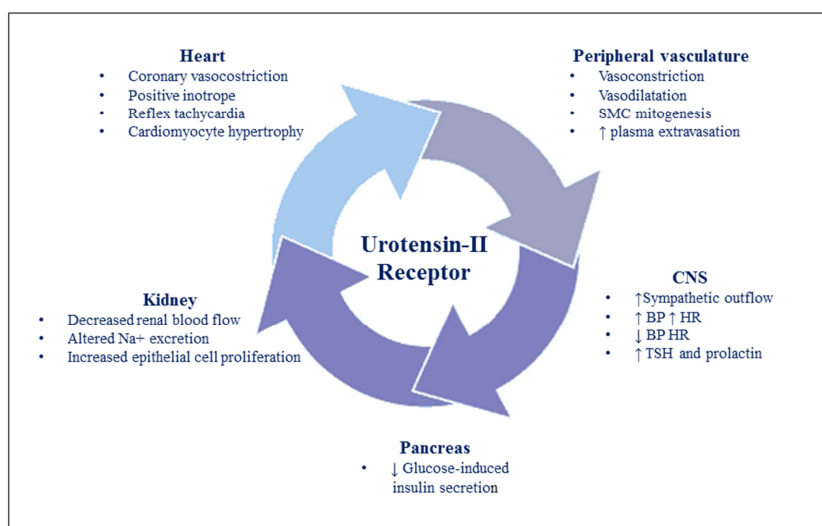


Figure 1. Physiological role of Urotensin-II receptor (UT receptor): UT receptor is expressed in the central nervous system (CNS) as well as other tissues, such as kidney, small intestine, prostate, pituitary, and adrenal gland and circulates in human plasma; the presence of UT receptor in the motor neurons in the spinal cord and the brain stem suggests a potential role in CNS; UT receptor can cause the vasoconstriction of coronary, mammary and radial arteries. In the kidney, UT receptor affects sodium transport, lipid and glucose metabolism.

Urotensin-II is a cyclic peptide originally isolated from the urophysis (a neuroendocrine gland placed in the caudal part of the spinal cord) of the teleost fish *Gillichthys mirabilis* [3]. The U-II precursor has been cloned in diverse vertebrate species including carp, flounder, frog, rat, pig, monkey and human [4]. The amino acids sequence of urotensin-II is structurally related to

somatostatin and cortistatin. Cyclic C-terminal hexapeptide sequence, [Cys-Phe-Trp-Lys-Tyr-Cys], is conserved in all U-II isoforms which is chargeable of the biological activity. On the other hand, the N-terminal zone of U-II differs in sequence conditional upon the animals species [5]. An acidic residue (Asp/Glu) on its N-terminal side and a bulky hydrophobic residue (Val/Ile) on its C-terminal side are unchangingly surround the cyclic core of the U-II isoforms (Figure 2). U-II is encoding by the UTS2 gene, mRNA express in brain, heart, aorta, leukocytes, spinal cord, kidney, and other tissues, with the high frequency in the ventral horn of spinal cord. The human isoform of urotensin-II (*hU-II*), a cyclic undecapeptide, H-Glu-Thr-Pro-Asp-[Cys-Phe-Trp-Lys-Tyr-Cys]-Val-OH, the amino acid sequence of U-II is similar with somatotstatin, is potent mammalian vasoconstrictor. U-II is highly engaged in the development of diseases, therefore, the antagonism effect of U-II to treat cardiovascular diseases has disclosed progressions in hemodynamics and cardiovascular remodeling [6]. In 1998 Coulouarn et al. has demonstrated the expression of U-II in the brain of amphibians and mammals [7] and in 1999 Ames et al., using a reverse molecular pharmacology approach, recognized that U-II is the endogenous ligand of a new human GPCR homologous to the GPR14 orphan receptor from rat [1].

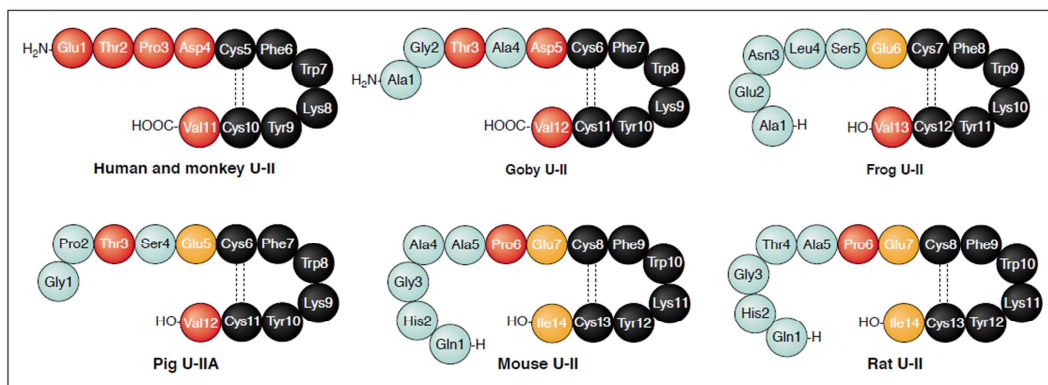


Figure 2. Urotensin-II isoforms. Comparison of Urotensin-II (U-II) isoforms. Amino acids in white circle represent the *core-sequence* conservation among U-II sequences isolated from different species of organisms.

1.2. Human Urotensin-II receptor

The receptor for *hU-II* is the orphan G-protein-coupled receptor 14 (GPR14) (Figure 3) [1]. U-II binds to its receptor in a “pseudo-irreversible” manner, and its extended activation and a functionally silent system due to the sluggish dissociation rate from the urotensin-II receptor

(UT receptor) that mediates complex hemodynamic effects and influences neuromuscular physiology. The structural homology between UT receptor and the somatostatin receptor (sst4) suggest some caution must be taken when we decide to design a UT receptor selective agonist or antagonist [8]. Potent vasoconstrictor effects has been demonstrated in vascular beds of UT receptor high levels and it has also been involved in osmoregulation. The human gene encoding the UT receptor is located on chromosome 17q25.3 [9].

Human urotensin-II receptor is a 389-amino acid polypeptide chain with seven transmembrane domains and its exhibits highly expression levels in the peripheral vasculature, heart and kidney, pancreas, adrenal gland and in the central nervous system (CNS) [10].

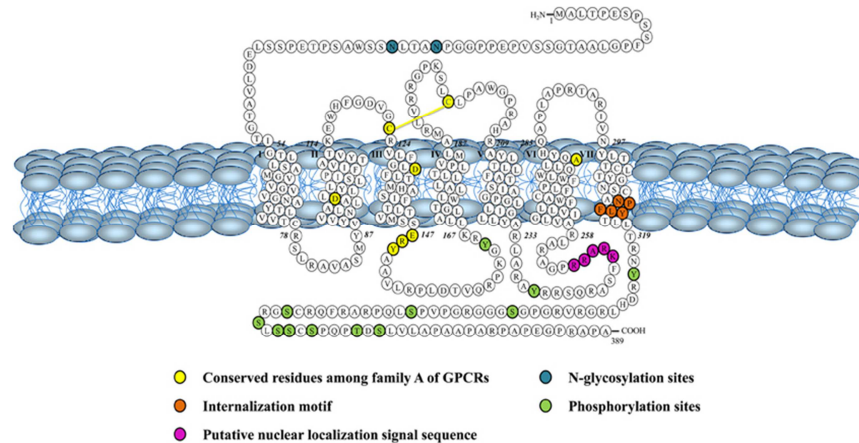


Figure 3. Human urotensin-II receptor. The receptor for *hU-II* is the orphan G-protein-coupled receptor 14 (GPR14).

The signal transduction is carrying out by the activation of the UT receptor coupled protein G_{α} , that leads to an increasing of inositol triphosphate and mobilization of intracellular Ca^{2+} (Figure 4). The mechanism by which *hU-II* evokes contraction of the smooth muscle is complex which includes small GTPase RhoA and its downstream effector Rho-kinase [11], phospholipase C, protein kinase C and tyrosine kinase, PKC-independent phosphorylation of myosin light chain (MLC-2) as well as the Ca^{2+} -calmodulin/MLC kinase system, extracellular signal-regulated kinase (ERK) and p38 mitogen-activated protein kinase. Rho signalling pathway and ERK included also in U-II-induced vascular smooth muscle cell proliferation. The proteolysis of prepro-U-II by specific urotensin-converting enzyme (UCE) at the presumed site, $K^{126}K^{127}R^{128}$, in the splice variant, and $K^{111}K^{112}R^{113}$ in the splice variant b,

brought out the U-II. The biological activity due to enzymatic cleavage. UCE has not been identified, but the proteolytic cleavage can fulfil led by several enzymes. In 2004 Russell et al., has studied the conversion of a 25-amino acid C-terminal fragment of prepro-U-II to mature U-II, documenting that furin, an endoprotease, expressed in the transGolgi network cells, may function as an intracellular UCE. The same authors also showed that trypsin, a serine protease, may act on prepro-U-II in the circulation [12, 13].

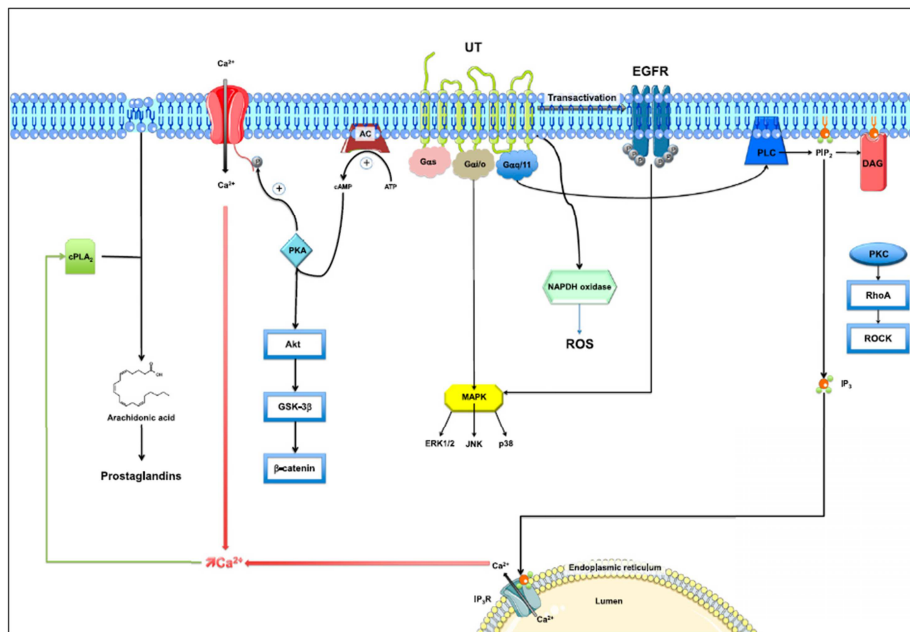


Figure 4. Urotensin-II receptor pathways. Vasoconstriction, vasodilatation, cell proliferation and hypertrophy caused by the binding of U-II to a G-protein-coupled UT, leading to hydrolysis of phosphatidylinositol 3,4,5-trisphosphate (PIP₂) to inositol 3,4,5-trisphosphate (IP₃) and diacylglycerol (DAG) by phospholipase C (PLC). IP₃ increases the release of Ca²⁺ from the sarcoplasmic reticulum or endoplasmic reticulum [14].

Recently, U-II/UT receptor pathway may represent a novel target in erectile dysfunction, we have demonstrated the involvement of U-II/UT receptor pathway in erectile function for the endogenous synthesis and local releasing of U-II in the human corpus cavernosum [15]. The human receptor of urotensin was always expressed at low intensity in hyperplastic tissues and at high intensity in well-differentiated carcinomas. Recently, we also have evaluated the biological role of UT receptor in prostate adenocarcinoma by the effects of an antagonist of UT receptor, urantide, on migration and invasion of LNCaP cells [16, 17]

The patho-physiological crucial role played by urotensin-II receptor made it a prey for discovering new ligands, peptide (Table 1), and nonpeptide analogues [18]. In order to

investigate new structure-activity relationship studies, I developed new Urotensin-II peptide analogues with with different backbone geometry, side-chain orientation and side chain functionalization as reported in the present unit of this dissertation.

Table 1. Urotensin-II peptide analogues:

Name	Sequence
PRL-2903	H-Fpa-[Cys-Pal-DTrp-Lys-Tle-Cys]-(2')Nal-NH ₂
SB-710411	H-Cpa-[DCys-Pal-DTrp-Lys-Val-Cys]-Cpa-NH ₂
BIM-23127	H-D(2')Nal-[Cys-Tyr-DTrp-Orn-Val-Cys]-(2')Nal-NH ₂
BIM-23042	H-D(2')Nal-[Cys-Tyr-DTrp-Lys-Val-Cys]-(2')Nal-NH ₂
[Orn ⁸]U-II	H-Glu-Thr-Pro-Asp-[Cys-Phe-Trp-Orn-Tyr-Cys]-Val-OH
P5U	H-Asp-[Pen-Phe-Trp-Orn-Tyr-Cys]-Val-OH
Urantide	H-Asp-[Pen-Phe-DTrp-Orn-Tyr-Cys]-Val-OH
UFP-803	H-Asp-[Pen-Phe-DTrp-Dab-Tyr-Cys]-Val-OH
URP	H-Ala-[Cys-Phe-Trp-Lys-Tys-Cys]-Val-OH
Urocontrin	H-Ala-[Cys-Phe-Bip-Lys-Tys-Cys]-Val-OH
GSK248451	H-Cin-[DCys-Pal-DTrp-Orn-Val-Cys]-His-NH ₂

2. STRUCTURE-ACTIVITY RELATIONSHIP STUDIES

Urotensin-II has a wide range of biological activities and a potential therapeutic use. The human urotensin-II (*hU-II*) is a cyclic undecapeptide, H-Glu-Thr-Pro-Asp-[Cys-Phe-Trp-Lys-Tyr-Cys]-Val-OH, recognized as the natural ligand of an orphan G-protein coupled receptor. The role played by the exocyclic region in the receptor interaction has been investigated by a series of truncated peptides related to *hU-II*. The discovery of the minimal active fragment of human urotensin-II (*hUII*₍₄₋₁₁₎), H-Asp-[Cys-Phe-Trp-Lys-Tyr-Cys]Val-OH confirm the exocyclic region is not significant for the binding (Figure 5) [19]. *U-II*₍₄₋₁₁₎ preserves high affinity and potency for the human receptor of urotensin-II, showing also similarity to somatostatin-14 in which truncation of the segment led to active analogues. The structural homology between UT receptor and the somatostatin receptor (*sst4*) suggest some caution must be taken when we decide to design a UT receptor selective agonist or antagonist. As shown in Figure 6, the similarity between *hU-II* and somatostatin consisting in *core-sequence*, Lys-Trp-Phe, which plays a crucial role in the binding of UT receptor [1]. Indeed, PRL-2903 (Table 1), H-4Fpa-[Cys-Pal-DTrp-Lys-Tle-Cys]-Nal-NH₂ represent a somatostatin analogues, resulted in the ability to block the *hU-II*-induced rat aorta ring tone at micromolar concentrations, although it showed low species selectivity [18]. Another peptide somatostatin analogue, named SB-710411 (Table 1), H-Cpa-[DCys-Pal-DTrp-Lys-Val-Cys]-Cpa-NH₂, described by Coy et al. in 2000, showed moderate affinity for UT receptor which was also able to inhibit *U-II*-induced contraction in rat isolated thoracic aorta in a surmountable manner (*pK_b*= 6.28) [20]. As cyclosomatostatin octapeptide analogue that shares structural similarities with SB-710411, the peptide neuromedin B receptor antagonist BIM-23127, H-D(2')Nal-[Cys-Tyr-DTrp-Orn-Val-Cys]-(2')Nal-NH₂ (Table1) [21], was investigated by functional activity at recombinant and native UT receptors [22].

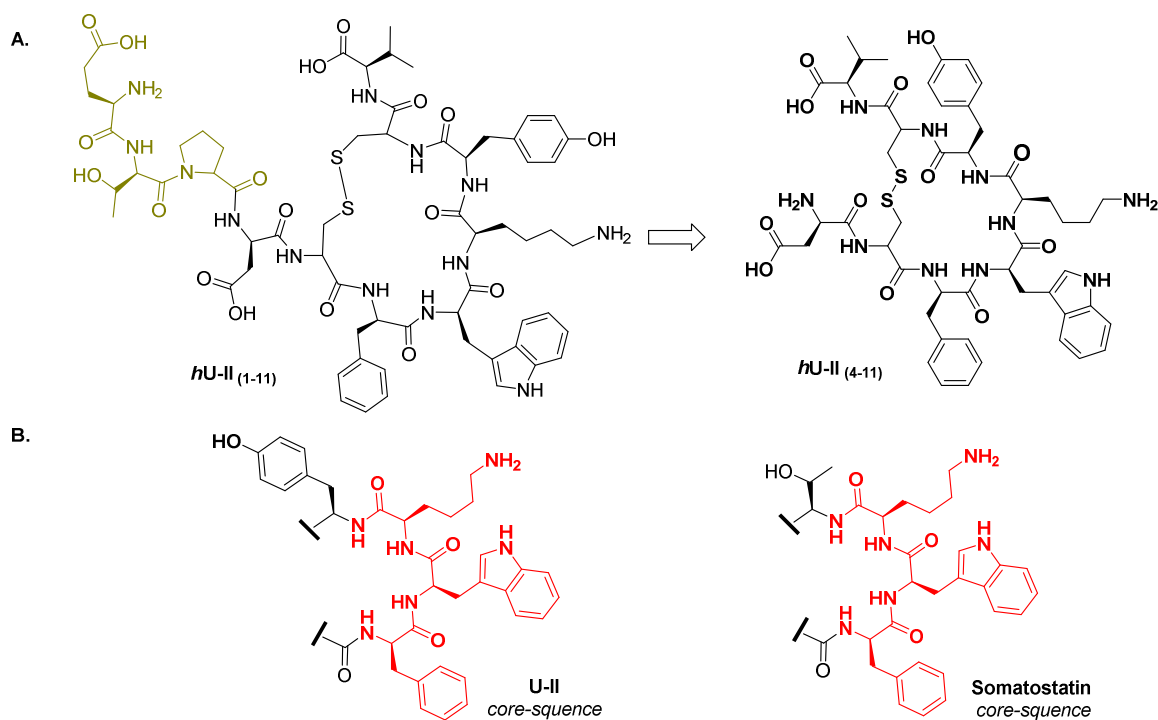


Figure 5. (A) Structures of human urotensin-II (1-11) and U-II(4-11). In green we have the exocyclic region without significant role in the activity of urotensin-II. (B) Structure similarity between urotensin-II and somatostatin. The part in red represent the core-sequence similarity between U-II and somatostatin.

In 2003 a report from Sugo *et al.* shown the existence of a paralogue of U-II named Urotensin-II Related Peptide (URP), H-Ala-[Cys-Phe-Trp-Lys-Tyr-Cys]-Val-OH (Figure 6), a novel peptide first isolated from the extract of rat brain and subsequently observed as the endogenous ligand for the UT receptor in rat, mouse and possibly in human. URP exhibits high binding affinity for UT receptor in transfected cell lines and high contractile potency in the rat aortic ring assay, suggesting that some physiological effects could be not completely attributed to U-II [23]. In 2014 Brancaccio *et al.*, has demonstrated that distinct pathophysiological roles of URP and *hU-II* are not related to different conformations of the two peptides, but they likely arise from their different interactions with the UT receptor (Figure 8). Those interaction can stabilize different active conformations of UT receptor that, in turn, can select specific subset of secondary messengers depending on the ligand-induced adopted conformation [24].

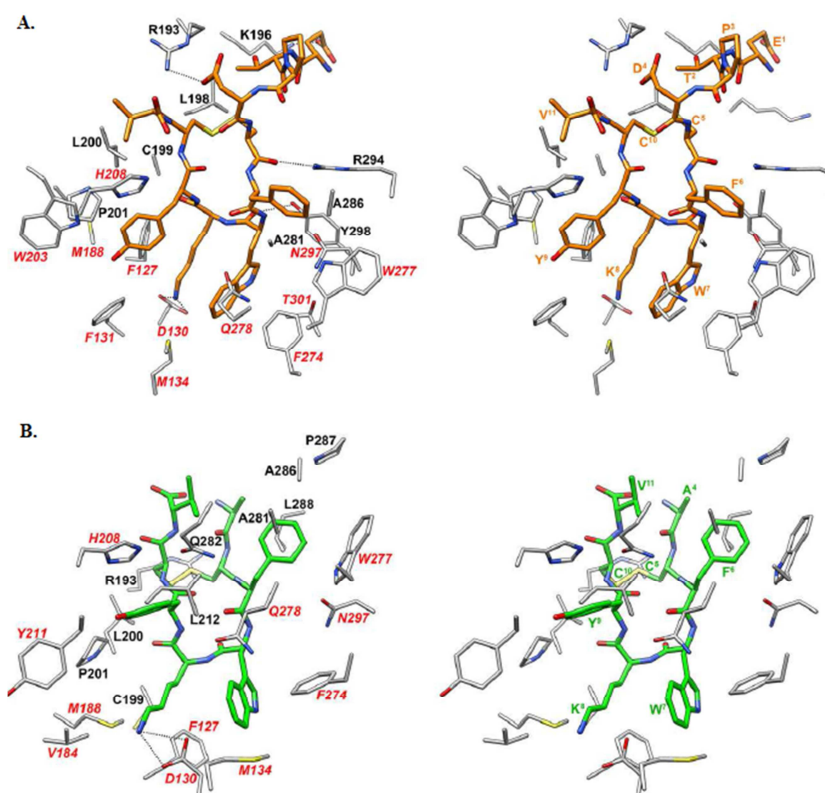


Figure 6. (A) N-terminal region of *hU-II* establish large interactions with extracellular loops EL2 of UTR. (B) Those interaction cannot be present in URP/UTR binding.

The disulphide bond is essential for the activity. Indeed, in 1986 McMaster et al. made evident the crucial role of the cyclic conformation for the interaction with UT receptor by the corresponding “ring-opened” analogue with a lack of biological activity [25]. In 2002 Grieco et al., has demonstrated by the replacement of the disulfide bridge by a chemically more stable lactam bridge, the contractile activity on the rat isolated thoracic aorta was found to be dependent upon the dimension of the ring [26]. $hU-II_{(4-11)}$ was conformationally constrained by replacement of Cys⁵ by penicillamine (β,β -dimethylcysteine), in order to stabilize the putative bioactive conformation. This substitution led to the identification of a UT receptor agonist showing ultrapotent activity in the rat aorta, [Pen⁵] $hU-II_{(4-11)}$, subsequently renamed P5U (Figure 7) [27]. The replacement of Lys⁸ by ornithine in the endocyclic portion of [Pen⁵] $hU-II_{(4-11)}$ provoked a shift from a very efficacious agonist to an antagonist endowed with residual low agonist efficacy: [Pen⁵,Orn⁸] $hU-II_{(4-11)}$ [28]. Finally, the inversion of the configuration of the Trp residue in position 7, was suggested by the presence of the same

modification in both BIM-23127 and SB-710411 (Table 1). This further modification yielded urantide: [Pen⁵, DTrp⁷, Orn⁸]hU-II(4–11) (Figure 7).

Conformational studies on urantide performed in 2005 by Grieco et al. showed that the distance between Trp⁷ and Tyr⁹ side chains was greater than that observed in the peptide agonist P5U because of the inversion of L-Trp⁷ into the corresponding D-isomer in urantide [29].

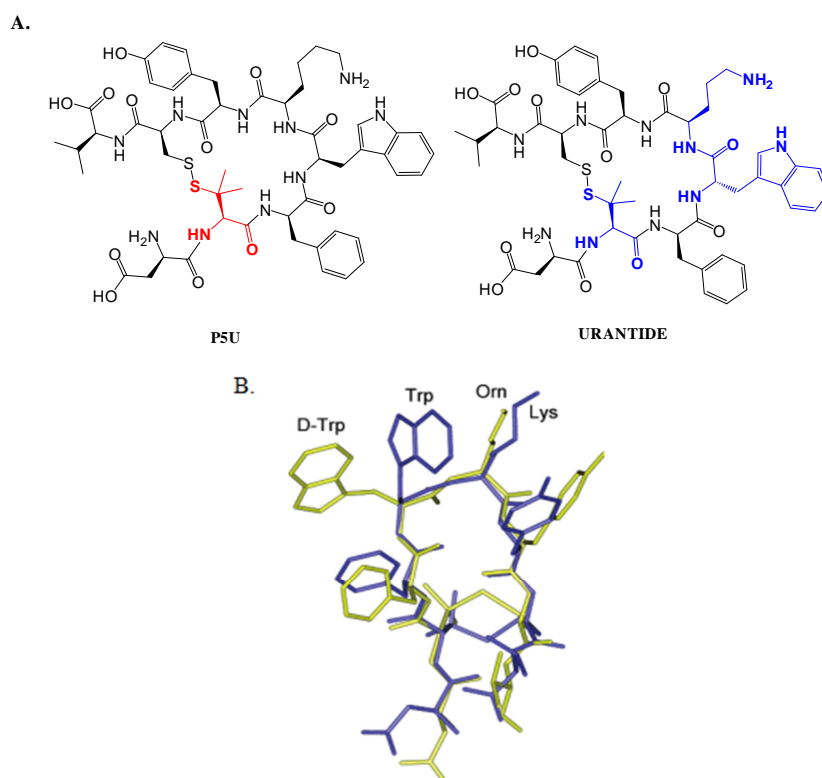


Figure 7. (A) P5U represent the full-agonist and urantide the most potent antagonist to date. The uncoded amino acids which differ from hU-II(4-11) sequence are in red and blue. (B) Representation of overlap 3D structures of P5U (blue) and urantide (yellow).

By Ala-scan studies has demonstrated that the replacement of Trp⁷, Lys⁸, and Tyr⁹ is crucial for the maintenance of biological activity, indicating that the hydrophobic side chains of Trp⁷ and Tyr⁹ and the positive charge of Lys⁸ represent pharmacophoric elements [30].

The *core-sequence* within urotensin-II peptide is essential for binding and activation of the receptor. The hydrophobic side chains of Trp⁷ and Tyr⁹ and the positive charge of Lys⁸ represent key pharmacophoric elements. Herein, we summarized all significant substitutions carried out on the cyclic region or *core-sequence* of urotensin-II [31]:

- ***Phe⁶ residue.*** This moiety is the most tolerant residue within the cyclic region of U-II [32]. Analogues have been designed in which this residue has been replaced by nonpolar aromatic or aliphatic amino acids in U-II₍₄₋₁₁₎. Substitution of the Phe⁶ residue with the isostere (2-thienyl)-alanine (Thi) or (3-benzothienyl)-alanine (BzThi) yields to retain high binding affinity but are 3 and 107 times less potent than U-II(4-11) in the rat aortic ring assay, respectively (Figure 8). On the other hand, replacement of the Phe⁶ residue by 4-tbutyl-Phe reduces by 48-fold the binding affinity but does not modify the contractile activity. High binding affinity of the peptide was verified by the substitution of the Phe⁶ residue of *h*U-II by the sterically bulky 4-benzoyl-L-phenylalanine moiety (Bpa) [33].
- ***Trp⁷ residue.*** Ala-substitution of Trp in position 7 reduces activity of the U-II analogs by approximately 1000-fold, while D-Trp substitution is tolerant for the activity (Figure 8). The role of indole NH was investigated by the replacement of Trp⁷ residue of *h*U-II by a 4-benzoyl-L-phenylalanine moiety yields to [Bpa7]U-II which has less binding affinity and lower potency on inositol phosphate production in UT-transfected COS-7 cells [31], suggesting that indole NH function may establish a hydrogen bond with some UT receptor (Figure 8) [34].
- ***Lys⁸ residue.*** The lysine in position 8 residue appears to be one of the most crucial pharmacophoric points of the core sequence of U-II and URP. The replacement of Lys⁸ with lipophilic residues leads to totally inactive analogs. Hydrophilic but not basic amino acids substitutions leads to loss of the activity, indicating that the basic nature of the lysine side-chain is important for the biological activity. Side-chain basic nature is one of the important parameters, the [Arg⁸]U-II analog is 50-fold less active while the [(*N,N*Me₂)Lys⁸]U-II analog is almost as potent as U-II(Figure 8) Less basic character such as pyridylalanine and 4-aminophenylalanine leads to be inactive. Thus, the primary aliphatic amine at position 8 is a crucial for U-II activity [35]. The distance between the primary aliphatic amine and the peptide backbone is important to generate potent analogues because the distance of 3 and 2 methylene groups gradually reduces the potency and efficacy such as Orn, Dap and Dab (Figure 8).
- ***Tyr⁹ residue.*** The tyrosine in position 9 has a paramount role in the binding of UT receptor (Figure 8). The substitution of Tyr⁹ with Ala or D-Tyr of U-II and URP

observed inactive analogues. Methoxy (-OMe), nitro (-NO₂), amino (-NH₂), methyl (-CH₃), fluoro (-F), or by a hydrogen atom does not affect the potency and the efficacy of the U-II analogs in the rat aorta bioassay [36]. The mono-iodinated analogue [3-iodo-Tyr⁶]U-II₍₄₋₁₁₎ was found to be five times more potent than the parent peptide in producing rat aortic ring contraction [31]. The [3-nitro-Tyr⁹]U-II₍₄₋₁₁₎ analogue shows a moderate decrease in binding affinity and in contractile activity. The [4-carboxy-Phe⁹]U-II₍₄₋₁₁₎ analogue, in which the hydroxyl group of the tyrosine moiety is replaced by a carboxyl radical, exhibits a significant reduction of both affinity and potency, whereas the amino counterpart, the [4-amino-Phe⁹]U-II₍₄₋₁₁₎ analog, retains affinity but shows a marked decrease in contractile activity [36]. Recently we have optimized P5U and urantide, two important ligands at UT receptor, designing several analogues by the exchange of the Tyr⁹ residue with different unnatural aromatic amino acids. This study allowed us to discover novel ligands with improved activity. In particular, the replacement of the Tyr⁹ residue by (pCN)Phe or (pNO₂)Phe within the urantide sequence led to pure antagonist activity toward UT receptor in a rat aorta bioassay. More interestingly, the replacement of the Tyr⁹ with the Btz or the (3,4-Cl)Phe residues (Figure 8) led to superagonists with pEC₅₀ values at least 1.4log higher than that of 1, being the most potent UT receptor agonists discovered to date. These ligands represent new useful tools to further characterize the urotensinergic system in human physiopathology [37].

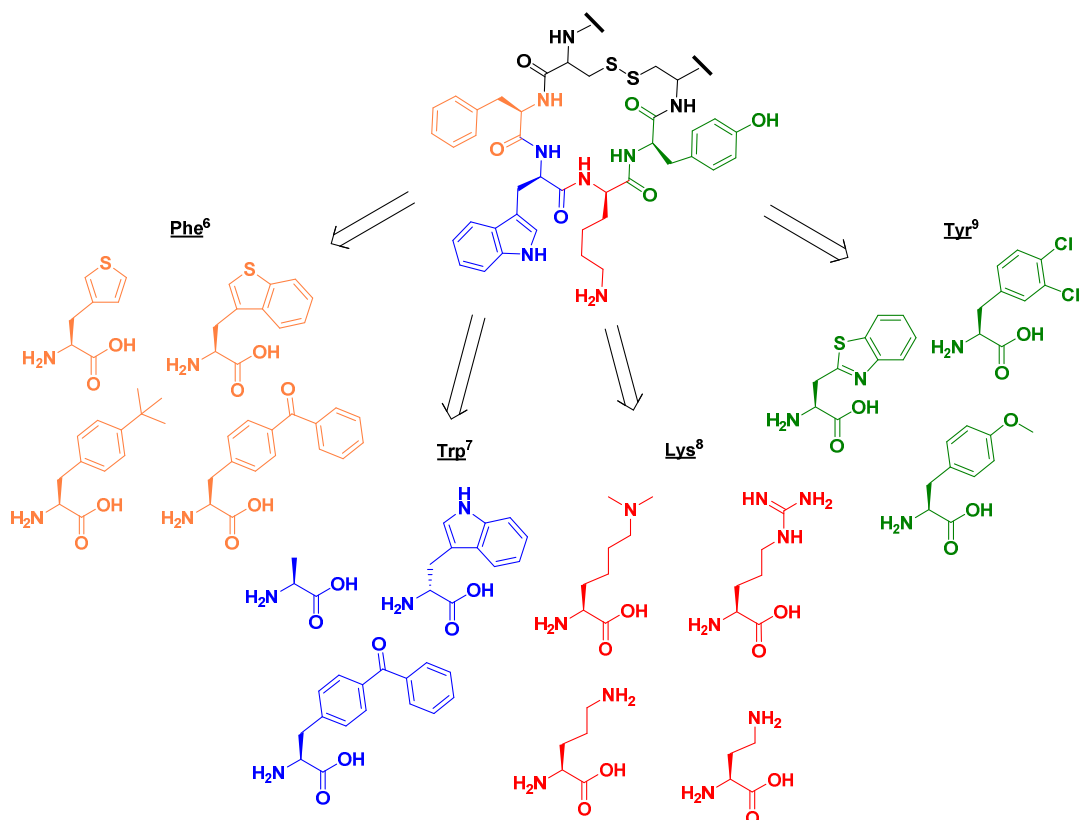
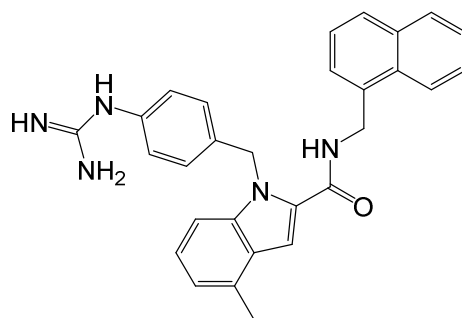


Figure 8. Substitutions of Urotensin-II *core-sequence* amino acid residues. Phe⁶ substitutions (Orange), Trp⁷ (Blue), Lys⁸ (Red) and Tyr⁹ (Green).

By high-throughput screening (HTS) studies from 500 compounds has been identified S7616 with an IC₅₀ of 400nM (Figure 9). The phenyl ring of the indole and the naphthalenemethylamine side chain are localized onto the two aromatic features of the pharmacophore. The basic benzamidine group in S6716 was shown to form a charged interaction with Asp130 residue within TM3 of UT receptor.



S7616

Figure 9. Structure of S7616

The identification of nonpeptide agonists and antagonists of *hU-II* is of great importance for the development of novel therapeutic strategies for cardiovascular pathologies. The first nonpeptide agonist named AC-7954 with a pEC₅₀ of 6.5 (Figure 10) was identified by Croston et al.[38]. Following classical optimization with modulation of the hydrophobic properties of the initial ligand, Lehmann et al. [39] identified the compound 2 named FL68 (Figure 11). The introduction of substituents into either of the two aromatic functions is tolerated, but substitution at the 4-position was detrimental to affinity.

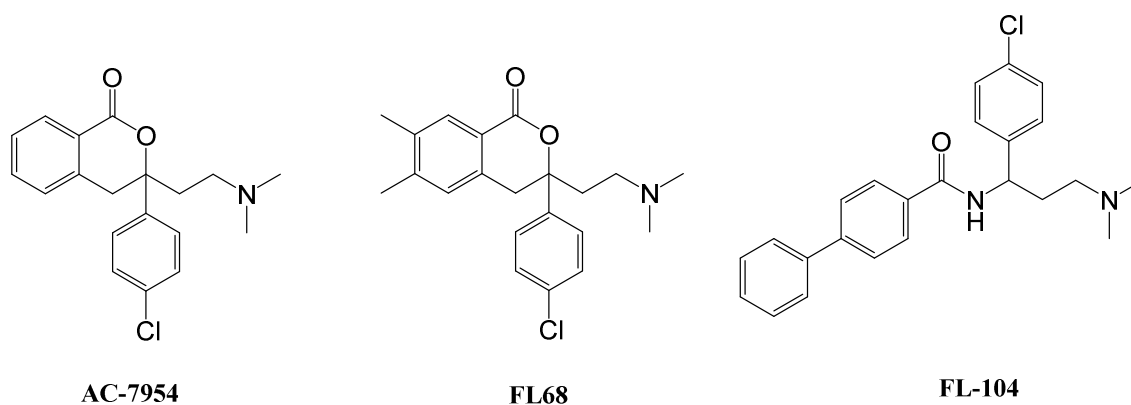


Figure 10. The most active *hU-II* nonpeptide agonists developed by Acadia Pharmaceuticals.

Molecular similarity based on structures AC-7954, FL68 and FL-104 led to the discovery of compounds 1, 2 and 3 (Figure 11). These three compounds have agonist activity toward the UT receptor of 4.0, 6.3 and 5.0 mM, respectively, as shown by a mammalian cell-based R-SAT assay [40]. Indeed, these structures have a clear relationship compared to the previous one, with two aromatic groups and a tertiary amine bound by an alkyl group to the heterocyclic ring.

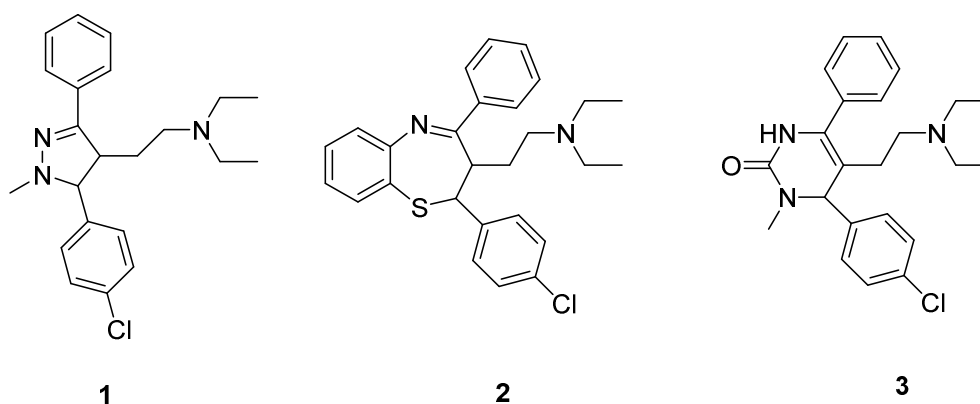
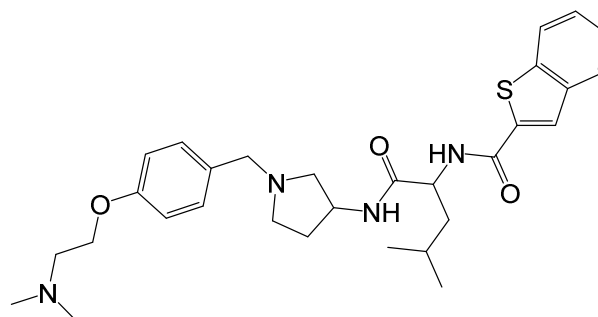
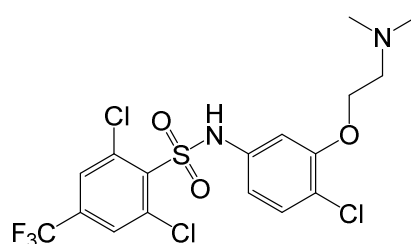


Figure 11. Structures of compound 1, 2 and 3.

The first series of nonpeptide antagonists corresponds to aminoalkoxybenzyl pyrrolidine derivatives that were identified by the GlaxoSmithKline Company. SB328872 represent the most potent compound of this series, showing a good binding affinity to UT receptor (Figure 13). Subsequent optimization of these hits led to the identification of SB-611812, which is as a potential therapeutic for heart failure (Figure 12) [41].



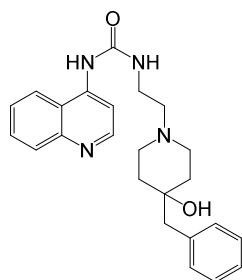
SB328872



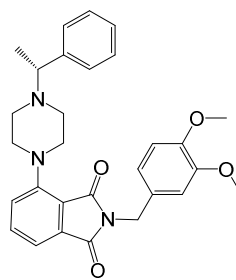
SB-611812

Figure 12. Structure of compounds SB328872 and SB611812.

The preparation of NH-substituted quinolones as *hU*-II antagonists. In 2004, Actelion described the discovery and characterization of urea derivative ACT-058362 (Palosuran) (Figure 13) with pIC_{50} values of 7.2 and 7.1, respectively (binding of [125 I]U-II to TE-671 cells and to recombinant CHO cells). Lawson and coworkers in 2009 [42] realized these novel series starting from the identification of the compound 5, also known as JNJ-28318706.



ACT-058362



JNJ-28318706

Figure 13. JNJ-28318706 with piperazine moiety has potent activity on UT receptor. ACT-058362 (known also as Palosuran) is a potent and specific antagonist of UT receptor with the quinoline moiety.

Despite all these structure-activity relationship studies carried out by developing small organic molecules of UT receptor in the last decade, urantide, represent the most potent antagonist discovered to date for being 50- to 100-fold more potent than any other compound described thus far in the rat isolated aorta bioassay.

3. *NEW UROTENSIN-II ANALOGUES*

3.1. Peptoids of Urotensin-II

Peptoids, *N*-Substituted glycine oligomers (NSG) are a class of peptidomimetics whose side chains are appended to the nitrogen atom of the peptide backbone, rather than to the α -carbons, otherwise referred to as α -peptoids, are a readily accessible class of synthetic, non-natural peptide mimic of modular design into which a plethora of structural elements can be readily incorporated (Figure 14). Zuckermann et al., in 1992 has reported the first NSG [43]. The higher flexibility of peptoid oligomers due to the flexibility of the main-chain methylene groups and the absence of stabilizing hydrogen bond interactions along the backbone are well-known for their higher flexibility and to be conformationally unstable. The choice of appropriate side-chains represent an important tool to form specific steric or electronic interactions that favour the formation of stable secondary structures like helices [44]. In general, NSG's present a platform for the study of protein interactions beyond those approachable by small molecules defined by Lipinski's rules and α -peptides.

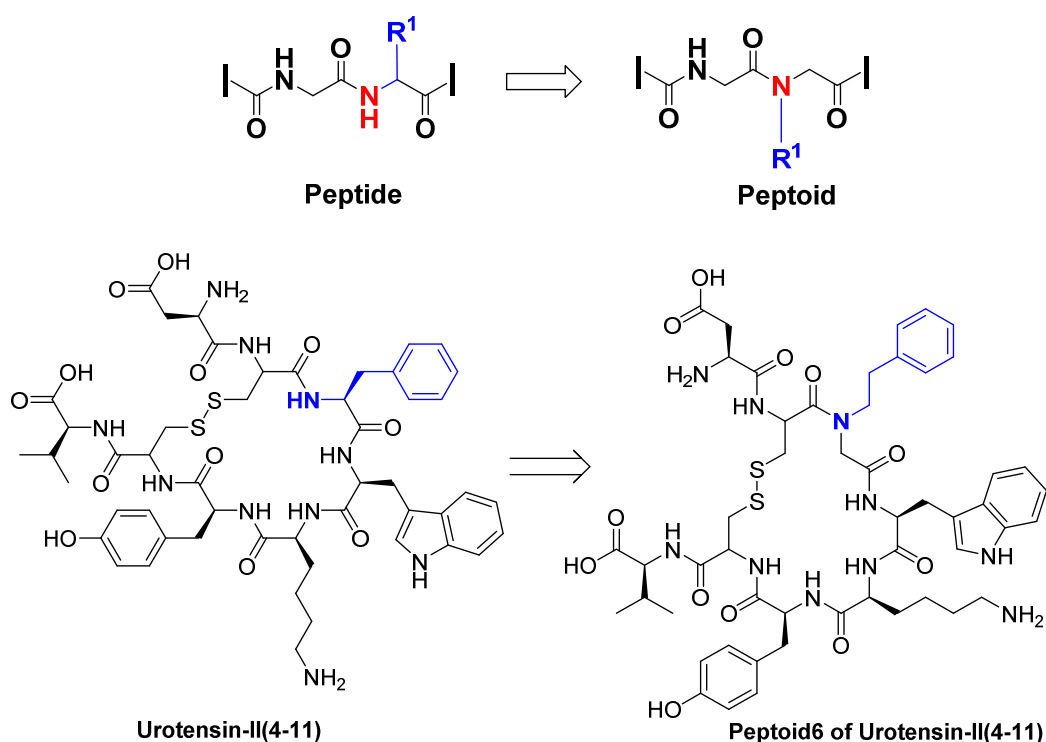


Figure 14. Schematic representation of Peptoids (NSG) and urotensin-II peptoid6 analogue.

The purpose of the present part of this thesis is to investigate urotensin-II structure-activity relationship studies by the development of U-II peptoid analogues. Based on the crucial role of the cyclic region of urotensin-II, [Cys-Phe-Trp-Lys-Tyr-Cys] (see paragraph 2), in the binding of UT receptor, we developed peptoid analogues (Table 4) of the cyclic region by shifting the side-chain of each amino acid from α -carbon to nitrogen.

Table 5. Urotensin-II peptoid analogues:

Peptoid	Sequence
Peptoid5	H-Asp[N-mercaptoethylGly-Phe-Trp-Lys-Tyr-Cys]Val-OH
Peptoid6	H-Asp[Cys-N-EthylphenylGly-Trp-Lys-Tyr-Cys]Val-OH
Peptoid7	H-Asp[Cys-Phe-N-EthylindoleGly-Lys-Tyr-Cys]Val-OH
Peptoid8	H-Asp[Cys-Phe-Trp-N-(5-aminopentyl)Gly-Tyr-Cys]Val-OH
Peptoid9	H-Asp[Cys-Phe-Trp-Lys-N-(4-hydroxyphenylethyl)Gly-Cys]Val-OH
Peptoid10	H-Asp[Cys-Phe-Trp-Lys-Tyr-N-mercaptoethylGly]Val-OH

3.2. Azasulfurylpeptides analogues of Urotensin-II

Peptide bonds can be broken by hydrolysis. Proteolytic enzymes mediate many key biological events by hydrolyzing specific peptide bonds. The tetrahedral transition states found in enzyme-catalyzed amide bond hydrolysis became a pride of many enzyme inhibitors by the replacement of amide bond with its isosteres, for example, the replacement of the amide carbonyl by a tetrahedral phosphorus atom using α -aminophosphonamides and α -aminophosphonamidates has provided inhibitors of human cyclophilin, HIV-1 proteinase, human neutrophil collagenase, enkephalinase and angiotensin-converting enzyme [45]. On the other hand, the replacement of amide bond by β -aminosulfonamides have been demonstrated to less successful as tetrahedral mimics in enzyme inhibitors due to their rapid decomposition [46].

Azapeptide (semicarbazide moiety) or azasulfurylpeptide (N-Aminosulfamide moiety) have been performed turn conformations and higher stability to enzymatic and chemical degradation, relative to the natural peptide. Azapeptides [47, 48], in which the α -carbon of one or more of the amino acid residues is replaced with a nitrogen atom, exhibit a propensity for

adopting β -turn conformations. In peptide scanning, the applications of aza-amino acid and aza-peptide building blocks have been fruitful, albeit their solution-phase synthesis from hydrazine starting materials may be tedious and may also limit side-chain diversity [49]. Azasulfurylpeptides are peptidomimetics possess an amino acid residue from which the C α H and the carbonyl are respectively replaced by a nitrogen atom and a sulfonyl group represented by N-aminosulfamide peptide1 (Figure 15) [50]. Although few examples of these peptidomimetics have been reported, their potential to mimic the tetrahedral geometry during amide bond hydrolysis was exploited by the insertion of azasulfurylphenylalanine (AsF) into a transition-state mimic, micromolar inhibitor of the human immunodeficiency virus-1 (HIV-1) proteinase, azasulfurylpeptide 2 (Figure 15) [50].

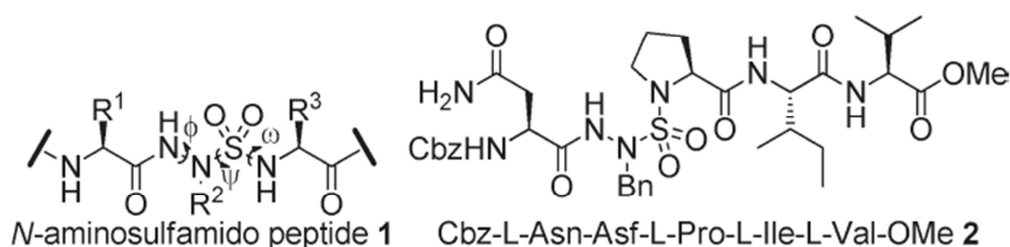


Figure 15. N-aminosulfonamide moiety in peptide structure 1 and Azasulfurylphenylalaninyl peptide 2.

Azasulfurylpeptide analogues combine characteristics of aza- and α -sulfonamido-peptides [46], albeit with firmer and more stable structures, potentially relevant for modification of backbone geometry. The sulfonyl group possesses a tetrahedral sulfur, which adopts ω torsion angle values around $\pm 60^\circ$ and $\pm 100^\circ$ (instead of amide *cis*-(E) and *trans*-(Z) conformations at respectively 0° and $\pm 180^\circ$) separated by a lower S-N rotational barrier ($\Delta G^\ddagger \approx 35$ kJ/mol), relative to the amide C-N ($\Delta G^\ddagger \approx 75$ kJ/mol) (Figure 16) [51]. Furthermore, the S-N bond length is longer than the C-N, due to lack of an amide bond resonance and greater sp^3 versus sp^2 character of the sulfonamide nitrogen (Figure 16). Based on these considerations, in 2012 Turcotte et al., has developed a new method for the synthesis of N-aminosulfamide moiety changing the geometry of the peptide backbone [52].

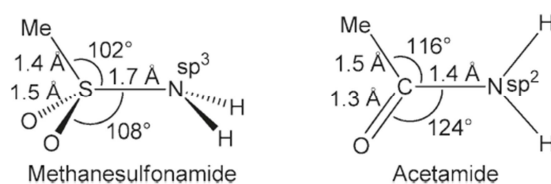


Figure 16. Backbone geometry of N-aminosulfamide moiety.

Basic amino acid residues, such as lysine and arginine, function in numerous biological processes including posttranslational modifications, transport across membranes, and as enzymatic cleavage sites [53]. In 2014 Traoré et al., has developed the synthesis of azapeptides with basic amino acid residues (aza-Lysine, aza-Ornithine, and aza-Arginine) [54]. According to the crucial role of Lys⁸ of the U-II *core-sequence* in the binding to UT receptor, I synthesized azasulfurylpeptide analogues of U-II with basic amino acid as Lys and its derivatives represented by **Azasulfuryl-Lys⁸ U-II** and **Azasulfuryl-*N,N*-Me₂-Lys⁸ U-II**, starting with protected tripeptide building block (Figure 17) to investigate first of all, the role of *N*-aminosulfamide moiety in the biological activity and to provide further structure-activity relationship studies of Lys in position 8 of urotensin-II.

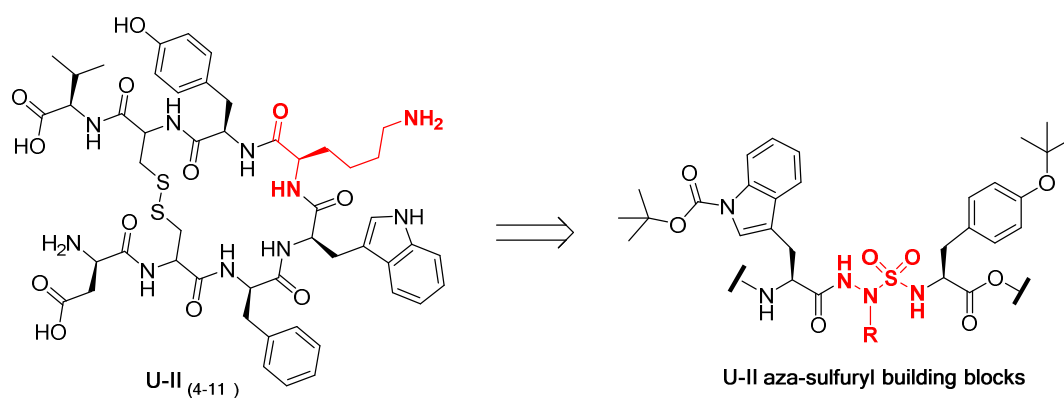


Figure 17. (A) Building blocks of urotensin-II aza-sulfuryl analogues. (B) Library of U-II azasulfuryl analogues: Azasulfuryl-Lys⁸ U-II and Azasulfuryl-*N,N*-Me₂-Lys⁸ U-II.

4. SYNTHETIC STRATEGIES

4.1. Peptoids of U-II analogues synthesis

Peptoids provide major advantages as research and pharmaceutical tools include economy of synthesis, highly variable backbone and side-chain chemistry possibilities. The present thesis provides two approaches for the synthesis of *N*-substituted glycine oligomers (α -peptoids) of urotensin-II.

4.1.1. Peptoids 7 and 9

The invention of the submonomer solid-phase synthesis method for peptoids by Zauckermann was a major breakthrough because it greatly increased the synthetic efficiency, synthesis yields, and available side chain diversity, while also dramatically reducing time and costs [55]. The first series of U-II peptoid analogues (**Peptoid 7 and 9**) were synthesized by solid phase approach (Figure 18).

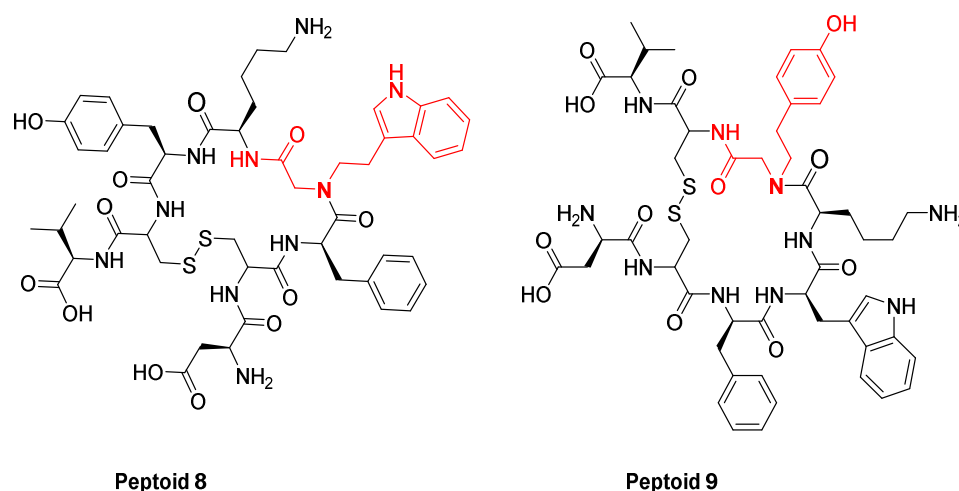
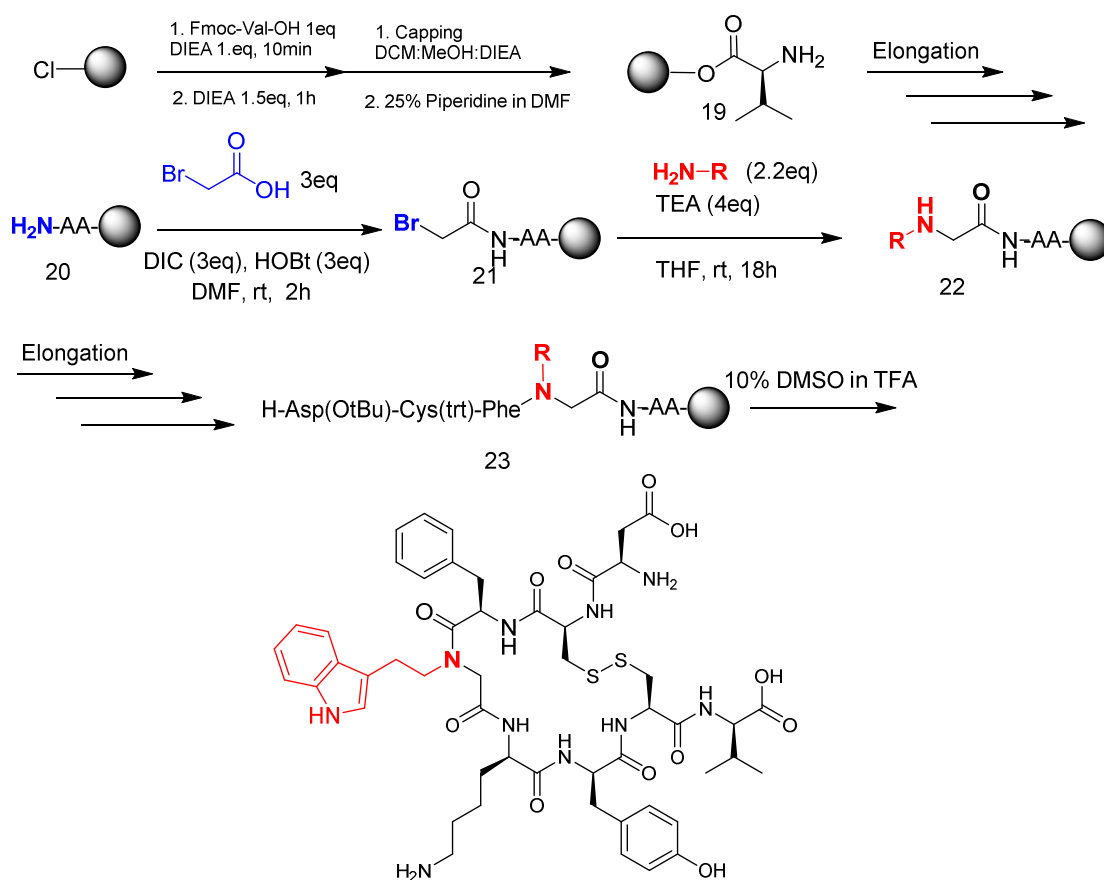


Figure 18. First library of U-II peptoids. Peptoid 8 with side chain of Trp in position 8 and Peptoid 9 with side chain of Tyr in position 9.

As shown in (Scheme 1), the synthesis was carried out in solid phase, using a 2-chlorotrityl Resin (0.312g, 0.8mmol/g), swelled for 30 minutes in dichloromethane (DCM). The first coupling was carried out using 1.0 equivalent of N^{α} -Fmoc-Val-OH, dissolved in 5mL of DCM. The amino acid solution was added to 2-chlorotrityl Resin. To the resulting mixture was added 1.0 equivalent of DIPEA, agitated in the shaker for 10 minutes then 1.5 equivalents of DIPEA were added. The mixture was agitated vigorously for 60 minutes. To endcap any remaining reactive 2-chlorotrityl groups, a

mixture of DCM/MeOH/DIPEA (80:15:5, v/v/v) was added and mixed for 30 minutes. For removing the Fmoc protecting group from the first amino acid, the resin was suspended in 25% solution of piperidine in dimethylformamide (DMF) (1x5 minutes and 1x25 minutes). The following protected amino acids were then added stepwise, N^α-Fmoc-Zaa-OH, (Zaa = Cys(Trt) and Tyr(tBu)). Each coupling reaction was carried out using a 3-fold excess of amino acid with HBTU (3eq) and HOBt (3eq) in the presence of (6eq) of DIPEA. The peptide resin was washed with DCM (3x), DMF (3x) and the deprotection protocol was repeated after each coupling step. The N^α-terminal on the resin is first acylated by a pre-activated bromoacetic acid, with *N,N*-diisopropylcarbodiimide (DIC) and HOBt. Then bromo was displaced by a primary amine, commercially available, by S_N2 reaction, in the presence of triethylamine (TEA) for 18hours at room temperature. After the elongation of the peptide sequence on resin, the N-terminal Fmoc group was removed as described above, using protected amino acids were then added stepwise, N^α-Fmoc-Zaa-OH, (Zaa = Cys(Trt), Trp(Boc), Phe and Asp(OtBu)). The cleavage and cyclization were carried out using the cocktail of TFA:DMSO:TIS (89:10:0.1, v/v/v/) for 3 hours. Crude peptides were recovered by precipitation from the filtrate using chilled ether to give a powder, which was purified by RP-HPLC using a semi-preparative C18-bonded silica column (Phenomenex, Jupiter 4μ Proteo 90Å, 1.0 x 25 cm) with a gradient of MeCN and water containing 0.1% TFA (from 10 to 90% over 40 min) at a flow rate of 5.0 mL/min. The product was obtained by lyophilization of the appropriate fractions after removal of the MeOH by rotary evaporation under reduced pressure. Analytical RP-HPLC indicated >95% purity and the correct molecular ions were confirmed by LC/ESI-MS.



Scheme 1. Solid-Phase Synthesis of Peptides by the Submonomer Strategy.

4.1.2. Peptoids 5, 6, 8 and 10

The synthetic strategy for the development of the second series of U-II peptoid analogues (**Peptoid5, 6, 8 and 9**) (Figure 19) represent a combination of solution and solid phase synthesis, consisting in the synthesis of the side-chains in solution and the alkylation step was carried out on resin.

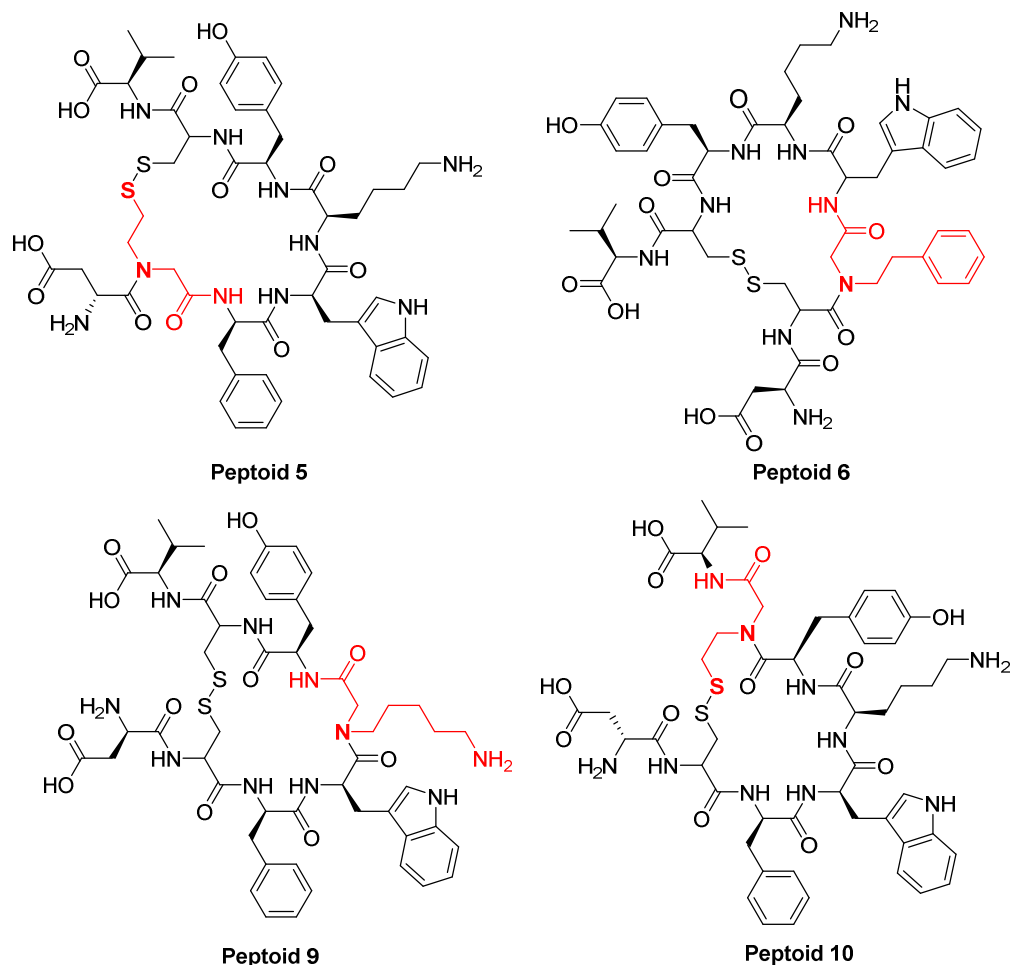
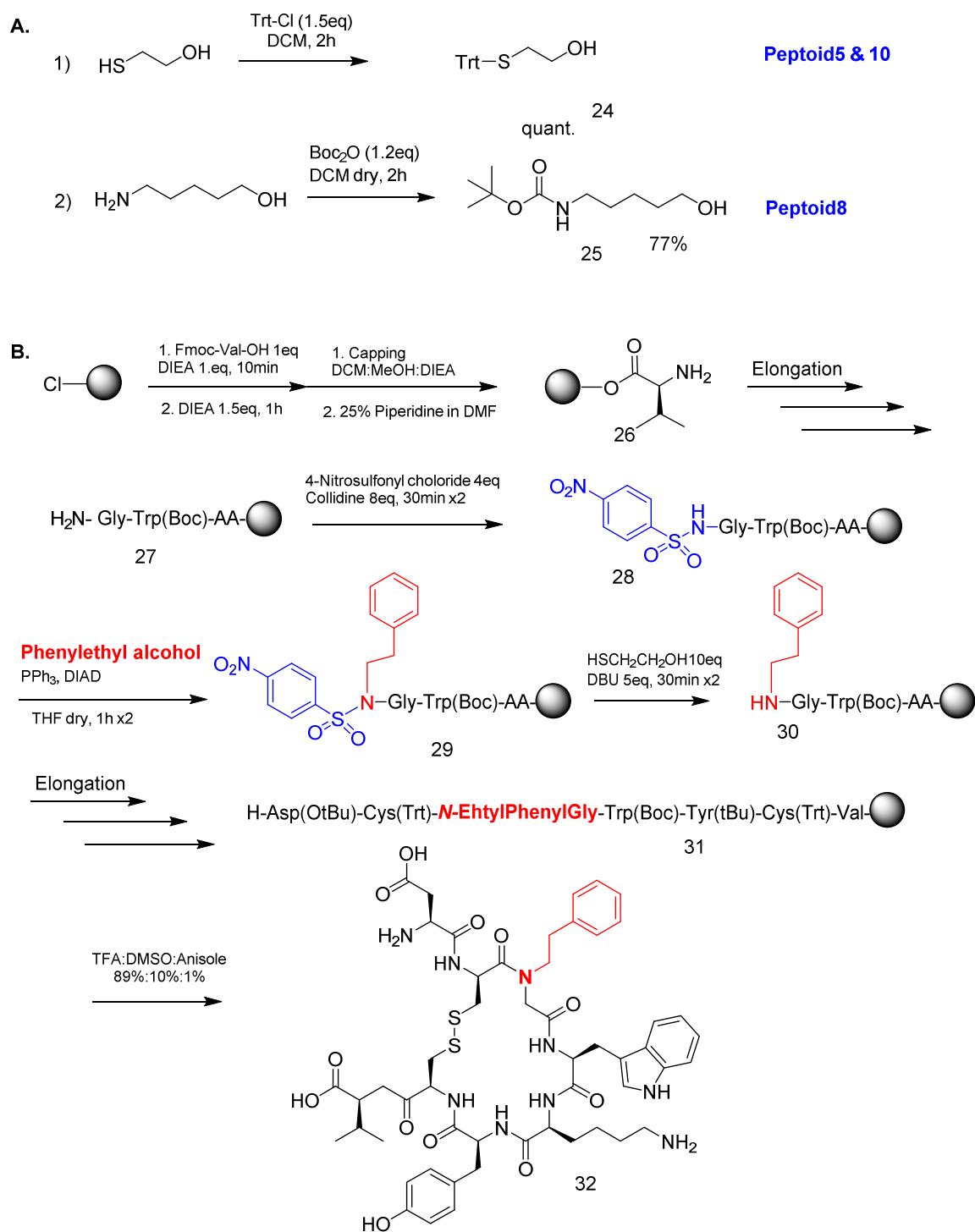


Figure 19. Second library of U-II peptoid. Peptoid 5 and 10 with side chain of Cys in positions 5 and 10, and peptoid 6 with side chain of Phe 6 and Peptoid 8 with side chain of Lys 8.

The side chain of Peptoid5 and 10 represented by Cys⁵ and Cys¹⁰ in original sequence of U-II were synthesized, treating β -mercaptoethanol with trityl chloride in DCM for 2hours. The side-chain of peptoid8, which mime the Lys⁸ residue, was obtained using 5-aminopentenol with di-tert-butyl dicarbonate in dry DCM for 2 hours (Scheme 2). On the other hands, the elongation of the peptide on resin was carried out using fmoc-chemistry approach (see paragraph 4.1.1). The *N*-alkylation step was accomplished using Fukuyama–Mitsunobu approach in solid phase [56]. The alkylation of secondary sulfonamides is achieved alcohols under Mitsunobu conditions, with triphenylphosphine and azo-reagent. After the elongation of the peptide on resin, the free amine was activated using 4-nitrobenzensulfonyl chloride, generating the sulfonamide. The acidity of the latter was employed for the *N*-alkylation step with

alcohol derivative. At this point the 4-nitrophenyl sulfanyl group was released using β -mercaptoethanol and DBU. As shown in Scheme 2, I reported the synthesis of peptoid6 which represent the analogue of Phe⁶ residue in the original sequence of urotensin-II.



Scheme 2. Synthetic strategy of peptoids 5, 6, 8 and 10. (A) Side-chains synthesis in solution of peptoids 5, 8 and 10. (B) Synthesis and alkylation in solid phase.

4.2. Azasulfurylpeptides of U-II synthesis

In 2012 Turcotte et al., has developed a new method for the synthesis of *N*-aminosulfamide peptides featuring the coupling of *p*-nitrophenylsulfamidates and *N*-(Boc)-amino acid hydrazides under microwave irradiation [52]. Chemoselective alkylation of azasulfuryl-glyciny peptides was used to add side-chain diversity and prepare other azasulfuryl amino acid residues. In 2014 Traore' et al, has developed diversity-oriented synthesis of azapeptides with basic amino acid residues [52]. The synthesis of azasulfuryl Lys⁸ peptide analogues of urotensin-II, **azasulfuryl Lys⁸ UII** and **azasulfuryl-*N,N*-Lys⁸ UII** (Figure 20), represent a combination of the two papers mentioned above.

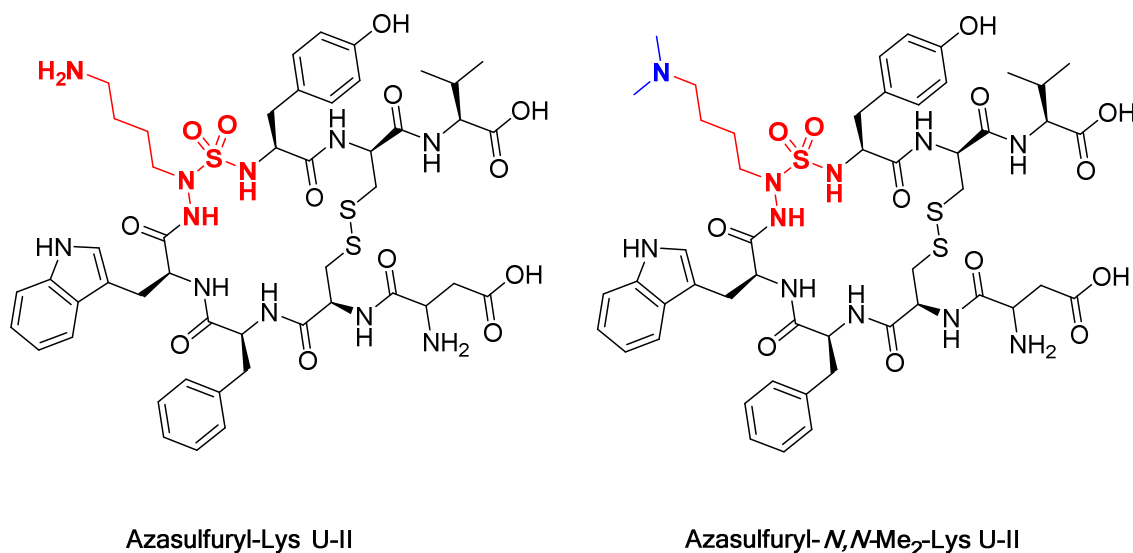


Figure 20. Azasulfurylpeptide analogues of urotensin-II: Azasulfuryl Lys⁸ UII and Azasulfuryl-*N,N*-Me₂-Lys⁸ UII.

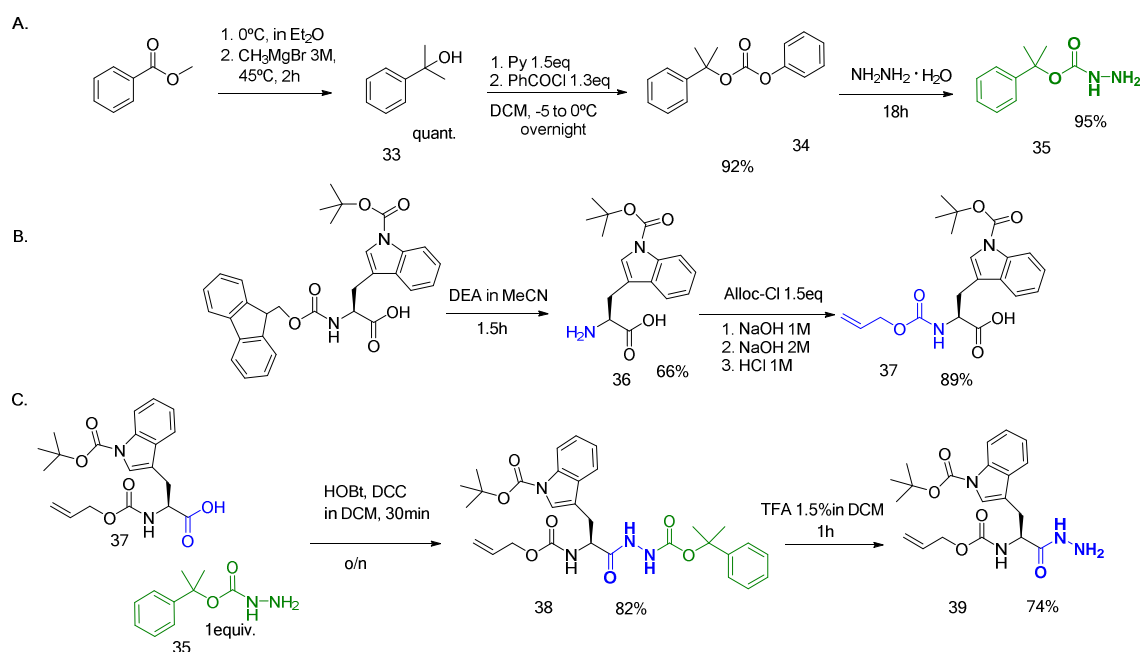
The synthesis of azasulfurylpeptides of U-II consisted of four parts:

4.2.1. Hydrazone of tryptophan synthesis

The hydrazone of tryptophan was critical to prepare for the hard choice of protecting groups. The hydrazone of tryptophan was synthesized using phenyl-isopropoxy carbonyl hydrazine **35** [57, 58]. It can be removed under mildly acidic conditions and with good yields, leaving other side-chains protecting groups intact such as Boc, tBu, and Pbf. The synthesis was carried out starting with methyl benzoate

which treated with methylmagnesium bromide solution (3M in diethyl ether) for generating the 2-phenyl-2-propanol (cumyl alcohol) **33**. The latter has been activated by phenyl chloroformate to give the corresponding phenyl-isopropyl carbonate **34**. At this point, to the resulting carbonate was added hydrazine hydrate (50-60% H₂O) in excess to give the corresponding phenyl-isopropoxyxycarbonyl hydrazine **35** (Scheme 3).

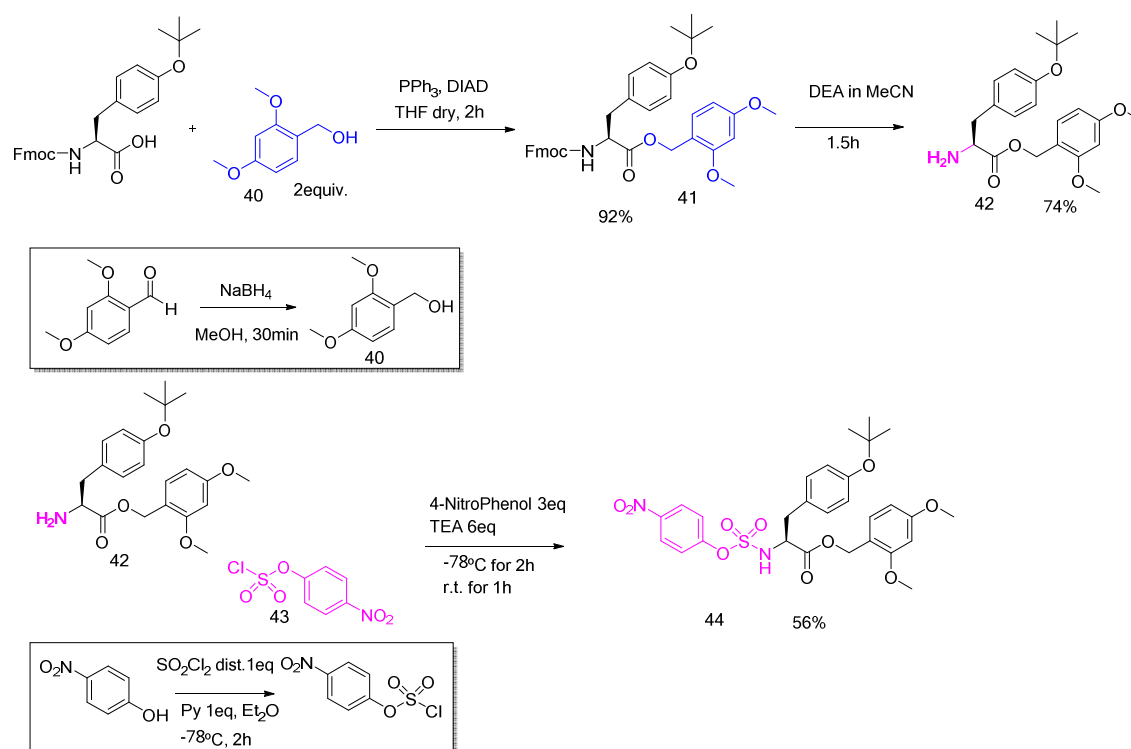
On the other hands, N^α-Fmoc-Trp(Boc)-OH was dissolved in a solution of 20% diethylamine in MeCN for removing the N^α-Fmoc protecting group, the crude was dissolved in MeOH and washed with heptane to extract the fluorenylmethyl-*N,N*-diethylamine. The free amine **36** was protected with Alloc using allyl chloroformate. The coupling step between the hydrazide of cumyl **35** and the pre-activated N^α-Alloc-Trp(Boc)-OH **37** was carried out in DCM overnight. Phenyl-isopropoxyxycarbonyl was removed with a solution of 2% TFA in DCM for 1h, keeping Boc intact (Scheme 3).



Scheme 3. Synthetic strategy of hydrazide of triptophan.

4.2.2. Sulfamate of tyrosine synthesis

The esterification of N^α-Fmoc-Tyr(tBu)-OH with 2,4-dimethoxybenzyl alcohol (previously prepared by treating 2,4-dimethoxybenzyl aldehyde with sodium borohydride in methanol for 30min) employing Mitsunobu reaction in presence of DIAD and PPh₃ for 2 hours. Then the N^α-Fmoc protecting group was removed using diethylamine in MeCN. 4-Nitrophenyl chlorosulfate (prepared according reference [59]) was dissolved in dry DCM and treated drop-wise with a solution of N^α-Tyr(tBu)-Odmcb, 4-Nitrophenol and triethylamine in dry DCM at –78 °C. A 2 equivalents amount of 4-nitrophenol was necessary as an additive to avoid formation of symmetric sulfamide. The sulfamate **45** could be stored for several months without decomposition (Scheme 4).



Scheme 4. Synthesis of the sulfamate of tyrosine.

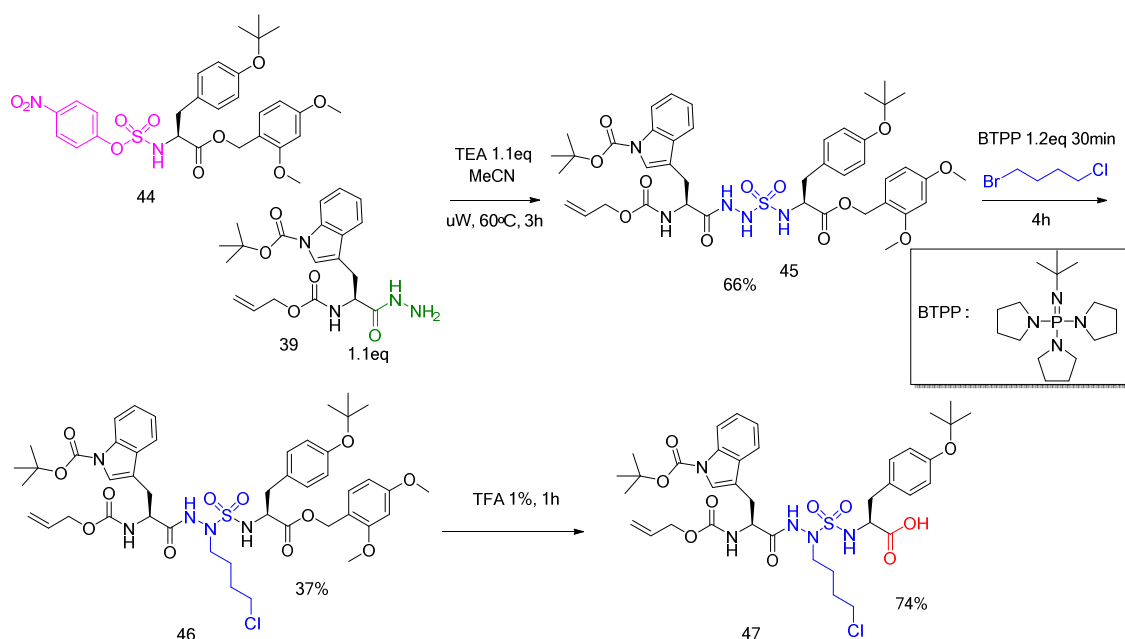
4.2.3. Synthesis of protected azasulfuryl protected tripeptide

The coupling between the hydrazide **39** and the sulfamate **45** was accomplished using microwave irradiation. Microwave irradiation has been demonstrated to be crucial to improve the yield of the formation of the N-aminosulfamides and favored

coupling between the two precursors (80% yield using microwave heating and only a 36% yield in normal conditions [52]).

Based on the findings developed by Turcotte et al., side chains may in principle be introduced onto the *N*-aminosulfamide moiety. By switching to the phosphazene base, tertbutylimino- tri(pyrrolidino)-phosphorane (BTPP), the alkylation yield was improved. Bis-alkylation was minimized by employing stoichiometric amounts of base and alkylating reagent [52].

In the case of this present project I alkylated with 1-bromo-4-chlorobutane to mime the side chain of Lys residue in position 8 in the *core-sequence* of urotensin-II using 1equiv. of BTPP at 0°C for 30 minutes and the 2equiv. of 1-bromo-4-chlorobutane were added for 12 hours, the yield was 66% and I had 5% of di-alkylation. The 2,4-dimethoxybenzyl alcohol was removed using 1% TFA in DCM for 1 hour for generating the carboxylic acid to be subsequently coupled on resin (Scheme 5).

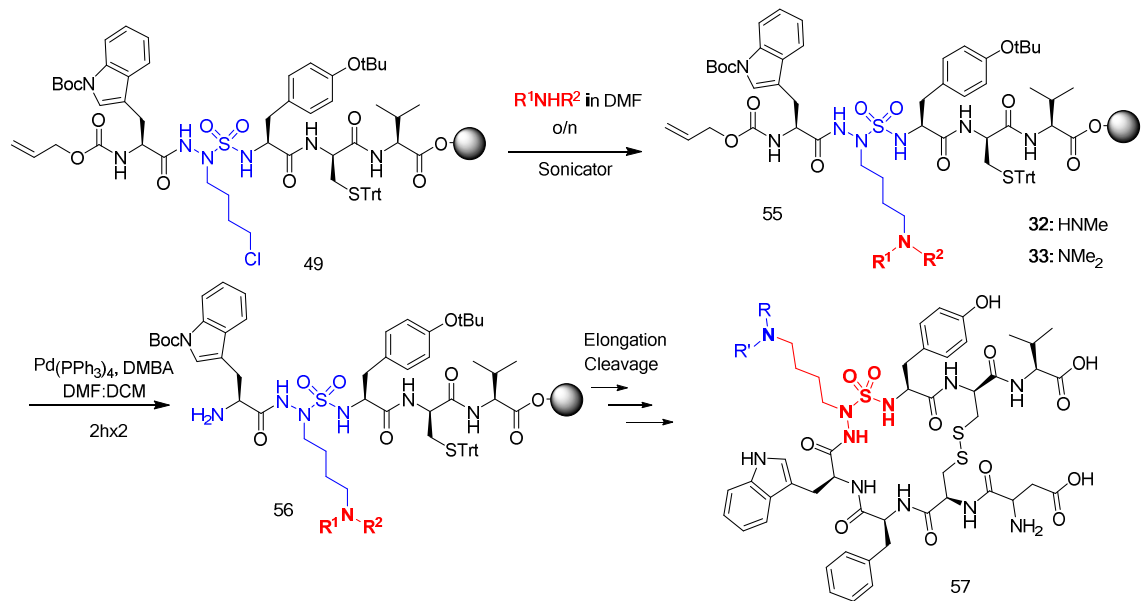


Scheme 5. Synthesis of the azasulfuryl protected tripeptide.

4.2.4. Solid phase synthesis

The azasulfuryl protected tripeptide **48** was coupled to the pre-built dipeptide on resin **49** using HOBt and DIC in DCM:DMF for 12 hours (Scheme 6).

In case of compound **Azasulfuryl-Lys⁸ III**, the chloride was replaced by azide using sodium azide in DMF under sonication overnight [52]. The *N*-terminal Alloc protecting group was removed using tetrakis(triphenylphosphine)-palladium(0) and *N,N'*-dimethylbarbituric acid in DCM/DMF for 2h at room temperature under aegon, and the reaction was repeated. The elongation of peptide was carried out with the same protocol reported in paragraph 4.1.1, using N^α-Fmoc-Phe-OH, N^α-Fmoc-Cys(trt)-OH and N^α-Boc-Asp(OtBu)-OH. The reduction of azide into amine was performed using *tris*(2-carboxyethyl)phosphine hydrochloride (TCEP) in THF:H₂O for 24h (Scheme 5). The cleavage and disulphide bond formation was accomplished in one-pot reaction using 10% DMSO in TFA with the presence of scavenger.



Scheme 7. Synthesis of Azasulfuryl *N,N*-Me₂-Lys⁸ U-II compound in solid phase.

5. CONCLUSIONS

The cyclic region of Urotensin-II became pride of our SARs by the development of new peptide analogues with different backbone geometry, side-chain orientation and side chain functionalization. Herein we summarized all goals achieved by the second unit of the present thesis:

- Major advantages of peptoids as research and pharmaceutical tools include the economy of synthesis, highly variable backbone and side-chain chemistry possibilities. At the same time, peptoid have been demonstrated as highly active in biological systems while resistant to proteolytic decay. I developed a library of Urotensin-II peptoid analogues to investigate new SARs by shifting the side-chain from α -carbon to nitrogen, in the meantime the role of non-chiral peptide backbone.
- The synthesis of new azasulfurylpeptides of urotensin-II can be an important tool for providing innovative SARs of UT receptor. *N*-aminosulfamide moiety in the core sequence of U-II confer to the peptide different backbone geometry. In particular, new *N*-aminosulfamide analogue has been developed by the replacement of Lys⁸ with the aza-sulfuryl amino acid carrying the side chain mimics of the native 5-aminobutane moiety.
- Diversity-oriented synthesis of azasulfurylpeptides with basic amino acid Residues: **Azasulfuryl-Lys UII** and **azasulfuryl-*N,N*-Me₂-Lys UII**. This approach should find significant applications in the study of various events featuring the post-translational modification and activity of lysine and arginine containing peptide structures.

6. CHARACTERIZATION

Peptoid 5: Purified purity >95%; LCMS chromatogram (10 to 90% MeCN in water (0.1% TFA), $t_R = 11.99$ min, over 15 min, flow rate of 1.0 mL/min), chemical formula: $C_{52}H_{67}N_9O_{12}S_2$, calculated mass; 1074.28, found: 1075.98 $[M+H]^+$.

Peptoid 6: Purified purity >95%; LCMS chromatogram (10 to 90% MeCN in water (0.1% TFA), t_R : 10.79 min over 15 min, flow rate of 1.0 mL/min), chemical formula: $C_{52}H_{67}N_9O_{12}S_2$, calculated mass; 1074.28, found: 1075.98 $[M+H]^+$.

Peptoid 7: Purified purity >95%; LCMS chromatogram (10 to 90% MeCN in water (0.1% TFA), t_R : 10.83 min, over 15 min, flow rate of 1.0 mL/min); LRMS for chemical formula: $C_{52}H_{67}N_9O_{12}S_2$, calculated mass; 1074.28, found: 1075.98 $[M+H]^+$.

Peptoid 8: Purified purity >95%; LCMS chromatogram (10 to 90% MeCN in water (0.1% TFA), t_R : 11.27 min over 15 min, flow rate of 1.0 mL/min); LRMS for chemical formula: $C_{52}H_{67}N_9O_{12}S_2$, calculated mass; 1074.28, found: 1075.98 $[M+H]^+$.

Peptoid 9: Purified purity >95%; LCMS chromatogram (10 to 90% MeCN in water (0.1% TFA), t_R : 11.65 min, over 15 min, flow rate of 1.0 mL/min); LRMS for chemical formula: $C_{52}H_{67}N_9O_{12}S_2$, calculated mass; 1074.28, found: 1075.98 $[M+H]^+$.

Peptoid 10: Purified purity >95%; LCMS chromatogram (10 to 90% MeCN in water (0.1% TFA), t_R : 10.92 min, over 15 min, flow rate of 1.0 mL/min); LRMS for chemical formula: $C_{52}H_{67}N_9O_{12}S_2$, calculated mass; 1074.28, found: 1075.98 $[M+H]^+$.

Azasulfuryl Lys⁸ UII: Purified purity >95%; LCMS chromatogram (10-90% MeCN in water (0.1% formic acid), 14 min, $t_R = 7.5$ min), purified on a Sunfire C18 analytical column (100Å, 3.5 μm, 4.6 mm X 100 mm); LCMS chromatogram (10-90% MeOH in water (0.1% formic acid), 14 min, $t_R = 8.7$ min), purified on a Sunfire C18 analytical column (100Å, 3.5 μm, 4.6 mm X 100 mm); HRMS for chemical formula: $C_{48}H_{63}N_{11}O_{13}S_3$, calculated mass $[M+2H]^{2+}$: 550.6172, found: 550.6153.

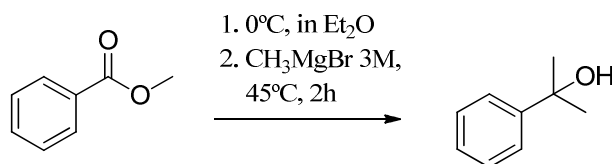
Azasulfuryl N,N-Me₂Lys⁸ UII: Purified purity >95%; LCMS chromatogram (0-80% MeCN (0.1% formic acid), 14 min, $t_R = 9.7$ min), purified on a Sunfire C18 analytical column (100Å, 3.5 μm, 4.6 mm X 100 mm); LCMS chromatogram (0-80% MeOH in water (0.1% formic acid), 14 min, $t_R = 10.9$ min), purified on a Sunfire C18 analytical column (100Å, 3.5 μm, 4.6 mm X 100 mm); HRMS for chemical formula: $C_{50}H_{67}N_{11}O_{13}S_3$, calculated mass $[M+2H]^{2+}$: 564.7192, found: 564.7173.

7. EXPERIMENTAL SECTION

4-nitrophenyl chlorosulfate (44) was synthesized according to literature methods [57]. 2,4-Dimethoxybenzaldehyd, mehtyl benzoate, allyl chloroformate, triethylamine (NEt₃), diisopropylethylamine (DIEA), mehtylmagnesium bromide, pyridine and diethylamine, all were purchased from Aldrich® and used as received. All amino acids, N^α-Fmoc-Zaa-OH, were purchased from GL Biochem® (Shanghai, China) Ltd. O-(Benzotriazol-1-yl)-N,N,N',N'-tetramethyluronium tetrafluoroborate (TBTU) was purchased from Albatross®. Methanol (MeOH) and trifluoroacetic acid (TFA) were respectively purchased from Fisher Chemical®, Aldrich®, J. T. Baker®, GenScript® Corporation and A&C Chemicals®, and used as received. Anhydrous solvents [tetrahydrofuran (THF), dichloromethane (DCM) and dimethylformamide (DMF)] were obtained by passage through a solvent filtration system (GlassContour®, Irvine, CA). Ethyl acetate (EtOAc) and hexanes were purchased from Fisher Chemical® and fractionally distilled prior to use. Microwave irradiation was accomplished using a 300 MW Biotage® apparatus on the high-absorption level; temperature was monitored automatically. Flash chromatography was on 230–400 mesh silica gel, and thin-layer chromatography was performed on silica gel 60 F254 plates from Merck®. Melting points were measured using a Gallankamp® apparatus and are uncorrected. Specific rotations, [α]_D values, were calculated from optical rotations measured at 20 °C in CHCl₃ or MeOH at the specified concentrations (c in g/100 mL) using a 1-dm cell (l) on a PerkinElmer Polarimeter 341, using the general formula: $[\alpha]_{20D} = (100 \times \alpha)/(l \times c)$. Accurate mass measurements were performed on a LC-MSD instrument from Agilent technologies in positive electrospray ionisation (ESI) mode at the Université de Montréal Mass Spectrometry facility. Sodium and proton adducts {[M+Na]⁺, [M+H]⁺ and [M+H]⁺+2} were used for empirical formula confirmation. ¹H NMR spectra were measured in CDCl₃ (7.26 ppm). ¹³C NMR spectra were measured in CDCl₃ (77.36 ppm). Coupling constant J values are measured in Hertz (Hz) and chemical shift values are reported in parts per million (ppm). Infrared spectra were recorded in the neat on an ATR Bruker® apparatus.

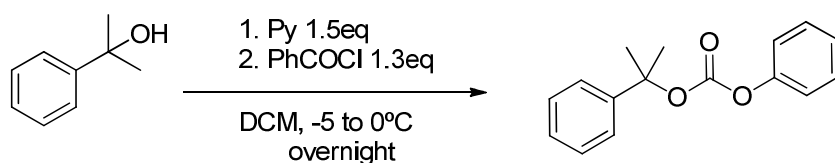
7.1. Solution synthesis:

Compound 33



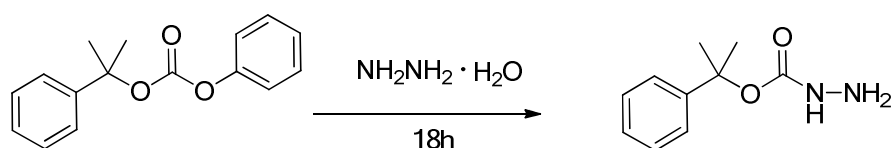
To a solution of methyl benzoate (630μL, 5mmol) in 5mL of anhydrous ether, 5mL of a solution of 3M methyl magnesium bromide in ether was added drop-wise at 0°C. The reaction was brought to 45°C with a warm water bath. After 2 h, TLC (3:7 EtOAc/hexanes) demonstrated completion conversion of the ester to 2-phenyl-propan-2-ol. The reaction mixture was poured slowly into an ice-cooled saturated solution of NH₄Cl, extracted with EtOAc (3 x 20mL). The organic phase were washed with brine (2 x 10mL), dried, filtered, and evaporated to afford 98% of 2-phenyl-propan-2-ol. ¹H-NMR δ 1.60 (s, 6H), 1.75 (s, 1H), 7.26 (t, 1H,J7.1), 7.36 (t, 2H,J7.5), 7.5 (d, 2H,J7.4); ¹³C-NMR δ 32.2, 72.5, 124.8, 127.1, 128.6, 150.0.

Compound 34



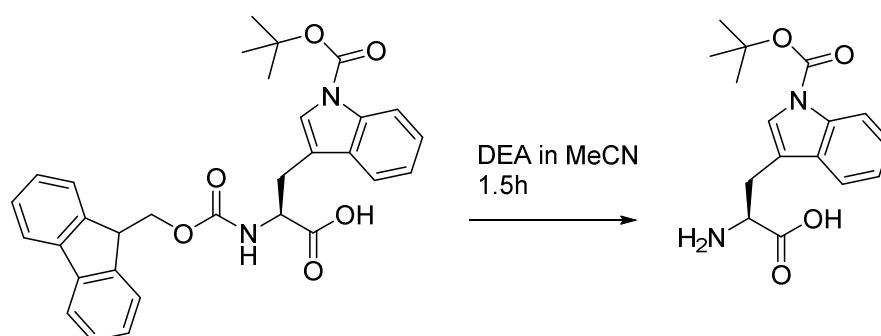
To a stirred solution of **33** (800mg, 5.88mmol) in 5mL of DCM and Py (750uL, 1.5equiv) at -5°C was added drop-wise over 30min a solution of phenyl chloroformate (1mL, 1.3equiv) in 4mL of DCM. A thick paste was gradually formed after the addition. The reaction mixture was further stirred overnight at 0°C. The mixture was diluted with DCM (50mL) and extracted with HCl 1N, NaOH 1N, H₂O and brine solution. The organic phase was dried, filtered, and evaporated, quantitative. ¹H-NMR δ 1.80 (s, 6H), 7.26 (t, 1H,J7.1), 7.29 (t, 2H,J7.5), 7.38 (t, 2H,J7.5), 7.42 (d, 2H,J7.4), 7.54 (d, 2H,J7.4); ¹³C-NMR δ 28.2, 84.5, 121.8, 124.1, 128.6, 129.4, 133.0,144.7, 151.1, 151.6.

Compound 35



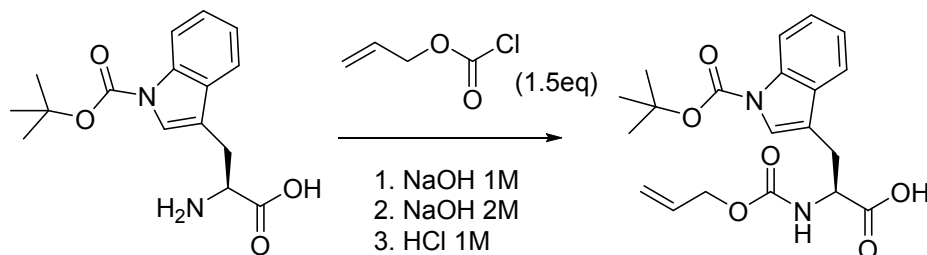
2.2 mL of hydrazine hydrate (50-60% in H₂O) was added to **34** (1gr, 3.9mmol) and the reaction was left and strong stirring for 18h. The mixture then poured into much ice water. The product was extracted of the aqueous phase with ethyl acetate (3x 20mL). The combined organic phase was washed with NaOH 1N, H₂O, and brine solution. Dried with sodium sulfate and the purification was carried out by trituration with hexane to afford 88% of yield. (R_f:0.15) in hexane:ethylacetate (6:4). ¹H-NMR δ 1.60 (s, 6H), 1.75 (s, 1H), 7.26 (t, 1H,J7.1), 7.36 (t, 2H,J7.5), 7.5 (d, 2H,J7.4); ¹³C-NMR δ 32.2, 72.5, 124.8, 127.1, 128.6, 150.0.

Compound 36



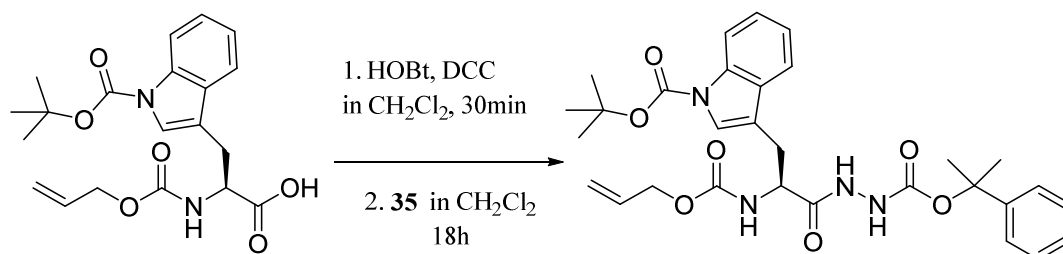
N^α-Fmoc-Trp(Boc)-OH (600mg, 1.2mmol) was dissolved in a solution of 25% of diethylamine in MeCN (20mL). It was stirred at room temperature for 1.5 h. After completion of the reaction, the volatiles were evaporated to a residue and the crude was dissolved in MeOH (20mL) and the fluorenylmethyl-*N*-diethylamine group was extracted with heptane (30mL x 5). White powder with 66% of yield. R_f: 0.09 in EtOAc ; mp: 133- 136°C; [α]_D²⁰ -20.1°; ¹H NMR (400 MHz, MeOD) δ 8.07 (d, *J* = 8.1 Hz, 1H), 7.68 (d, *J* = 7.7 Hz, 1H), 7.57 (s, 1H), 7.33 – 7.09 (m, 2H), 3.81 (dd, *J* = 9.2, 4.2 Hz, 1H), 3.39 (dd, *J* = 15.2, 3.6 Hz, 1H), 3.26 (dt, *J* = 3.2, 1.6 Hz, 1H), 3.07 (dd, *J* = 15.2, 9.3 Hz, 1H), 1.62 (s, 9H). ¹³C NMR (400 MHz, MeOD) δ 171.11 (s), 147.98 (s), 134.17 (s), 128.37 (s), 122.98 (s), 122.72 (s), 120.85 (s), 117.24 (s), 113.20 (d, *J* = 6.8 Hz), 81.95 (s), 52.79 (s), 46.68 (s), 46.47 (s), 46.25 (s), 46.04 (s), 45.83 (s), 45.61 (s), 45.40 (s), 25.43 (s), 25.14 (s). IR (neat) ν_{max}/cm⁻¹ 2973, 2934, 1728, 1590, 1366, 1152, 747; HRMS (ESI) *m/z* calculated for C₁₆H₂₁N₂O₄ 305.1497 found 305.1479.

Compound 37



36 (1.5g, 5mmol) was dissolved in NaOH 1M (20mL), allyl chloroformate (1.5equiv.) was then added to the mixture. The reaction was left under stirring at room temperature for 3.5h. During this period, a NaOH 2M (10mL) was added in 4 portions to the above mixture. After the completion of the reaction, HCl 1N was added to pH= 4-5. The resulting white suspension was extracted with EtOAc (20mL x 5). The organic phase was washed with water and brine solution, dried with dry sodium sulfate. The crude was purified with DCM:MeOH (9:1), *R_f*: 0.44. Brown oil with 89% of yield. ¹H NMR (400 MHz, CDCl₃) δ 10.65 (s, 1H), 8.12 (s, 1H), 7.62 – 7.42 (m, 2H), 7.40 – 7.12 (m, 2H), 5.94 – 5.64 (m, 1H), 5.42 (d, *J* = 7.9 Hz, 1H), 4.77 (s, 1H), 4.58 (s, 2H), 3.44 – 2.95 (m, 2H), 1.69 (s, 9H). ¹³C NMR (101 MHz, CDCl₃) δ 175.94 (s), 155.92 (s), 149.73 (s), 132.43 (s), 130.29 (s), 124.62 (s), 124.32 (s), 122.71 (s), 118.87 (s), 118.01 (s), 115.33 (s), 114.84 (s), 83.90 (s), 77.22 (d, *J* = 31.9 Hz), 76.74 (s), 76.61 – 76.26 (m), 66.05 (s), 53.76 (s), 28.21 (s), 27.54 (s). IR (neat) $\nu_{\text{max}}/\text{cm}^{-1}$ 2981, 1720, 1368, 1252, 1132, 745; HRMS (ESI) *m/z* calculated for C₂₀H₂₄N₂NaO₆ 411.4211 found 411.1513.

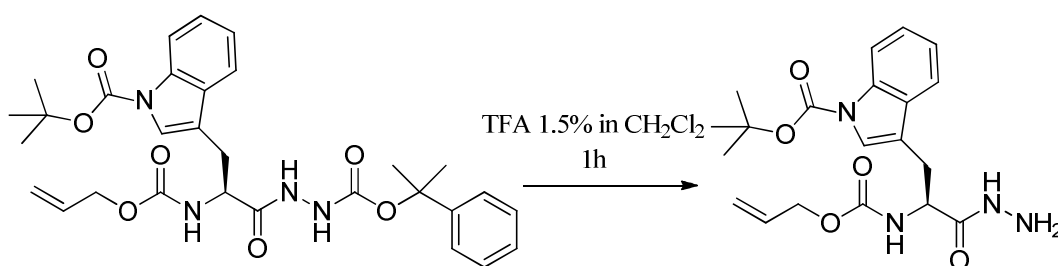
Compound 38



To a solution of **37** in 10mL of DCM was added HOBt (371mg, 1.1equiv) followed by DCC (566mg, 1.1equiv) and stirred for 30min at room temperature. Then a solution of **35** in 3mL of DCM was added and the reaction was left under stirring overnight. The work-up was carried out by the filtration of the crude and the evaporation to the residue. At this point the residue was treated with cold ethyl acetate to the further precipitation of *N,N'*-Dicyclohexylurea (DCU), filtered again and the EtOAc was washed with NaHCO₃, Brine and dried with sodium sulphate. The crude was then purified with a chromatography column eluting with EtOAc:hexane (3:7), white solid with *R_f* 0.32; $[\alpha]_{\text{D}}^{20}$ 40.1°; mp 75-77; ¹H NMR (400 MHz, CDCl₃) δ 8.41 (s, 1H), 8.13 (s, 1H), 7.63 – 7.44 (m, 2H), 7.42 – 7.15 (m, 7H), 6.93 (s, 1H), 5.86 – 5.65 (m, 2H), 5.37 – 5.02 (m, 2H), 4.61 (s, 1H), 4.45 (s, 2H), 3.31 – 3.15 (m, 1H), 3.08 (s, 1H), 1.80 (s, 6H), 1.66 (s, 9H). ¹³C NMR (101 MHz, CDCl₃) δ 170.91 (s), 156.13 (s), 154.64 (s), 149.66 (s), 145.50 (s), 135.41 (s), 132.39 (s), 130.32 (s), 128.31 (s), 127.12 (s),

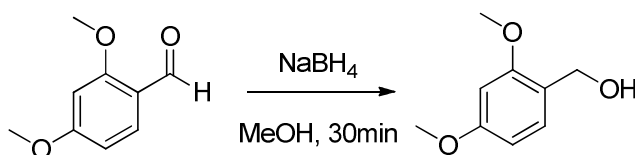
124.44 (d, $J = 17.0$ Hz), 122.68 (s), 118.98 (s), 117.90 (s), 115.26 (d, $J = 3.8$ Hz), 83.67 (s), 82.94 (s), 77.38 (d, $J = 11.4$ Hz), 77.11 (s), 76.80 (s), 66.04 (s), 60.46 (s), 53.22 (s), 28.79 (s), 28.03 (d, $J = 35.5$ Hz), 21.06 (s), 14.22 (s). IR (neat) $\nu_{\max}/\text{cm}^{-1}$ 3272, 2979, 2933, 1727, 1682, 1225, 745; HRMS (ESI) m/z calculated for $\text{C}_{30}\text{H}_{36}\text{N}_4\text{NaO}_7$ 587.2476 found 587.2480.

Compound 39



38 (1.2g, 2.3mmol) was treated with a solution 1.5%TFA in DCM 40mL. The reaction was left for 1h. The crude was then purified with a chromatography column eluting with EtOAc:hexane (6:4), pale yellow solid with R_f : 0.09; mp 84-86°C; ^1H NMR (CDCl_3 , 400 MHz) δ 1.66 (9H, s), 3.14 (1H, dd, $J = 8.1, 15.0$ Hz), 3.20 (1H, dd, $J = 6.6, 14.8$ Hz), 3.57-3.94 (2H, br), 4.48 (1H, dd, $J = 7.4, 14.8$ Hz), 4.55 (2H, d, $J = 5.7$ Hz), 5.21 (1H, d, $J = 10.4$ Hz), 5.27 (1H, d, $J = 17.2$ Hz), 5.42-5.64 (1H, br), 5.83-5.92 (1H, m), 7.20-7.58 (5H, m), 8.05-8.19 (1H, br); ^{13}C NMR (CDCl_3 , 100 MHz) δ 156.0, 149.7, 135.5, 132.5, 130.2, 124.8, 124.4, 122.8, 118.9, 118.2, 115.5, 115.2, 84.0, 66.2, 53.8, 29.2, 28.3; $[\alpha]_{\text{D}}^{20}$ 7.2° (THF, c 1.04); IR (neat) $\nu_{\max}/\text{cm}^{-1}$ 3290, 1726, 1452, 1367, 1252, 1154, 1085; HRMS (ESI) m/z calculated for $\text{C}_{20}\text{H}_{27}\text{N}_4\text{O}_5$ $[\text{M}+\text{H}]^+$ 403.1981; found 403.1981.

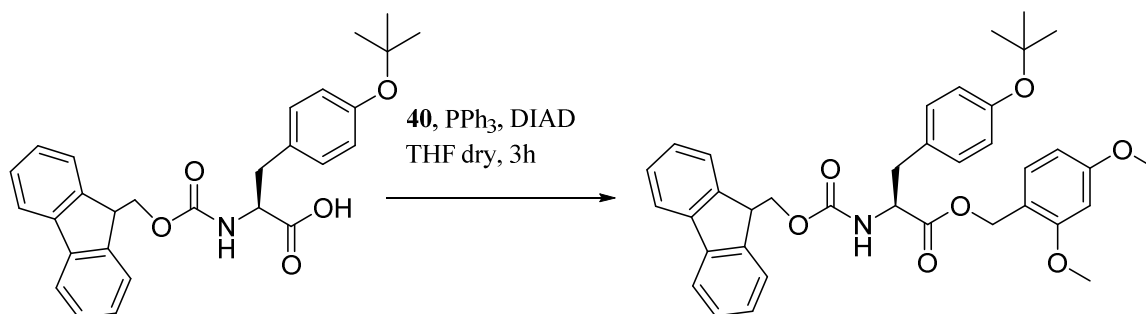
Compound 40



2,4-dimethoxybenzaldehyde (1g, 6mmol) was dissolved in 50mL of methanol. Then sodium borohydride (757mg, 2eq) was added slowly over 10min. The reaction was left for 30min, the reaction was checked by TLC eluting with Hexane:EtOAc (7:3). colorless oil with R_f : 0.46; yield 95%. ^1H NMR (CDCl_3 , 400 MHz) δ 7.29(1H, s), 7.18-7.16 (1H, d), 6.44-6.42(1H, d), 4.58(2H, s), 3.77(3H, s), 3.76(3H, s), 2.98(1H, s); ^{13}C NMR (CDCl_3 , 400 MHz) δ 55.1, 61.2,

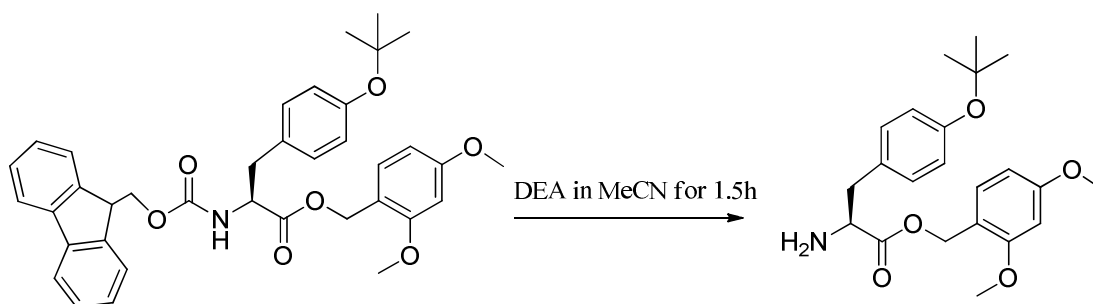
99.2, 105.1, 123.2, 130.1, 159.1, 161.2; HRMS (ESI) m/z calculated for $C_9H_{13}O_3$ $[M+H]^+$ 169.1159; found 169.1161.

Compound 41



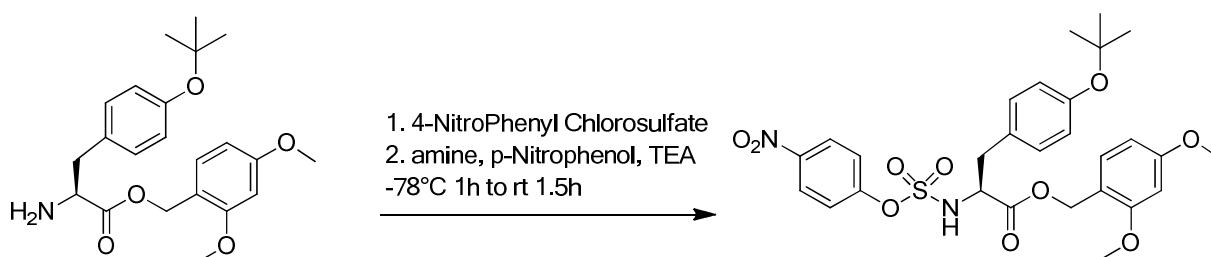
To a solution of Fmoc-Tyr(tBu)-OH (1.37g, 3 mmol) in THF dry (5mL) were added PPh_3 (1.57g mg, 6mmol) and **40** (1g, 6 mmol) followed by diisopropyl azodi-carboxylate (1.18mL, 6mmol), and the mixture was stirred at room temperature for 2 h. The reaction was concentrated and then diluted with EtOAc. The organic layer was washed with water, dried (Na_2SO_4) and concentrated. Purification by silica gel column chromatography, eluting with 5-30% EtOAc in hexanes, yielded the ester (1.53g, 83%) as pale yellow oil. 1H NMR ($CDCl_3$, 400 MHz) δ 1.36 (9H, s), 3.26 (1H, dd, $J = 5.9, 15.1$), 3.31 (1H, dd, $J = 5.6, 14.8$), 3.804 (3H, s), 3.810 (3H, s), 4.21 (1H, t, $J = 7.2$), 4.20-4.30 (2H, m), 4.75-4.85 (1H, m), 5.14 (2H, s), 5.47 (1H, d, $J = 8.1$), 6.43 (1H, s), 6.45 (1H, s), 6.91 (H, d, $J = 8.0$), 7.10 (1H, t, $J = 7.3$), 7.25-7.45 (5H, m), 7.46 (2H, s), 7.55-7.60 (2H, m); ^{13}C NMR ($CDCl_3$, 100 MHz) δ 28.9, 37.5, 47.23, 55.4, 56.1, 62.5, 66.9, 98.9, 104.1, 115.9, 120.0, 124.0, 125.2, 127.1, 127.4, 129.0, 130.9, 131.6, 141.6, 143.1, 143.2, 154.9, 155.0, 159.4, 161.9, 171.9; IR (neat) ν_{max}/cm^{-1} 1158, 1256, 1452, 1588, 1613, 1729, 2974, 3380; LRMS (ESI) m/z calculated for $C_{22}H_{29}NO_5$ $[M+H]^+$ 610.27; found 610.71.

Compound 42



N-(Fmoc)-(Tyrosine(tBu) 2,4-dimethoxybenzyl ester **42** (0.542 g, 0.89 mmol) was dissolved in MeCN (20 mL) and diethylamine (5mL) was added to the solution. It was stirred at room temperature for 1.5 h. After completion of the reaction, the volatiles were evaporated to a residue and the crude was purified by flash chromatography eluting with EtOAc:Hexane 2:3, buffed with 2% NEt₃ to afford amine (531 mg, 65 %) as an oil: *R*_f 0.26 (EtOAc:Hexane 2:3) + 2% NEt₃; [α]_D²⁰ = -8.5(CHCl₃, c 1.31); ¹H NMR (CDCl₃, 400 MHz) δ 1.43 (6H, s), 3.26 (1H, dd, *J* = 5.9, 15.1), 3.31 (1H, dd, *J* = 5.6, 14.8), 3.807 (3H, s), 3.804 (3H, s), 5.12 (2H, s), 6.40-6.50 (2H, m), 7.13 (1H, d, *J* = 7.9), 7.22 (1H, t, *J* = 7.4), 7.29 (1H, t, *J* = 7.3), 7.46 (1H, s), 7.55 (1H, d, *J* = 7.8); ¹³C NMR (CDCl₃, 100 MHz) δ 28.5, 40.8, 54.9, 55.71, 55.75, 62.8, 83.8, 98.9, 104.4, 116.6, 124.5, 124.8, 129.9, 131.8, 131.8, 154.9, 159.4, 161.7, 175.5; IR (neat) ν_{max}/cm⁻¹ 1158, 1256, , 1452, 1588, 1613, 1729, 2974, 3380; HRMS (ESI) *m/z* calculated for C₂₂H₃₀NO₅: 388.2118, found: 388.2109.

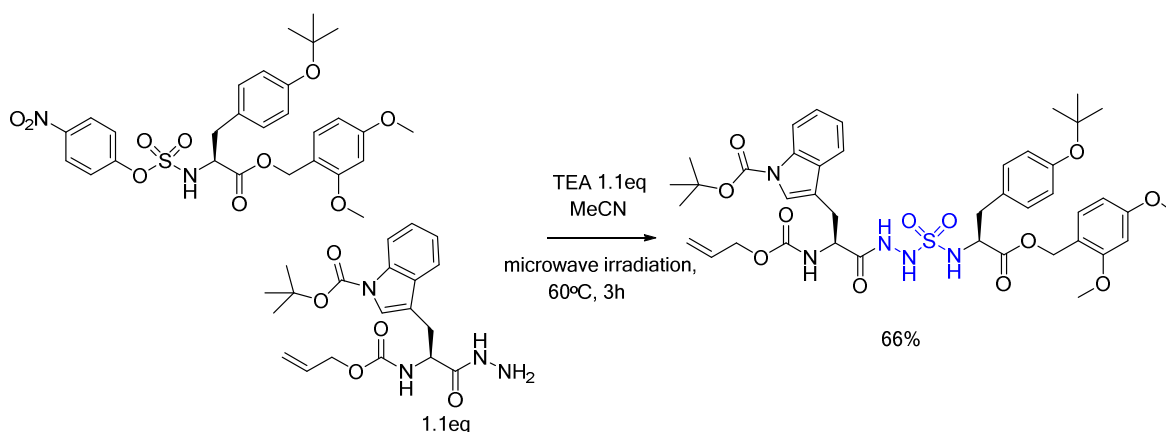
Compound 44



4-Nitrophenyl chlorosulfate (2.58g, 10.84 mmol, prepared according to reference [57]) was dissolved in dry DCM (10mL) and treated drop-wise with a solution of amine (2.089g, 5.42mmol), 4-nitrophenol (2.261g, 16.61 mmol) and triethylamine (4.5 mL, 32.52 mmol) in dry DCM (50 mL) at -78 °C. It was stirred at -78 °C for 2h. The reaction mixture was then allowed to warm at room temperature under stirring for 1 h. The reaction mixture was

evaporated to a residue, dissolved in DCM(20mL), washed with sat. NaHCO₃ (aq.) (3 x 25 mL), dried over MgSO₄, filtered. The crude was purified by flash chromatography eluting with hexane:ethyl acetate (8:2) to afford the sulfamidate contaminated with 4-nitrophenol. Yield 56% as a solid; *R_f*:0.30; mp 110-113°C; [α]_D²⁰ 6.2 (CHCl₃, c 0.97); ¹H NMR (CDCl₃, 400 MHz) δ 1.41 (9H, s), 3.14 (2H, dd, *J* = 5.0, 14.8), 3.83 (6H, s), 5.10 (2H, s), 6.46-6.48 (2H, m), 6.94(2H, d, *J* = 7.8), 7.20-7.30 (2H, m), 7.34 (1H, dt, *J* = 1.1, 7.2), 7.48 (1H, s), 7.44 (1H, d, *J* = 7.8), 8.15 (2H, m); ¹³C NMR (CDCl₃, 100 MHz) δ 27.5, 35.0, 56.73, 60.79, 62.4, 86.4, 100.5, 106.1, 116.9, 124.1, 126.7, 128.1, 129.4, 140.2, 154.6, 157.6, 159.2, 160.2, 171.7; IR (neat) ν_{max}/cm⁻¹ 728, 864, 1155, 1346, 1487, 1736, 2975; HRMS (ESI) *m/z* calculated for C₂₈H₃₂N₂O₁₀SNa: 611.1669, found: 611.1670.

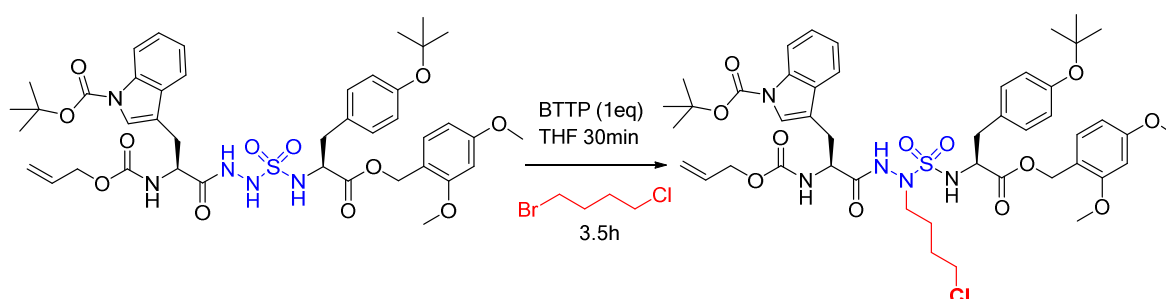
Compound 45



Hydrazide **39** (250 mg, 1.1equiv) and sulfamidate **44** (352mg, 0.60mmol) were dissolved in MeCN (6 mL) in a 2-5 mL microwave vessel. Triethylamine (93 μL, 1.1equiv) was then added to the mixture, at which point the solution turned yellow. The microwave vessel was sealed and the solution was heated at 60 °C under microwave irradiations for 3 h. The mixture was then evaporated to a residue. The crude was purified by flash chromatography eluting with EtOAc:Hexane (3:7); to afford sulfamide **46** (yield 60 %) as a pale yellow solid: *R_f* 0.23 (EtOAc:Hexane 3:7); mp 101-104°C; [α]_D²⁰ -8.3; (CHCl₃, c 1.10); ¹H NMR (CDCl₃, 400 MHz) δ 1.31 (9H, s), 1.66 (9H, s), 3.02-3.09 (4H, m), 3.82 (6H, s), 4.35-4.40 (1H, m), 4.42-4.48 (1H, m), 4.50-4.53 (2H, m), 5.09 (2H, s), 5.15 (1H, d, *J* = 10.5), 5.19 (1H, d, *J* = 10.5), 5.23 (1H, d, *J* = 17.2), 5.62 (1H, d, *J* = 7.7), 5.80-5.90 (1H, m), 6.41-6.45 (2H, m), 6.76-6.78 (2H, m), 6.96 (1H, s), 6.98 (1H, d, *J* = 7.8), 7.19-7.21 (2H, m), 7.23-7.25 (2H, m), 7.32-7.34 (2H, m) 8.05-8.10 (2H, m); ¹³C NMR (400 MHz, CDCl₃) δ 171.91 (s), 170.24 (s), 161.71 (s), 159.15 (d, *J* = 12.3 Hz), 155.80 (s), 154.58 (d, *J* = 14.8 Hz), 149.84 (s), 135.42 (s), 132.32 (s), 131.99 (d, *J* = 14.9 Hz), 130.38 – 129.57 (m), 125.06 (s), 124.77 (d, *J* = 14.0 Hz), 124.34 (s),

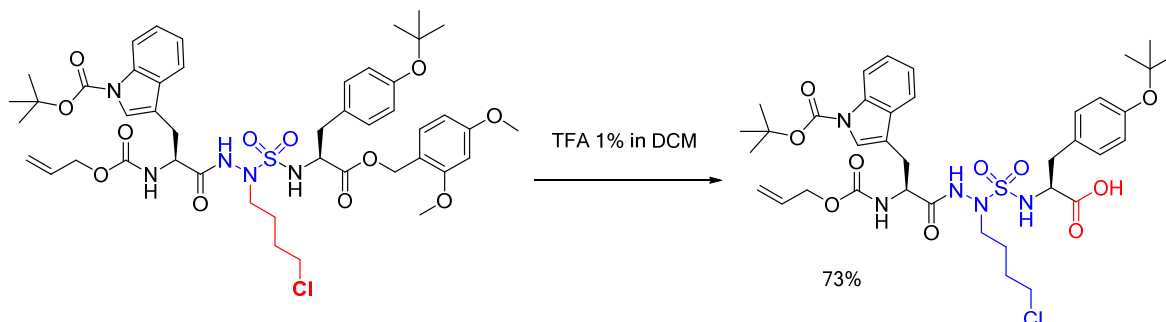
123.95 (s), 122.93 (s), 118.94 (s), 118.06 (d, $J = 25.0$ Hz), 115.46 (d, $J = 27.1$ Hz), 114.63 (s), 104.05 (s), 98.54 (s), 84.19 (s), 78.46 (s), 77.20 (s), 77.01 (s), 76.83 (s), 66.10 (d, $J = 22.5$ Hz), 63.52 (s), 57.16 (d, $J = 12.3$ Hz), 55.42 (t, $J = 6.7$ Hz), 53.52 (s), 37.85 (d, $J = 15.0$ Hz), 29.71 (s), 29.12 – 28.77 (m), 28.76 – 27.94 (m), 28.12 – 27.94 (m), 27.87 (s), 26.72 (s); LCMS monitoring [40-90% MeOH (0.1% FA) in water (0.1% FA) over 14 min, RT = 8.50 min]; IR (neat) $\nu_{\max}/\text{cm}^{-1}$ 1152, 1255, 1368, 1452, 1511, 1615, 1717, 2941, 3296; HRMS (ESI) m/z calculated for $\text{C}_{42}\text{H}_{53}\text{N}_5\text{NaO}_{12}\text{S}$ 874.3303; found 874.3295.

Compound 46



To a solution of **45** (0.74mmol) in THF (14mL) at 0°C under stirring was added BTTP (226 μL , 1 equiv.) and the reaction was left for 30min. Then 1-Bromo, 4-Chlorobutane (170 μL , 2 equiv.) was added quickly to the mixture. The reaction was left for 3.5h at 0°C . Then was warm to room temperature overnight. White powder (Yield: 66%); Rf: 0.34; mp 88-91 $^{\circ}\text{C}$; $[\alpha]_{\text{D}}^{20} = -7.1$ (CHCl_3 , c 1.10); ^1H NMR (400 MHz, CDCl_3) δ 8.15 (d, $J = 8.2$ Hz, 2H), 7.69 – 7.54 (m, 4H), 7.29 (ddd, $J = 30.7, 19.0, 7.7$ Hz, 7H), 6.99 (d, $J = 8.4$ Hz, 4H), 6.84 (t, $J = 5.5$ Hz, 4H), 6.54 – 6.41 (m, 4H), 5.90 (ddd, $J = 16.1, 10.9, 5.7$ Hz, 2H), 5.66 (s, 1H), 5.44 (d, $J = 7.2$ Hz, 2H), 5.33 – 5.05 (m, 8H), 4.55 (d, $J = 5.0$ Hz, 4H), 4.49 – 4.35 (m, 4H), 4.15 (q, $J = 7.2$ Hz, 1H), 3.84 (d, $J = 6.1$ Hz, 11H), 3.47 (t, $J = 6.5$ Hz, 4H), 3.26 – 3.13 (m, 7H), 3.06 (d, $J = 5.6$ Hz, 4H), 1.76 (dd, $J = 8.8, 5.8$ Hz, 5H), 1.68 (d, $J = 3.0$ Hz, 17H), 1.46 (s, 4H), 1.33 (d, $J = 2.8$ Hz, 17H); ^{13}C NMR (400 MHz, CDCl_3) δ 170.38 (s), 161.61 (s), 159.12 (s), 154.52 (s), 132.30 (s), 132.02 (s), 130.14 (s), 129.94 (s), 124.78 (s), 123.96 (s), 122.84 (s), 118.95 (s), 115.69 (s), 115.41 (s), 104.05 (s), 98.49 (s), 78.29 (s), 77.37 (s), 77.05 (s), 76.73 (s), 63.29 (s), 57.09 (s), 55.43 (d, $J = 6.0$ Hz), 50.68 (s), 44.45 (s), 37.97 (s), 30.93 (s), 29.13 (s), 28.86 (s), 28.18 (s), 24.28 (s), 14.21 (s); LCMS [40-90% MeOH (0.1% FA) in water (0.1% FA), 20 min, RT= 7.8 min]; IR (neat) $\nu_{\max}/\text{cm}^{-1}$ 3280, 1727, 1453, 1366, 1255, 1155, 1087; HRMS (ESI) m/z calculated for $\text{C}_{46}\text{H}_{61}\text{ClN}_5\text{O}_{12}\text{S}$ $[\text{M}+\text{H}]^+$ 942.3715; found 942.3705.

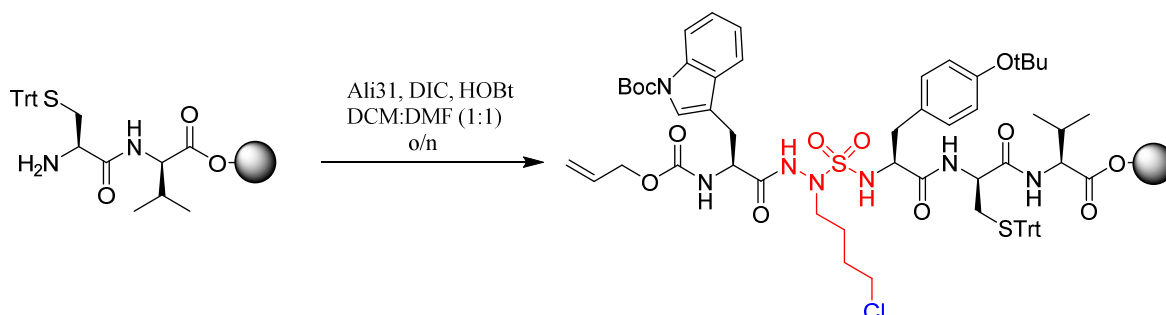
Compound 47



Sulfamide **46** (0.27mmol) was dissolved in a solution of 1% TFA in DCM (5mL) under stirring for 1h. The product was triturated in Et₂O. Pale yellow solid, 73% of yield. Rf: 0.21 in EtoAc:hexanes (4:1); mp 112-115°C; ¹H NMR (400 MHz, CDCl₃) δ 7.99 (d, *J* = 41.5 Hz, 2H), 7.66 (s, 1H), 7.43 – 7.23 (m, 3H), 7.16 (d, *J* = 8.3 Hz, 3H), 6.90 (d, *J* = 8.3 Hz, 2H), 6.08 (s, 1H), 5.93 – 5.70 (m, 2H), 5.22 (dd, *J* = 23.6, 13.9 Hz, 2H), 4.57 (s, 1H), 4.46 (d, *J* = 17.2 Hz, 3H), 3.86 – 3.60 (m, 2H), 3.49 (t, *J* = 6.0 Hz, 3H), 3.17 (dt, *J* = 40.2, 17.7 Hz, 5H), 1.76 (s, 2H), 1.74 – 1.58 (m, 10H), 1.47 (dd, *J* = 33.4, 25.2 Hz, 2H), 1.32 (d, *J* = 5.6 Hz, 10H). ¹³C NMR (400 MHz, CDCl₃) δ 174.30 (s), 156.29 (s), 154.39 (s), 149.80 (s), 135.28 (s), 132.30 (s), 130.80 – 130.61 (m), 129.91 (s), 129.60 (s), 124.48 (s), 123.93 (s), 122.34 (s), 118.01 (s), 117.52 (s), 115.08 (s), 114.28 (s), 84.13 (s), 78.00 – 77.80 (m), 66.37 (s), 56.41 (s), 53.73 (s), 53.52 – 53.33 (m), 50.74 (s), 50.49 (s), 44.37 – 44.17 (m), 37.31 (s), 24.35 (s). The reaction was by monitored with LCMS [40-90% MeOH (0.1% FA) in water (0.1% FA), 14 min, RT= 10.0 min]; IR (neat) ν_{\max} /cm⁻¹ 3280, 1727, 1453, 1366, 1255; HRMS (ESI) *m/z* calculated for C₃₇H₅₀ClN₅O₁₀S: 814.2859, found: 814.2864.

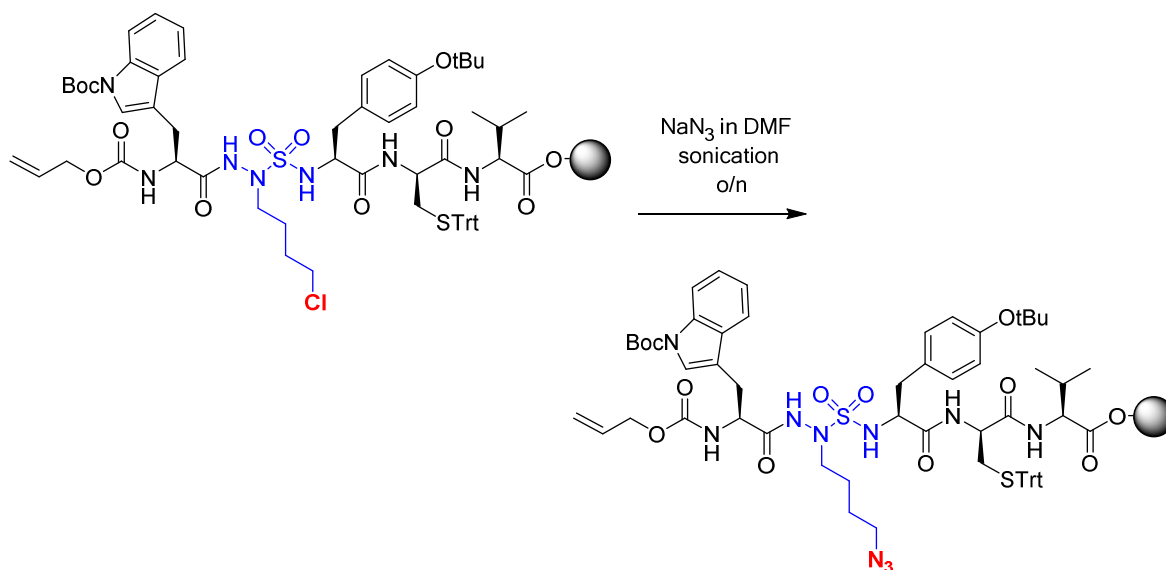
7.2. Solid phase synthesis:

Compound 49



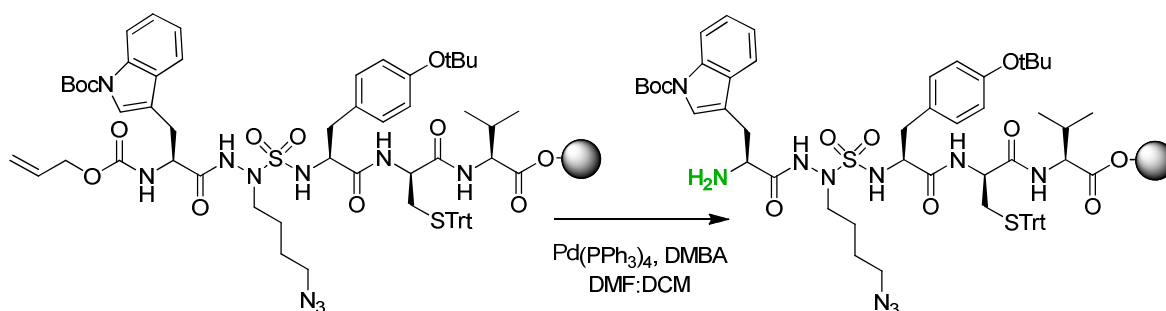
47 was dissolved in DCM:DMF (1:1), HOBt (28mg, 2equiv.) and DIC(126uL, 2equiv.) were added and the resulting mixture was added to **48** (0.1mmol). The reaction was left on the shaker at room temperature overnight. The resin was filtered, washed with DMF (3 × 10 mL), MeOH (3 × 10 mL), THF (3 × 10 mL), and DCM (3 × 10 mL), dried under vacuum, and stored in the fridge. By monitoring with LCMS [20-80% MeOH (0.1% FA) in water (0.1% FA), 20 min, RT= 7.5 min, 80% conversion] of the residue obtained from cleavage of a resin aliquot (3 mg) using 1 mL of TFA/TES/H₂O (95:2.5:2.5, v/v/v), resin filtration and evaporation.

Compound 50



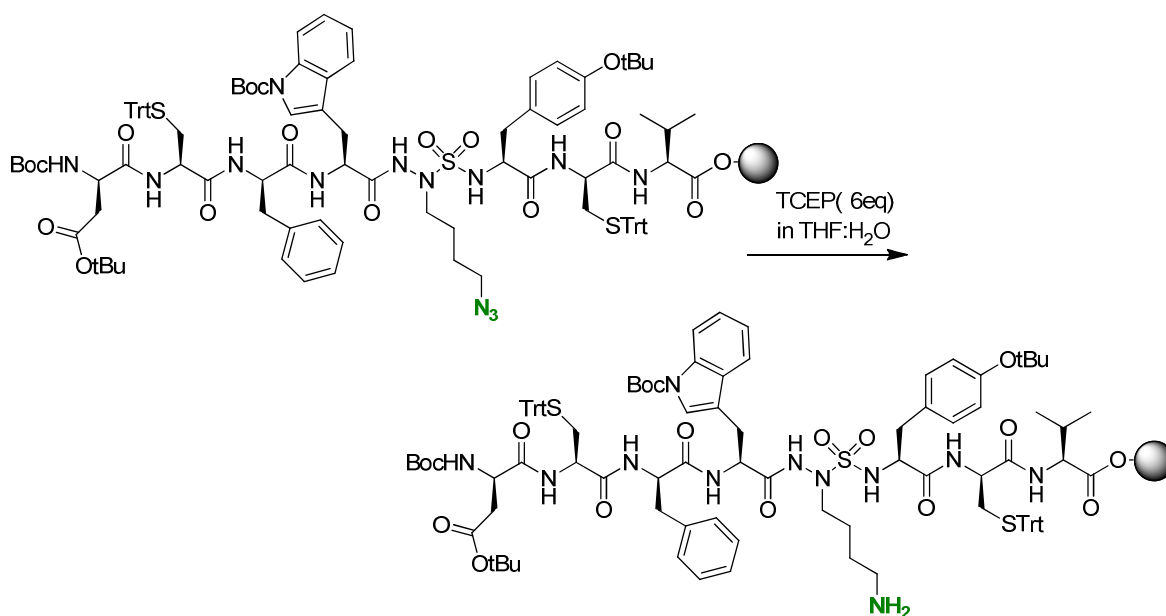
To a plastic syringe tube equipped with Teflon™ filter, stopper and stopcock containing a suspension of **49** (0.1mmol/g) in DMF (2 mL), solid NaN₃(10 equiv.) was added and the mixture was heated in a water bath with a sonication at 60°C overnight. The resin was filtered, washed with DMF (3 × 10 mL), MeOH (3 × 10 mL), THF (3 × 10 mL), and DCM (3 × 10 mL), dried under vacuum, and stored in the fridge. By monitoring with LCMS [20-90% MeOH (0.1% FA) in water (0.1% FA), 14 min, RT= 7.3 min, 80% conversion] of the residue obtained from cleavage of a resin aliquot (3 mg) using 1 mL of TFA/TES/H₂O (95:2.5:2.5, v/v/v), resin filtration and evaporation.

Compound 51



To a plastic syringe tube equipped with Teflon™ filter, stopper and stopcock containing a suspension of **50** (0.1mmol/g) in 4mL of DMF:DCM (3:1), solid yellow Pd(PPh₃)₄ (0.1 equiv.) and DMBA (10equiv.) was added and the mixture under argon for 1h and the process was repeat for a second time. The resin was filtered, washed with DMF (3 × 10 mL), MeOH (3 × 10 mL), THF (3 × 10 mL), and DCM (3 × 10 mL), dried under vacuum, and stored in the fridge. The reaction was shown to have gone to 90% conversion by monitoring with LCMS [10-90% MeOH (0.1% FA) in water (0.1% FA), 20 min, RT= 9.1 min, quantitative] of the residue obtained from cleavage of a resin aliquot (3 mg) using 1 mL of TFA/TES/H₂O (95:2.5:2.5, v/v/v), resin filtration and evaporation.

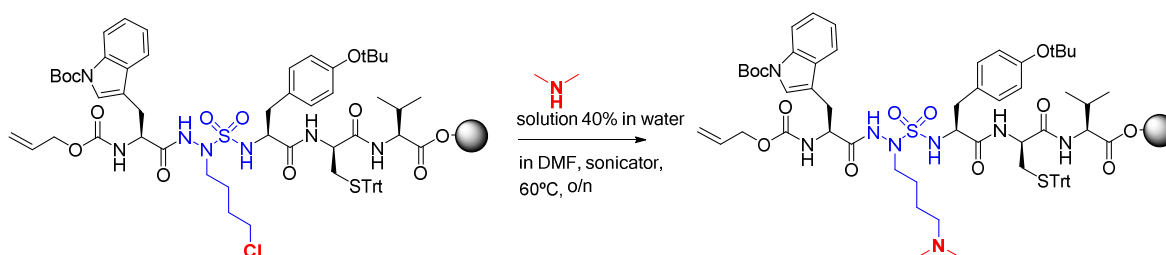
Compound 53



A plastic syringe tube equipped with Teflon™ filter, stopper and stopcock containing a suspension of azide derivative on resin (0.1 mmol/g) in THF/H₂O (9/1, v/v) (3 mL) was treated with TCEP (3 equiv.). The mixture was agitated for 24h at room temperature on an automated shaker. The resin was filtered, washed with DMF (3 × 10 mL), MeOH (3 × 10

mL), THF (3×10 mL), and DCM (3×10 mL), dried under vacuum, and stored in the fridge. Quantitative conversion was ascertained by LCMS monitoring [10-90% MeCN (0.1% FA) in water (0.1% FA) over 15 min, RT = 7.6 min, 90% conversion] of the residue obtained from cleavage of resin aliquot (3 mg) with 1 mL of TFA/TES/H₂O (95:2.5:2.5, v/v/v), resin filtration and evaporation.

Compound 55



To a plastic syringe tube equipped with Teflon™ filter, stopper and stopcock containing a suspension of **50** (250 mg, 0.1mmol/g), 600 μ L of 20% piperidine in DMF (6 mmol, 10 equiv.) were added, and the mixture was heated in a water bath with sonication at 60 °C for 4 h. The resin was filtered, washed with DMF (3×10 mL), MeOH (3×10 mL), THF (3×10 mL), and DCM (3×10 mL), dried under vacuum, and stored in the fridge. The reaction was shown to have a quantitative conversion by monitoring with LCMS [10-90% MeOH (0.1% FA) in water (0.1% FA), 14 min, RT = 9.1, quantitative] of a residue obtained from cleavage of a resin aliquot (3 mg) with 1 mL of TFA/TES/H₂O (95:2.5:2.5, v/v/v), resin filtration and evaporation.

8. REFERENCES

- [1] Ames RS, Sarau HM, Cambers JK, “Human urotensin II is a potent vasoconstrictor and agonist for the orphan receptor GPR14” *Nature* 1999;401:282-286.
- [2] Kwok Leung Ong, Karen S.L. Lam, Bernard M.Y. Cheung, “Urotensin II: Its Function in Health and Its Role in Disease” *Cardiovascular Drugs and Therapy* 19 65-75 2005.
- [3] Pearson D, Shively JE, Clark BR, Geschwind II, Barkley M, Nishioka RS, “Urotensin II: a somatostatin-like peptide in the caudal neurosecretory system of fishes” *Proc Natl Acad Sci USA* 1980;77:5021-4.
- [4] Chartrel N, Leprince J, Dujardin C, Chatenet D, Tollemier H, Baroncini M, “Biochemical characterization and immunohistochemical localization of urotensin II in the human brainstem and spinal cord” *J Neurochem* 2004;91:110-8.
- [5] Coulouarn Y, Jegou S, Tostivint H, Vaudry H, Lihrmann I, “Cloning, sequence analysis and tissue distribution of the mouse and rat urotensin II precursors” *FEBS Lett* 1999;457:28-32.
- [6] Tsoukas, P.; Kane, E.; Giaid, A., “Potential clinical implications of the urotensin II receptor antagonists” *Frontiers in Pharmacology* **2011**, 2, article 38.
- [7] Coulouarn Y, Jegou S, Tostivint H, Vaudry H, Lihrmann I, “Cloning, sequence analysis, and tissue distribution of the mouse and rat urotensin II precursor. *FEBS Lett* 1999;457:28-32.
- [8] Ames RS, Sarau HM, Chambers JK, Willette RN, Aiyar NV, Romanic AM, et al. Human urotensin-II is a potent vasoconstrictor and agonist for the orphan receptor GPR14. *Nature* 1999;401:282-6.
- [9] Muravenko, O.V.; Gizatulin, R.Z.; Al-Amin, A.N.; Protopopov, A.I.; Kashuba, V.I.; Zelenin, A.V.; Zabarovsky, E.R., Human ALY/BEF gene Map position 17q25.3, *Chromosome Research* **2000**, 8, 6, 562.
- [10] Maguire, J.J.; Kuc, R.E.; Davenport, A.P., Orphan-receptor ligand human urotensin II: receptor localization in human tissues and comparison of vasoconstrictor responses with endothelin-1, *British Journal of Pharmacology* **2000**, 131, 3, 441-446.
- [11] Sauzeau V, Le Mellionec E, Bertoglio J, Scalbert E, Pacaud P, Loirand G. Human urotensin II-induced contraction and arterial smooth muscle cell proliferation are mediated by RhoA and Rho-kinase. *Circ Res* 2001;88:1102-110.
- [12] Russell FD, Kearns P, Toth I, Molenaar P, “Urotensin-II-converting enzyme activity of furin and trypsin in human cells in vitro” *JPharmacol Exp Ther* 2004;310:209-214.
- [13] Kwok Leung Ong, Karen S.L. Lam, and Bernard M.Y. Cheung “Urotensin II: Its Function in Health and Its Role in Disease” *Cardiovascular Drugs and Therapy* 19 65-75 2005.

- [14] Vaudry H, Leprince J, Chatenet D, Fournier A, Lambert DG, Le Mével JC, Ohlstein EH, Schwertani A, Tostivint H, Vaudry D, “International union of basic and clinical pharmacology. XCII. Urotensin II, urotensin II-related peptide, and their receptor: from structure to function” *Pharmacol Rev* 67:214–258, January 2015.
- [15] D’Emmanuele R, Di Villa B, Fusco F, D’Aiuto E, Grieco P, Novellino E, Imbimbo C, Mirone V, Cirino G, Raffaella Sorrentino “Endogenous Urotensin II Selectively Modulates Erectile Function through eNOS” 2012, 7, 2, e31019.
- [16] Grieco P, Bozzuto G, Toccaceli L, Sgambato A, Marra M, Zappavigna S, Migaldi M, Rossi G, Striano S, Marra L, Gallo L, Cittadini A, Botti G, Novellino E, Molinari A, Budillon A, Caraglia M, “Urotensin II Receptor Predicts the Clinical Outcome of Prostate Cancer Patients and Is Involved in the Regulation of Motility of Prostate Adenocarcinoma Cells” *Journal of Cellular Biochemistry*, 112, 341–353 (2011).
- [17] Patacchini R, Santicioli P, Giuliani S, Grieco P, Novellino E, Rovero P, Alberto Maggi C, “Urantide: an ultrapotent urotensin II antagonist peptide in the rat aorta” *British Journal of Pharmacology*(2003) 140, 1155–1158).
- [18] Merlino F, Di Maro S, Yousif AM, Caraglia M, Grieco P, “Urotensin-II Ligands: An Overview from Peptide to Nonpeptide Structures” *Journal of Amino Acids* Volume 2013, Article ID 979016,15pp.
- [19] McMaster D, Kobayashi Y, Rivier J, Lederis K. Characterization of the biologically and antigenically important regions of urotensin II. *Proc West Pharmacol Soc* 1986;29:205–208.
- [20] Carotenuto A, Grieco P, Rovero P, Novellino E, “Urotensin-II receptor antagonists,” *Current Medicinal Chemistry*, 13, 3, 267–275, 2006.
- [21] Behm DJ, Herold CL, Ohlstein, EH, Knight SD, Dhanak D, Douglas SA, “Pharmacological characterization of SB-710411 (Cpa-c[D-Cys-Pal-D-Trp-Lys-Val-Cys]-Cpaamide), a novel peptidic urotensin-II receptor antagonist,” *British Journal of Pharmacology*, 137, 4, 449–458, 2002.
- [22] Orbuch JE, Taylor DH, Coy “Discovery of a novel class of neuromedin B receptor antagonists, substituted somatostatin analogues,” *Molecular Pharmacology*, 44, 4, 841–850, 1993.
- [23] Herold CL, Behm DJ, Buckley PT, “Theneuromedin B receptor antagonist, BIM-23127, is a potent antagonist at human and rat urotensin-II receptors,” *British Journal of Pharmacology*, vol. 139, 2, 203–207, 2003.
- [24] Sugo, T.; Murakami, Y.; Shimomura, Y.; Harada, M.; Abe, M.; Ishibashi, Y.; Kitada, C.; Miyajima, N.; Suzuki, N.; Mori, M.; Fujino, M., Identification of urotensin II-related peptide as the urotensin II-immunoreactive molecule in the rat brain, *Biochemical and Biophysical Research Communications* **2003**, 310, 3, 860-868.

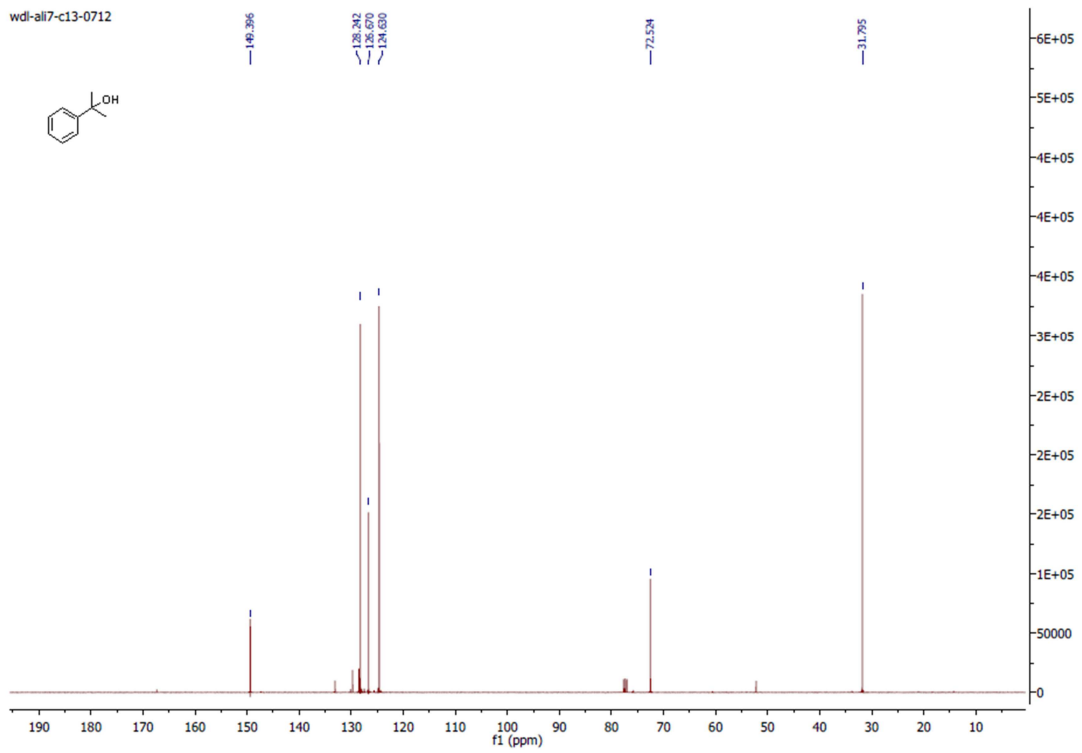
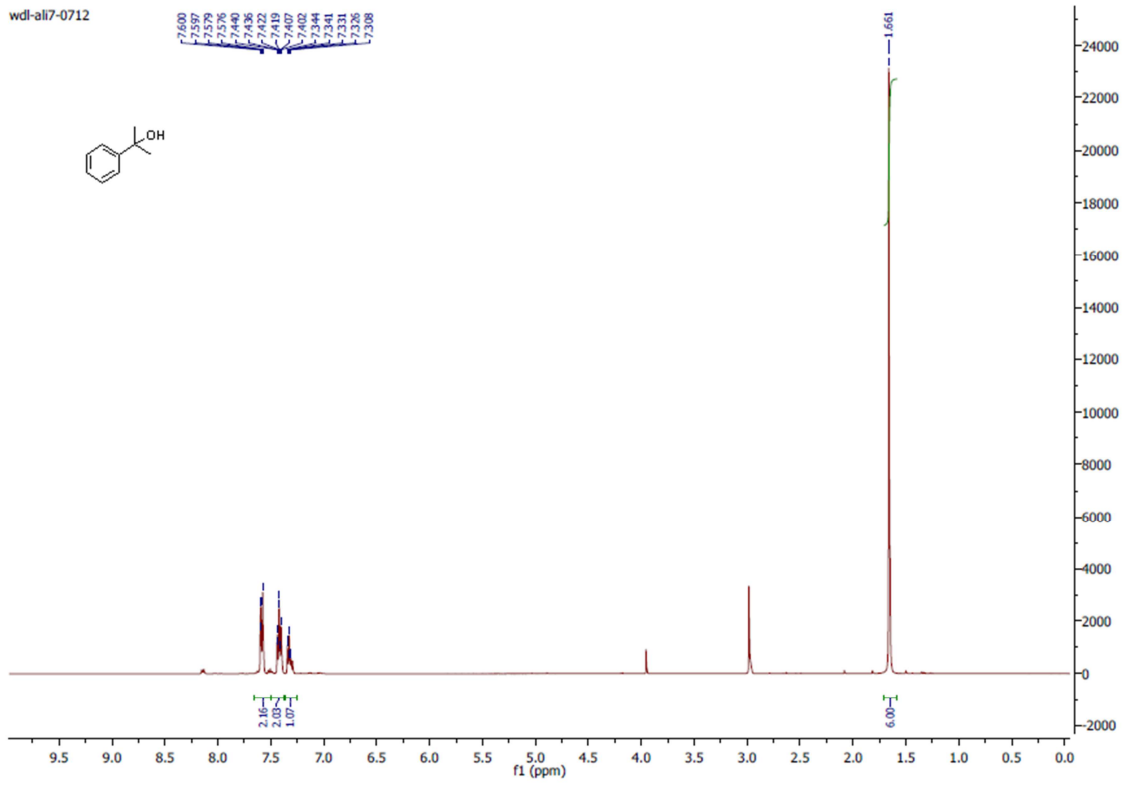
- [25] Brancaccio D, Merlino F, Limatola A, Yousif AM, Gomez IM, Campiglia P, Carotenuto A, Grieco P, "An Investigation into the Origin of the Biased Agonism Associated with the Urotensin-II Receptor Activation" *Journal of Peptide Science - PSC-14-0179*, DOI 10.1002/psc.2740.
- [26] McMaster D, Kobayashi U, Rivier J, Lederis K, "Characterization of the biologically and antigenically important regions of urotensin II," *Proceedings of the Western Pharmacology Society*, vol. 29, pp. 205–208, 1986..
- [27] Grieco P, Carotenuto A, Patacchini R, Maggi CA, Novellino E, Rovero P, "Design, Synthesis, Conformational Analysis, and Biological Studies of Urotensin-II Lactam Analogues" *Bioorganic & Medicinal Chemistry* 10 (2002) 3731–3739.
- [28] Grieco P, Carotenuto A, Campiglia P, Zampelli E, Patacchini R, Maggi CA, Novellino E, Rovero P, "A new, potent urotensin II receptor peptide agonist containing a Pen residue at the disulfide bridge" *Journal of Medicinal Chemistry* **2002**, 45, 20, 4391-4394.
- [29] Grieco P, Carotenuto A, Campiglia P, Marinelli L, Lama T, Patacchini R, Santicioli P, Maggi CA, Rovero P, Novellino E, "Urotensin-II receptor ligands. From agonist to antagonist activity" *Journal of Medicinal Chemistry* **2005**, 48, 23, 7290-7297.
- [30] Kinney WA, Almond Jr. HR, Qi J, "Structure function analysis of urotensin II and its use in the construction of a ligand-receptor working model" *Angewandte Chemie— International Edition*, vol. 41, no. 16, pp. 2940–2944, 2002.
- [31] Leprince J, Chatenet D, Dubessy C, Fournier A, Pfeiffer B, Scalbert E, Renard P, Pacaud P, Oulyadi H, Se'galas-Milazzo I, Guilhaudis L, Davoust D, Tonon M.C, Vaudry H, "Structure–activity relationships of urotensin II and URP" *Peptides* 29(2008) 658-673.
- [32] Flohr S, Kurz M, Kostenis E, Brkovich A, Fournier A, Klabunde T, "Identification of nonpeptidic urotensin II receptor antagonists by virtual screening based on a pharmacophore model derived from structure–activity" *Peptides*; 29(2008); 658-673.
- [33] Boucard AA, Sauve SS, Guillemette G, Escher E, Leduc R, "Photo-labeling the rat urotensin II/GPR14 receptor identifies a ligand binding site in the fourth transmembrane domain" *Biochem J.* ;370(2003); 829–38.
- [34] Boucard AA, Sauve SS, Guillemette G, Escher E, Leduc R. "Photo-labeling the rat urotensin II/GPR14 receptor identifies a ligand binding site in the fourth transmembrane domain" *Biochem J.* 2003;370:829–38.
- [35] Guerrini R, Camarda V, Marzola E, Arduin M, Calo G, Spagnol M, "Structure–activity relationship study on human urotensin II" *J Peptide Sci* 2005;11:85–90.

- [36] Chatenet D, Dubessy C, Boularan C, Scalbert E, Pfeiffer B, Renard P, “Structure-activity relationships of a novel series of urotensin II analogs: identification of a urotensin II antagonist” *J Med Chem* 2006;49:7234–8.
- [37] Carotenuto A, Auriemma L, Merlino F, Yousif AM, Marasco D, Limatola A, Campiglia P, Gomez-Monterrey I, Santicioli P, Meini S, Maggi CA, Novellino E, Grieco P, Lead Optimization of P5U and Urantide: Discovery of Novel Potent Ligands at the Urotensin-II Receptor *J. Med. Chem.*, **2014**, 57 (14), pp 5965–5974.
- [38] Croston GE, Olsson R, Currier EA, Burstein ES, Weiner D, Nash N, “Discovery of the first nonpeptide agonist of the GPR14/urotensin-II receptor: 3-(4-chlorophenyl)-3-(2-(dimethylamino)ethyl) isochroman-1-one (AC-7954)” *J Med Chem* 2002;45:4950–3.
- [39] Lehmann F, Lake L, Currier EA, Olsson R, Hacksell U, Luthman K. Design, parallel synthesis and SAR of novel urotensin II receptor agonists. *Eur J Med Chem* 2007;42: 276–85
- [40] Olsson R. Acadia Pharmaceuticals Inc. A combinatorial scaffold approach towards the pharmacophores of ligands II and somatostatin 5 receptors. *PCT Int Appl.*; 2004 (WO2004073642).
- [41] Bousette N, Hu F, Ohlstein EH, Dhanak D, Douglas SA, Giaid A. “Urotensin-II blockade with SB-611812 attenuates cardiac dysfunction in a rat model of coronary artery ligation” *J Mol Cell Cardiol* 2006;41:285–95..
- [42] Lawson EC, Luci DK, Ghosh S, “Nonpeptide urotensin- II receptor antagonists: a new ligand class based on piperazinophthalimide and piperazino-isoindolinone subunits”, *Journal of Medicinal Chemistry*, 52, 23, 7432–7445, 2009
- [43] Zuckermann RN, Kerr JM, Kent SBH, Moos WH, “Efficient method for the preparation of peptoids [oligo(N-substituted glycines)] by submonomer solid-phase synthesis” *J. Am. Chem. Soc.* **1992**, 114, 10646-10647.
- [44] Kirshenbaum K, Barron AE, Goldsmith RA, Armand P, Bradley EK, Truong KTV, Dill KA, Cohen FE, Zuckermann RN, “Sequence specific polypeptoids: a diverse family of heteropolymers with stable secondary structure” *Proc Natl Acad Sci U S A*, 1998, 95:4303-4308.
- [45] Camp NP, Perry DA, Kinchington D, Hawkins P, Gani D, “Synthesis of peptide analogues containing phosphoramidate methyl ester functionality: HIV-1 proteinase inhibitors possessing unique cell uptake properties” *Bioorganic & Medicinal Chemistry*, 3, 3, 297-312, 1995.
- [46] Gilmore WF, Lin HJ, “Synthesis of Carbamates of α -Amino Sulfonamides” *J. Org. Chem.* **1978**, 43, 4535-4537.
- [47] Gante, J, “Azapeptides” *Synthesis* **1989**, 405.

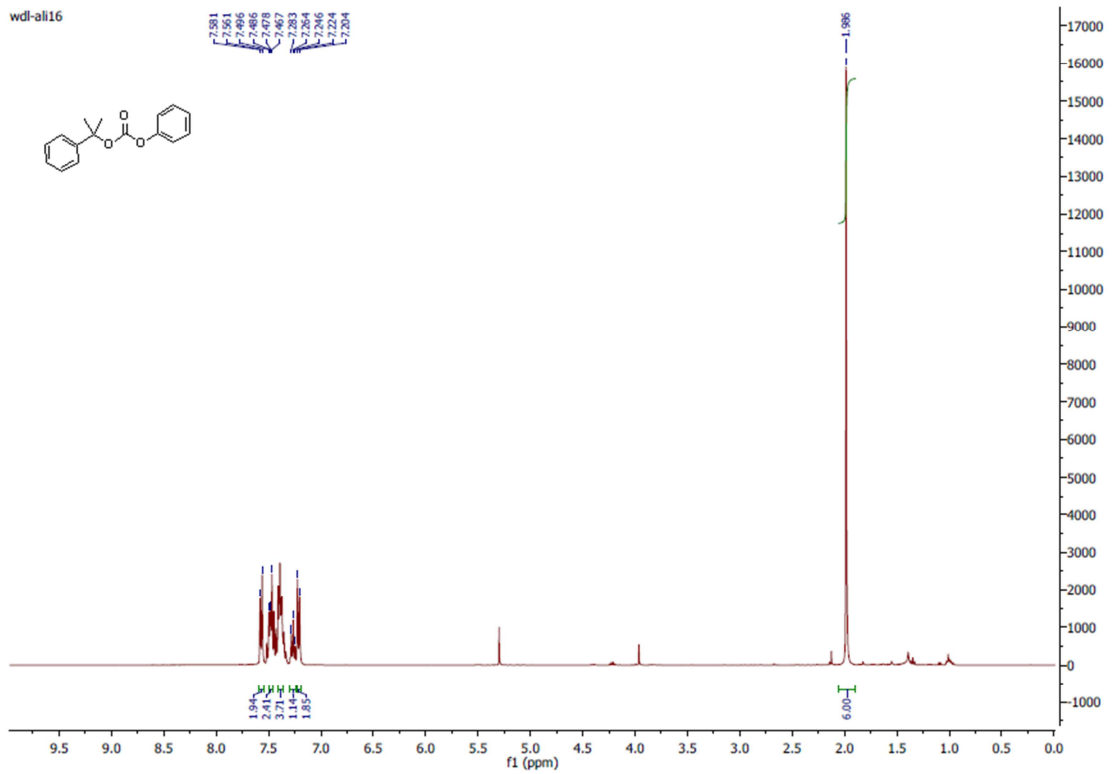
- [48] Zega A, Urleb U, "Azapeptides" *Acta Chim. SloV.* **2002**, *49*, 469.
- [49] Sabatino D, Proulx C, Klocek S, Bourguet CB, Boeglin D, Ong H, Lubell WD, "Exploring side-chain diversity by submonomer solid-phase Aza-peptide synthesis. *Org Lett* (2009);*11*:3650–3653.
- [50] Cheeseright, TJ, Edwards AJ, Elmore DT, Jones JH, Raissi M, Lewis EC, "Azasulfonamidopeptides as Peptide Bond Hydrolysis Transition State Analogues. Part 1. Synthetic Approaches" *J Chem Soc, Perkin Trans 1* 1994, 1595–1600.
- [51] Baldauf C, Gunther R, Hofmann H.J, "Conformational properties of sulfonamido peptides" *Theochem* **2004**, *675*, 19-28.
- [52] Turcotte S, Bouayad-Gervais SH, Lubell WD, "N-aminosulfamide peptide mimic synthesis by alkylation of Azasulfurylglycinyl peptides" *Org Lett* 2012, *14*, 1318–1321.
- [53] Sun AQ, Luo Y, Backos DS, Xu S, Balasubramaniyan N, Reigan P, Suchy FJ, *Mol. Pharmacol.* 2013, *83*, 1078–1086.
- [54] Traoré M, Doan ND, Lubell WD, "Diversity-Oriented Synthesis of Azapeptides with Basic Amino Acid Residues: Aza-Lysine, Aza-Ornithine, and Aza-Arginine" *Org. Lett.* (2014); *13*; 3588-91.
- [55] Zuckermann, R. N.; Kerr, J. M.; Kent, S. B. H.; Moos, W. H. *J. Am. Chem. Soc.* 1992, *114*, 10646–10647
- [56] Lin X, Dorr H, Nuss JM, "Utilization of Fukuyama's sulfonamide protecting group for the synthesis of *N*-substituted-amino acids and derivatives"
- [57] Brunwin M, Low G, "Total Synthesis of Nuclear Analogues of 7-Methyl-cephalosporin" *J.C.S. CHEM. COMM.*, 1972.
- [58] Tun-Kyi A, Schwyzer R, "(*p*-Phenylazophenyl)-isopropylloxycarbonyl, a new protecting group for peptide synthesis" *Helvetica Chimica Acta*, *59*, 5, 1976, 1642-46.
- [59] Fettes, K.J.; Howard, N.; Hickman, D.T.; Adah, S.; Player, M.R.; Torrence, P.F.; Micklefield, J., *J. Chem. Soc., Perkin Trans. 1* 2001, 485-495.

9. SPECTRA SECTION

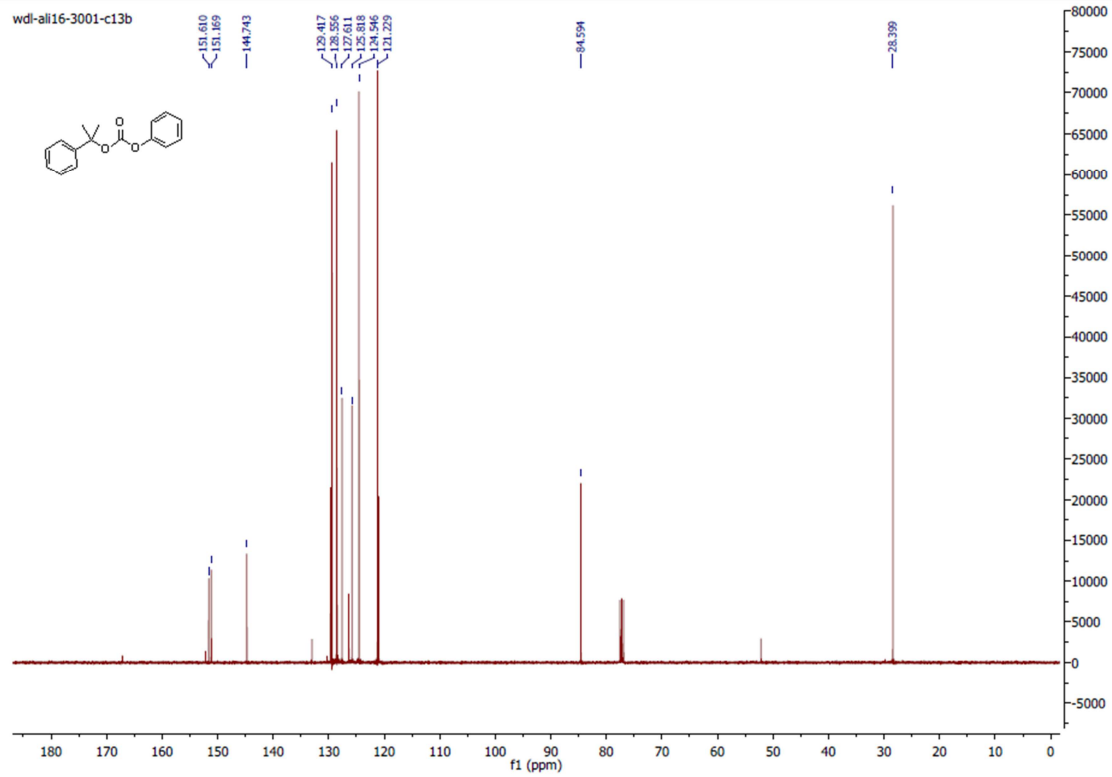
NMR Spectra

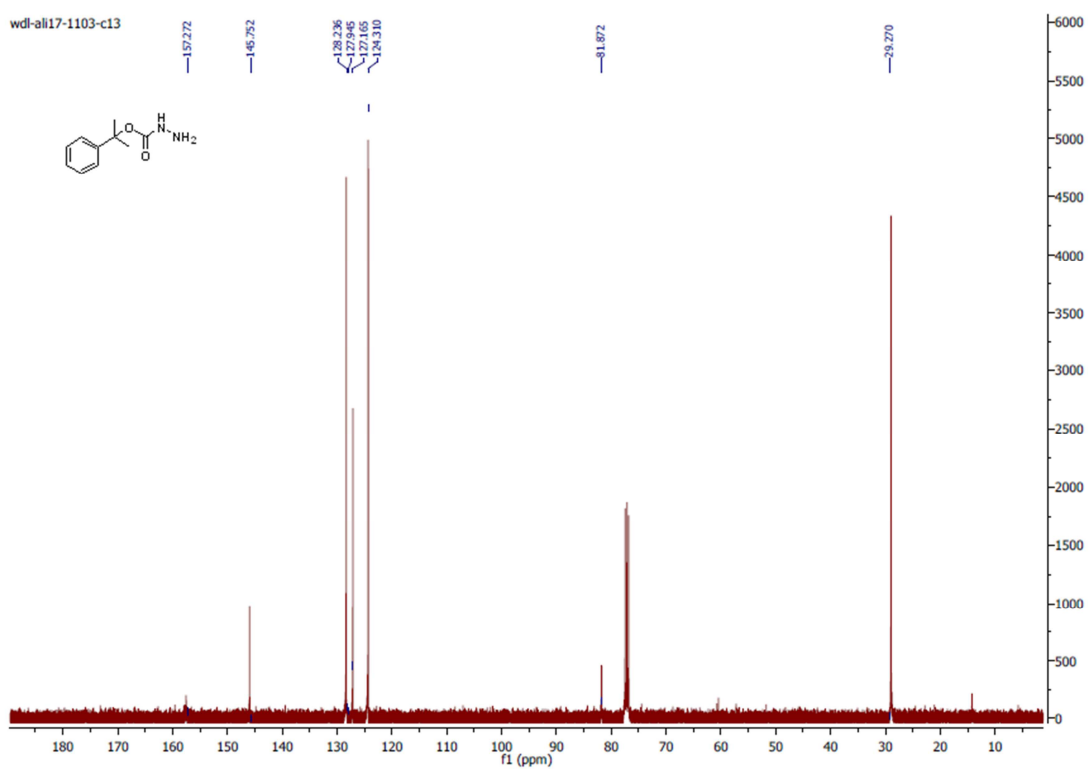
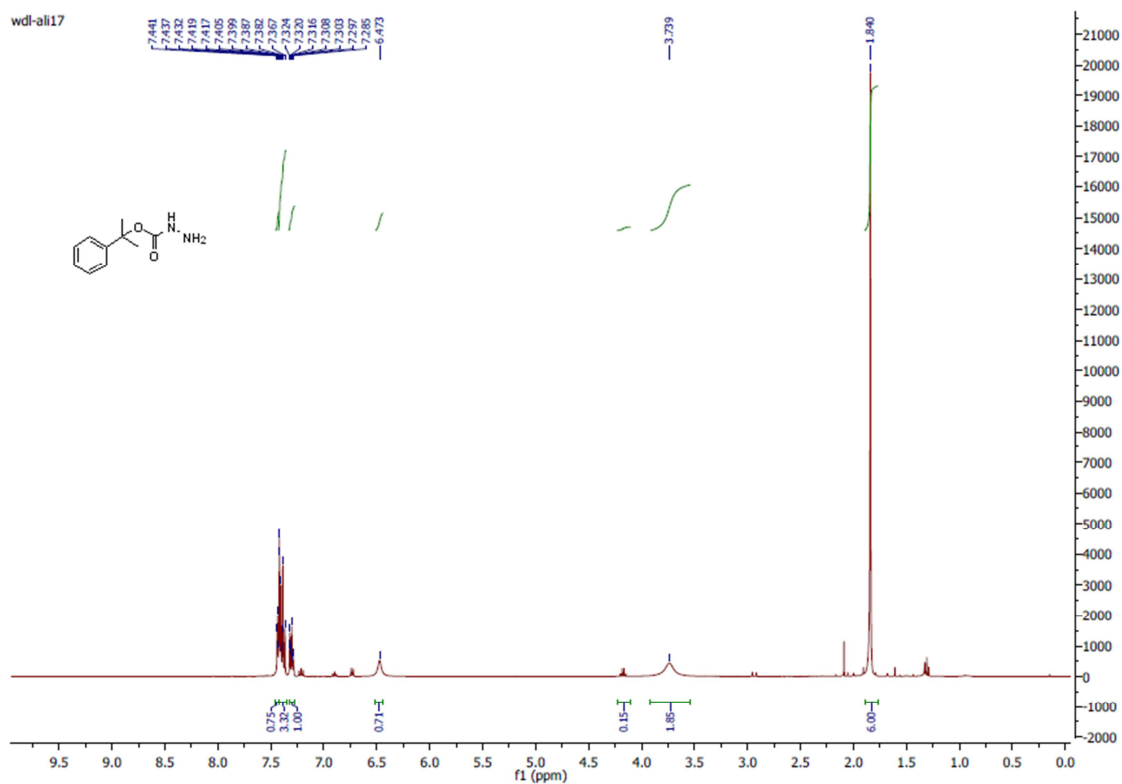


wdi-ali16

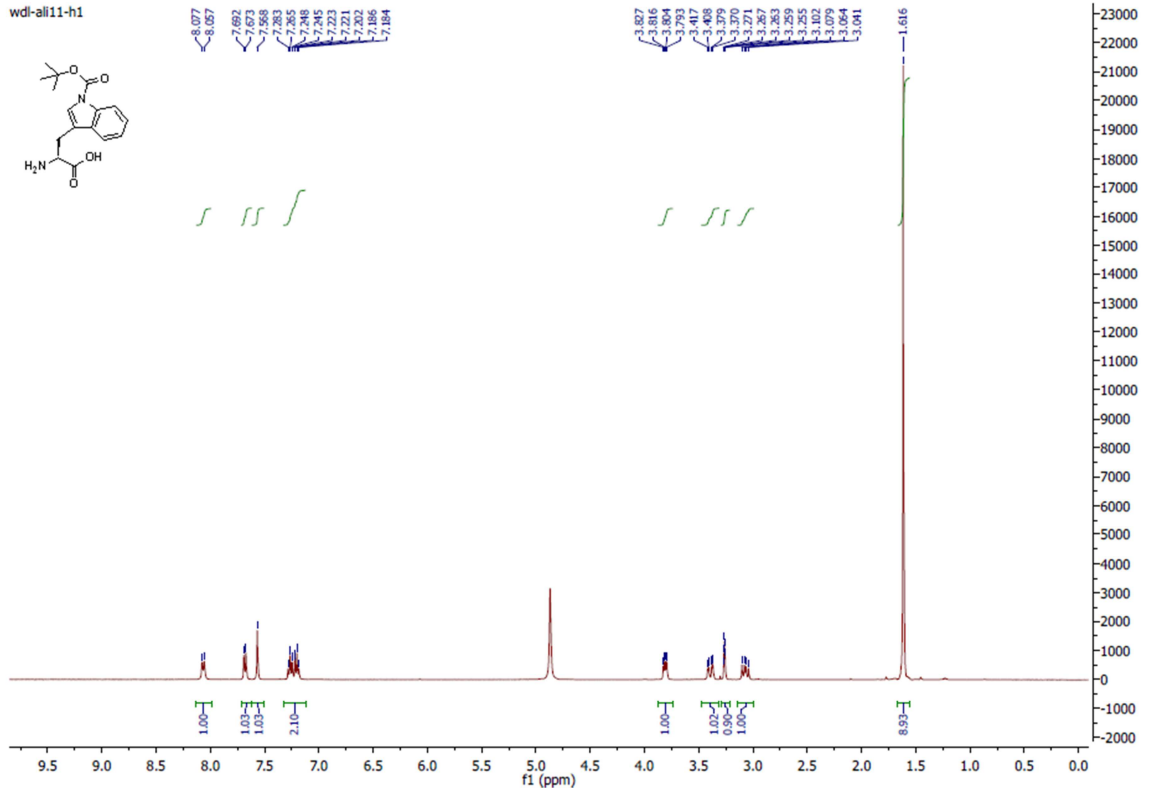


wdi-ali16-3001-c13b

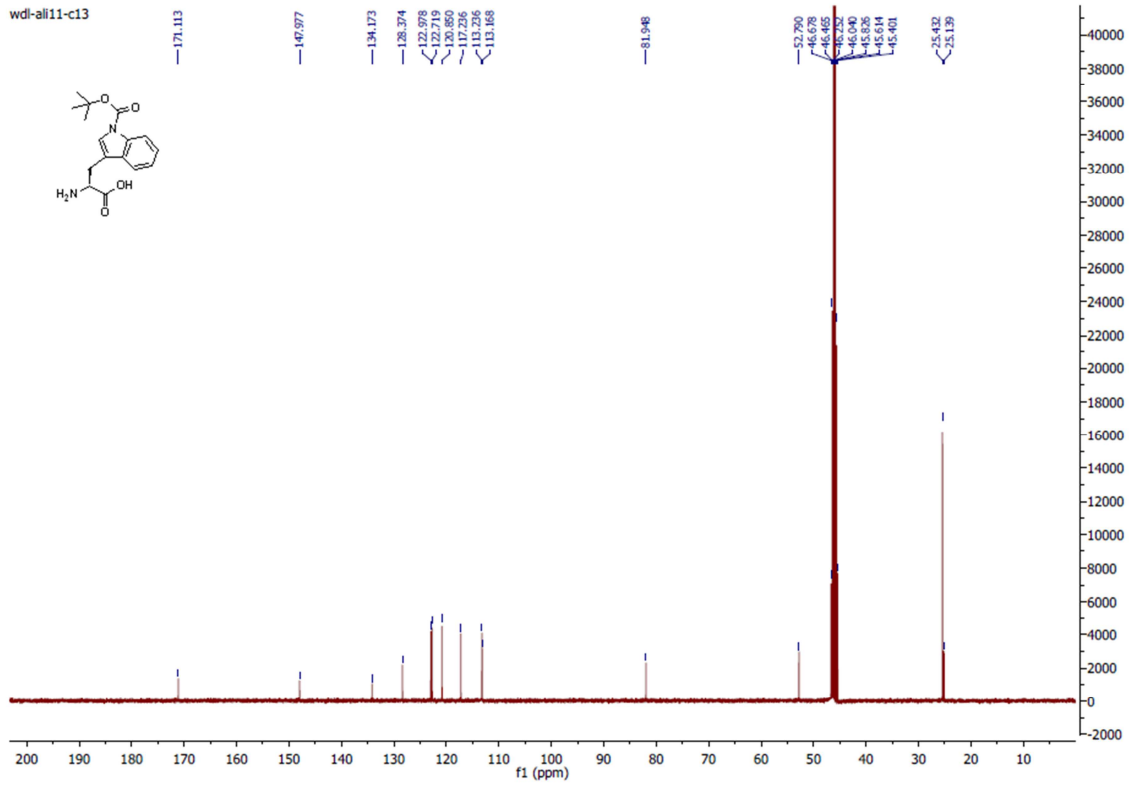


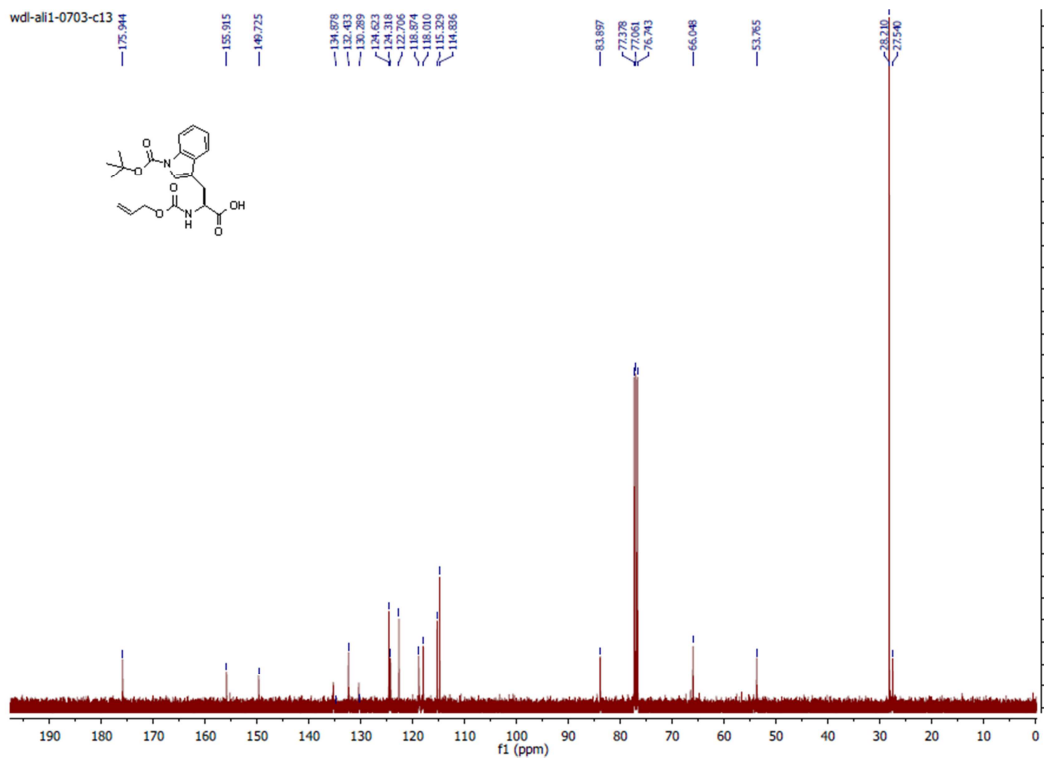
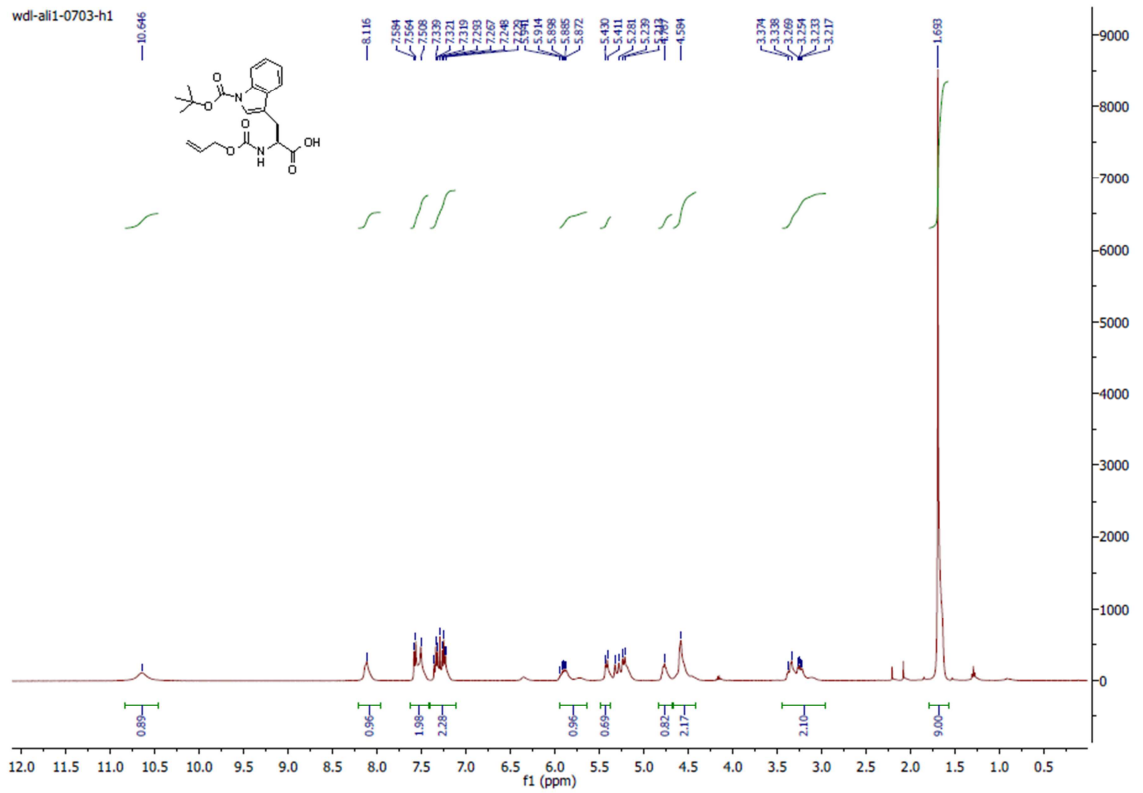


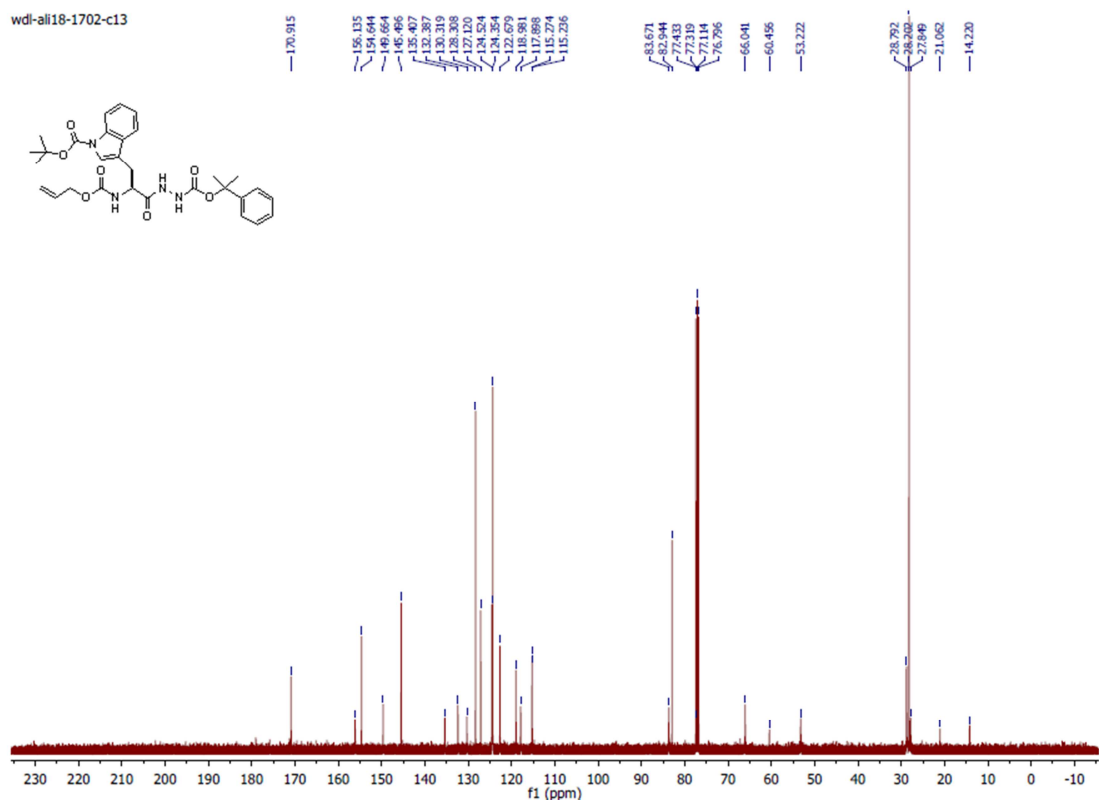
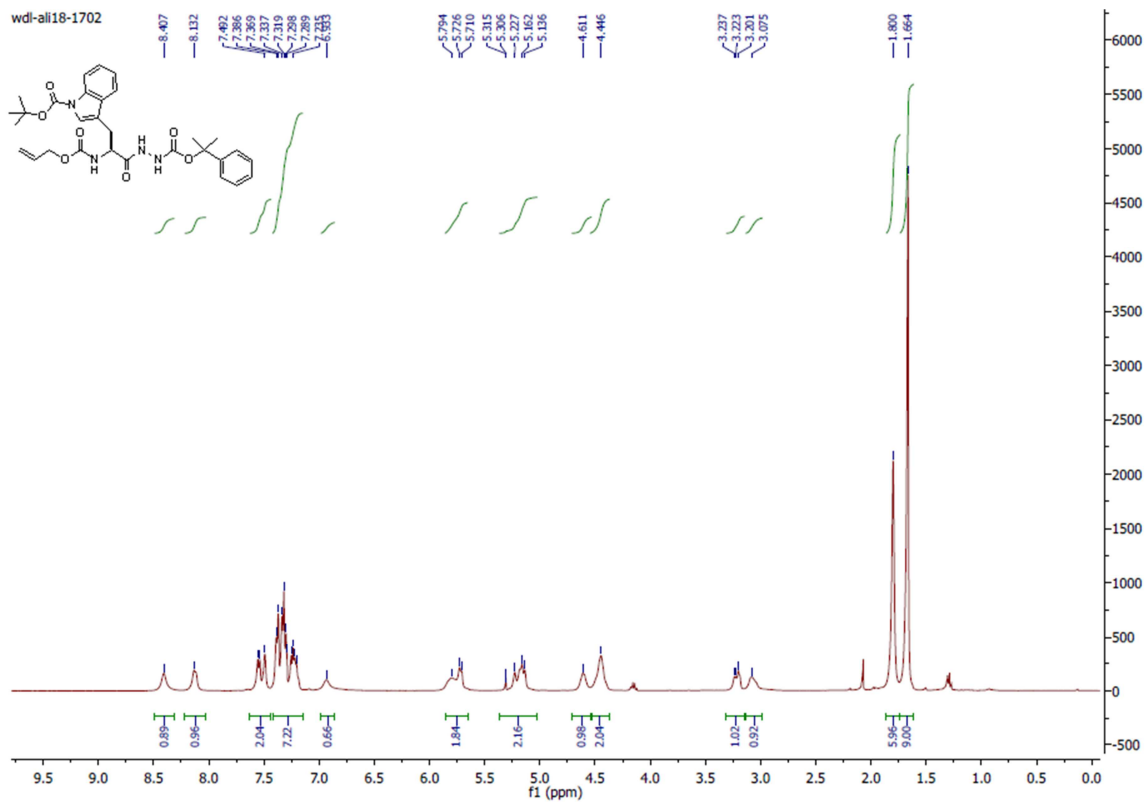
wdi-ali11-h1



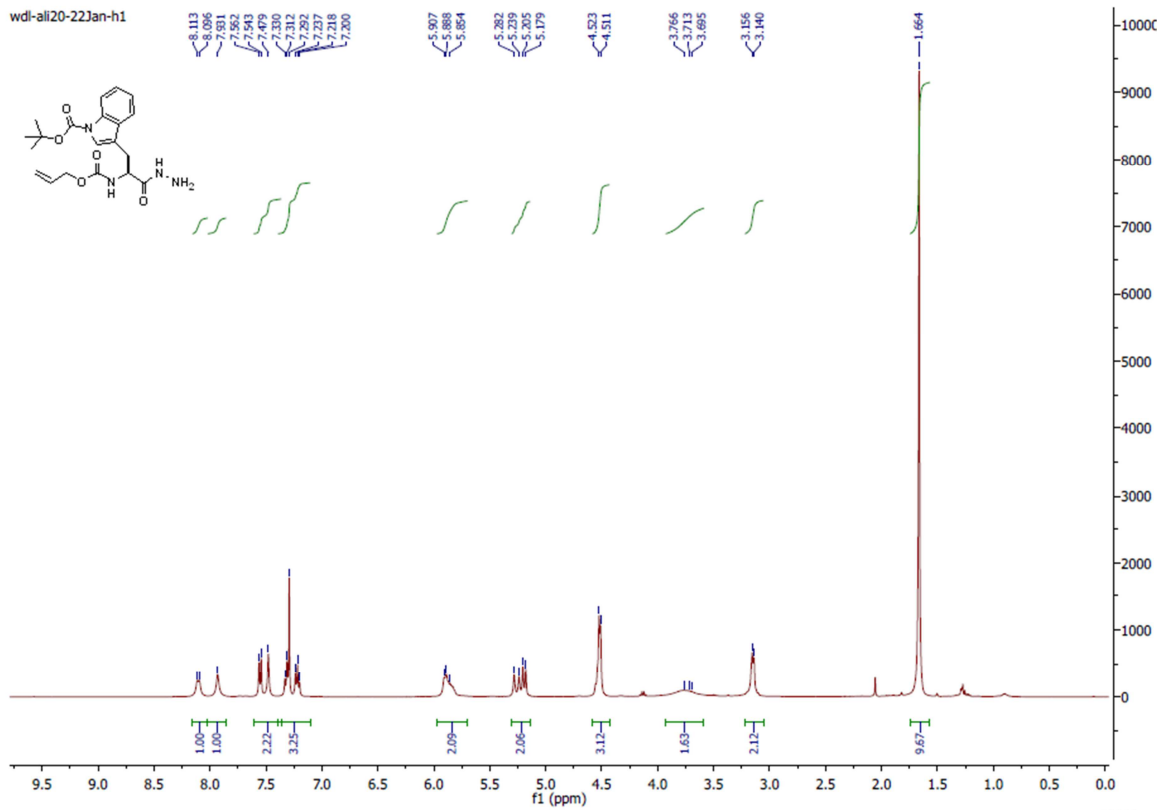
wdi-ali11-c13



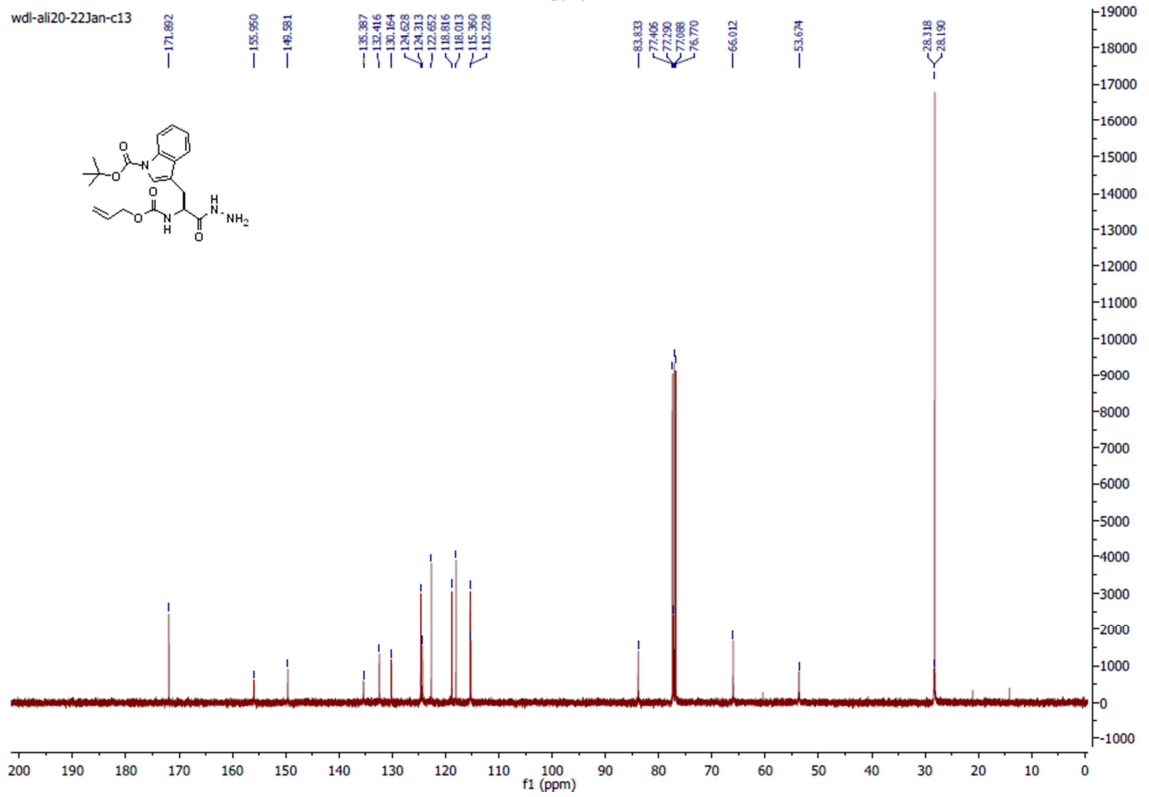


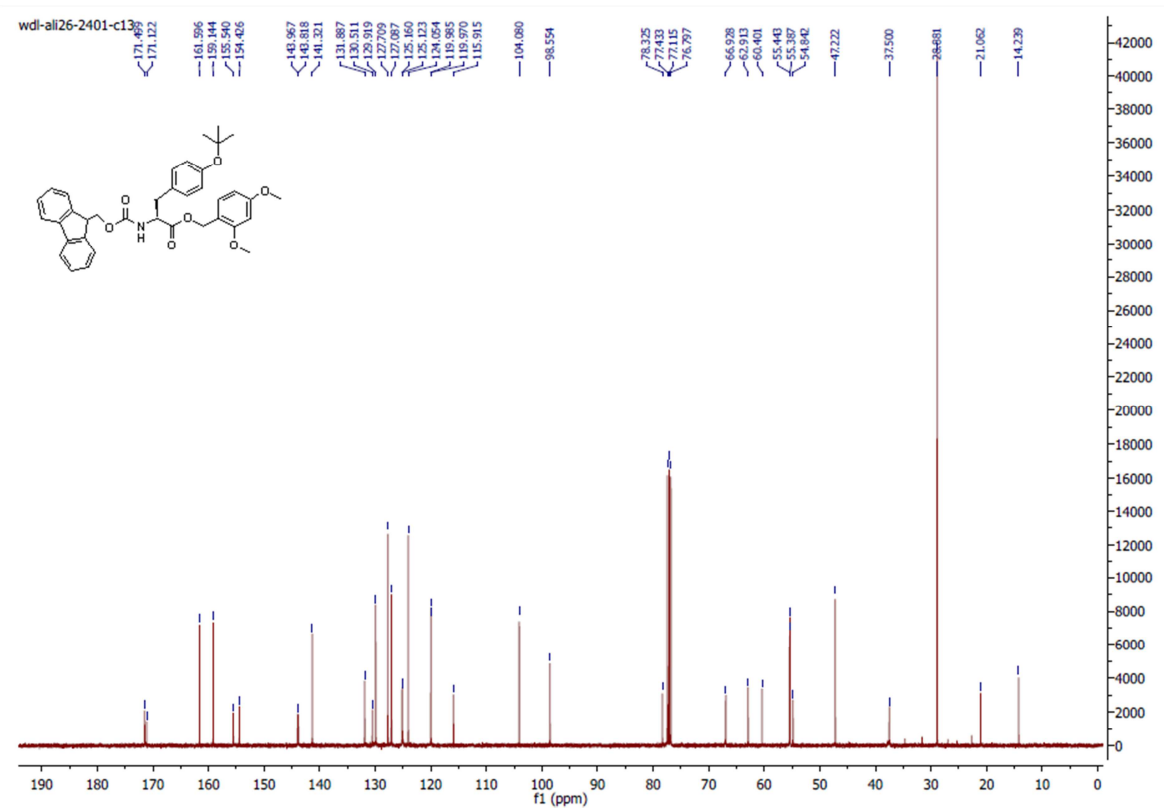
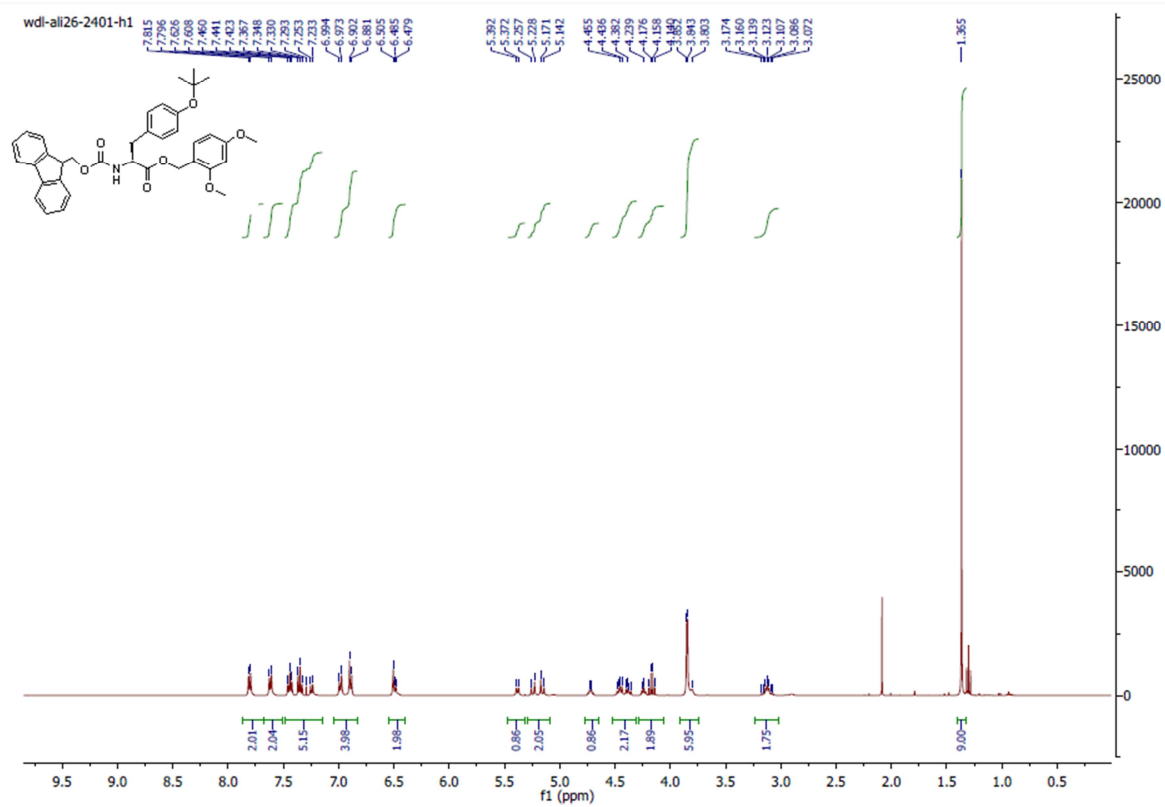


wdl-ali20-222Jan-h1

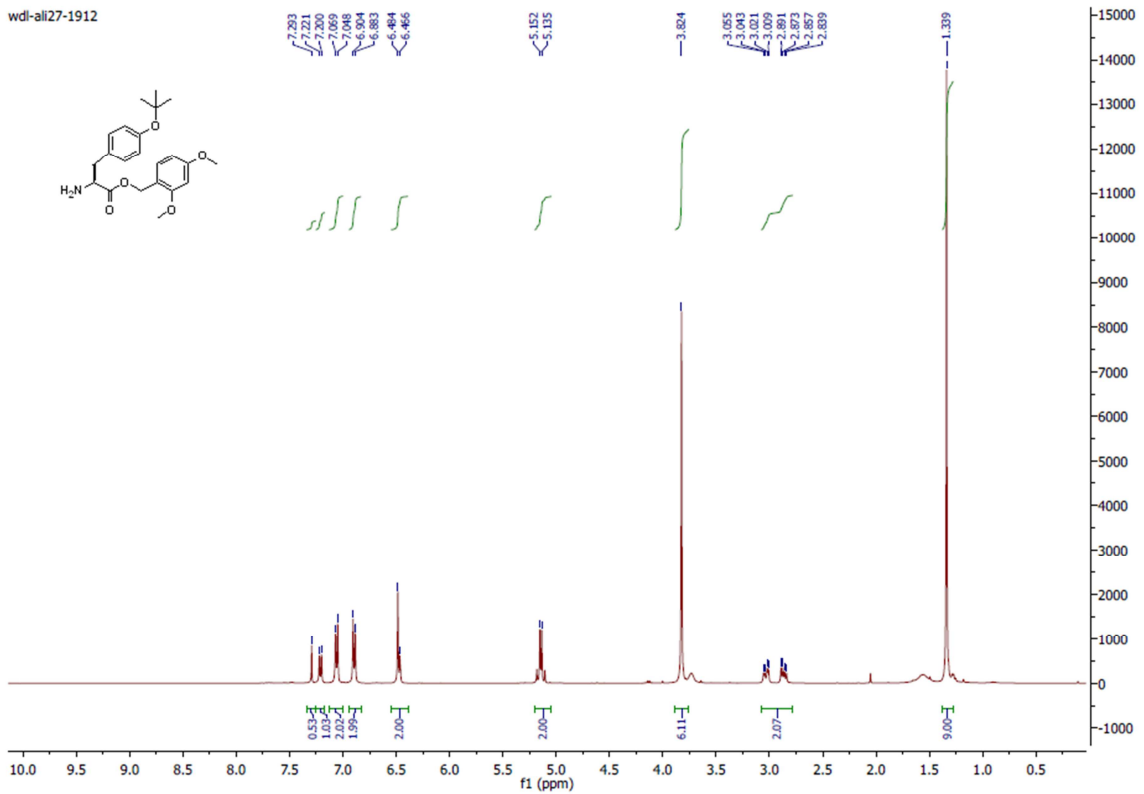


wdl-ali20-222Jan-c13

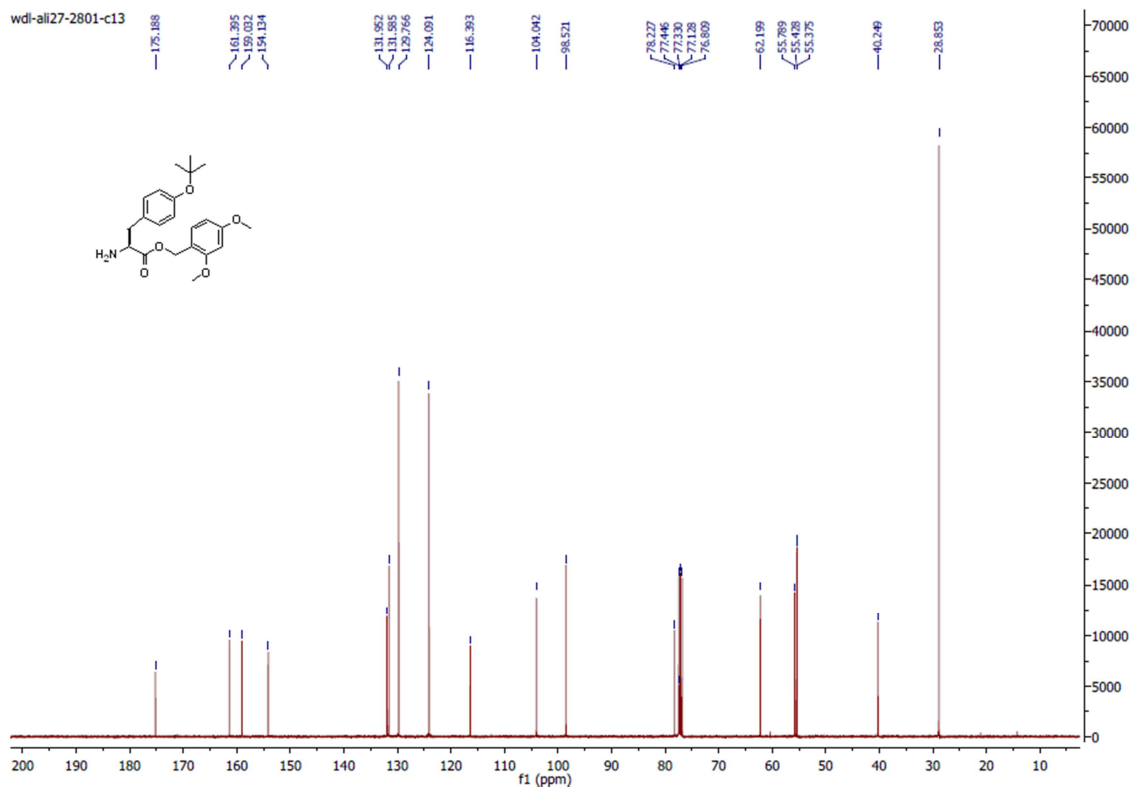


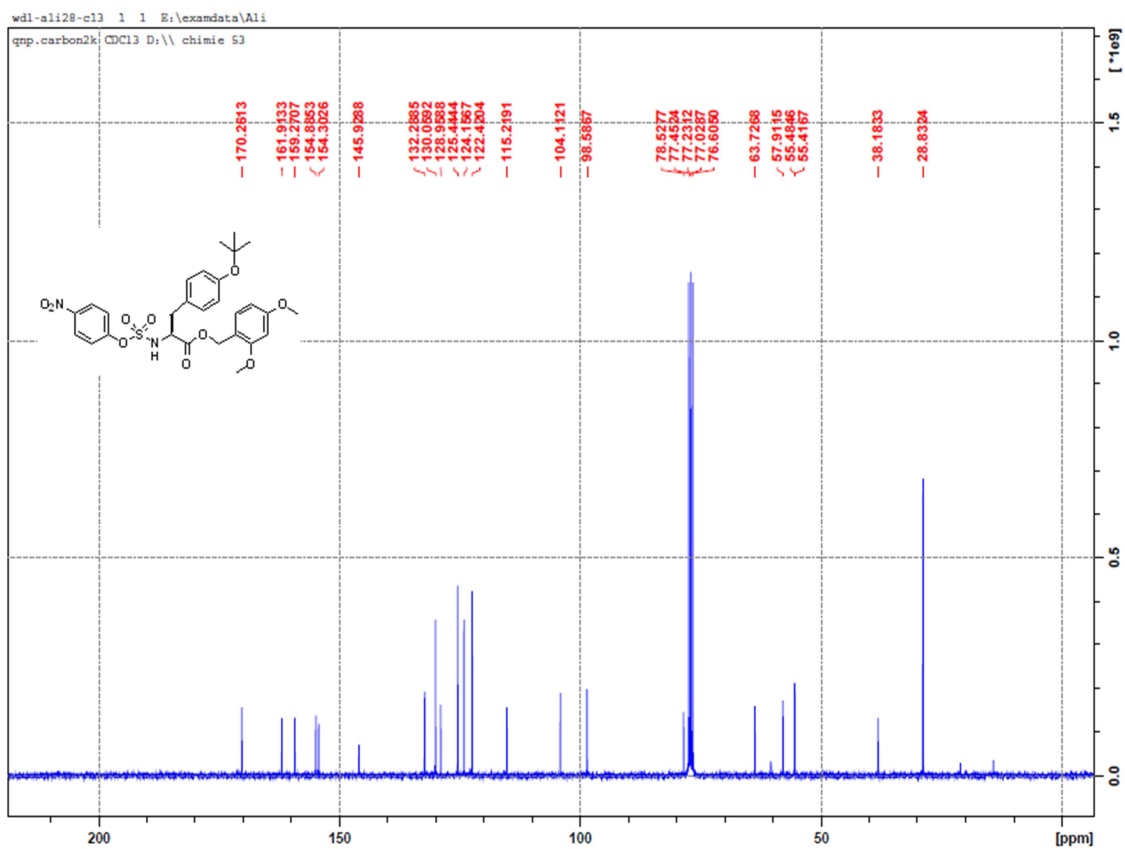
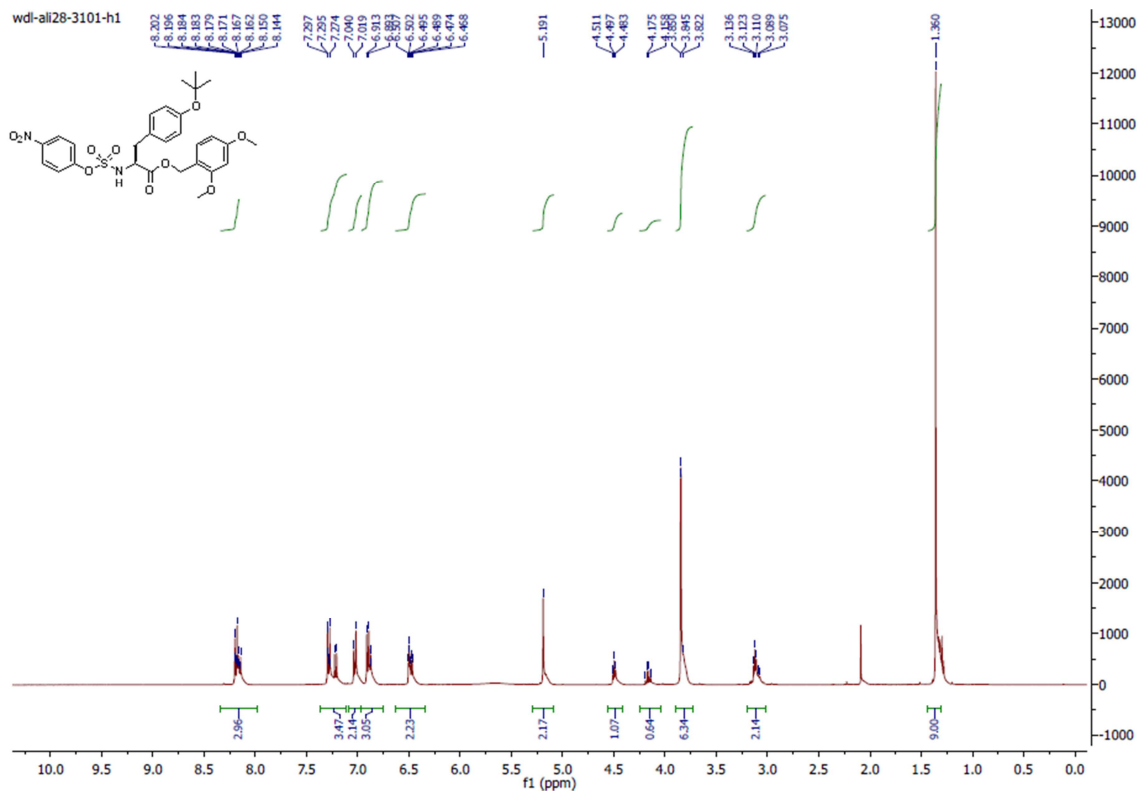


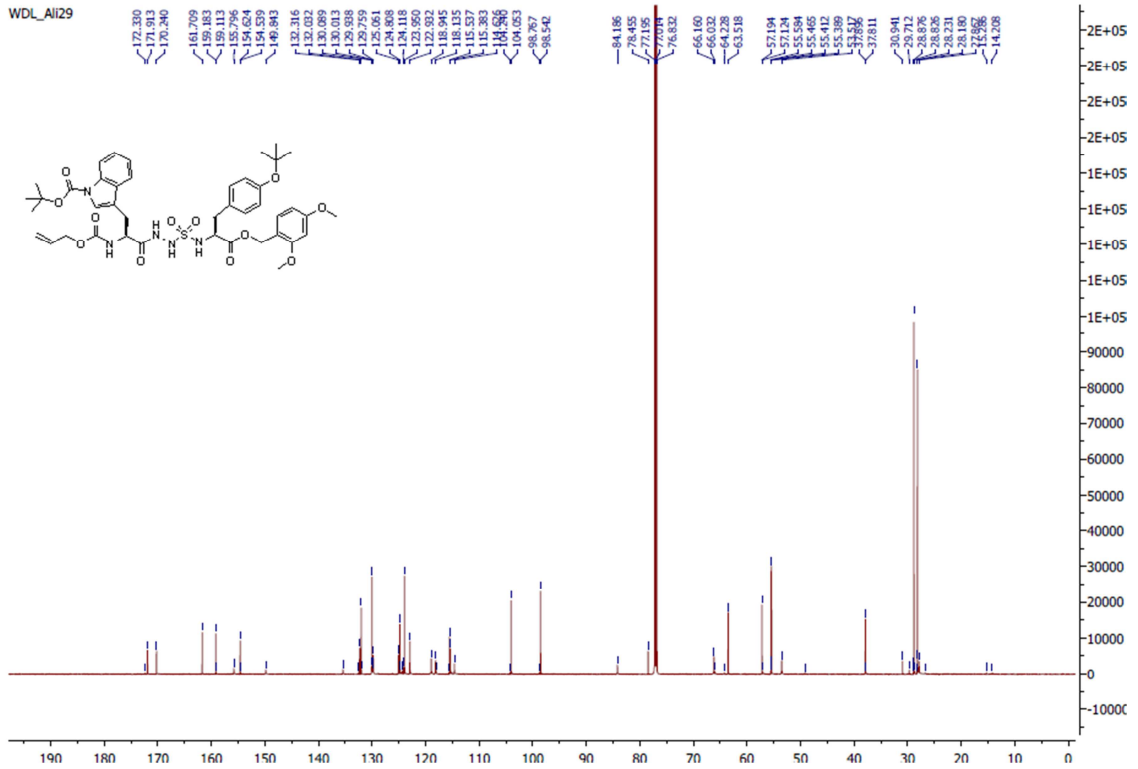
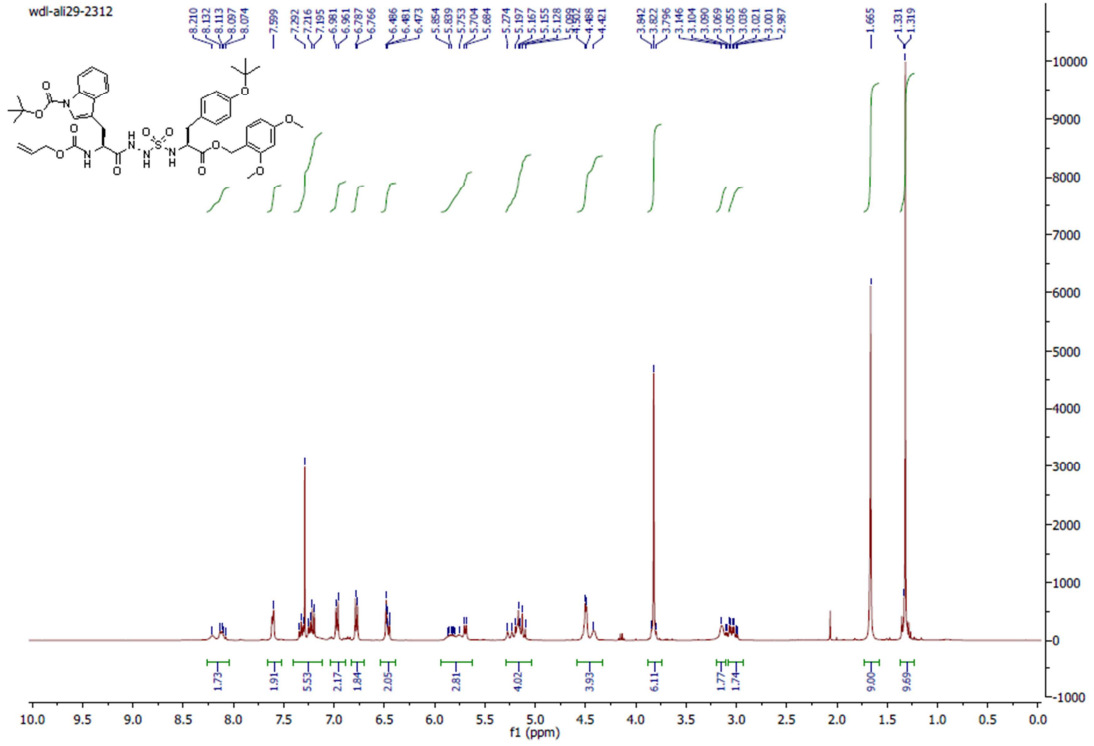
wdi-all27-1912

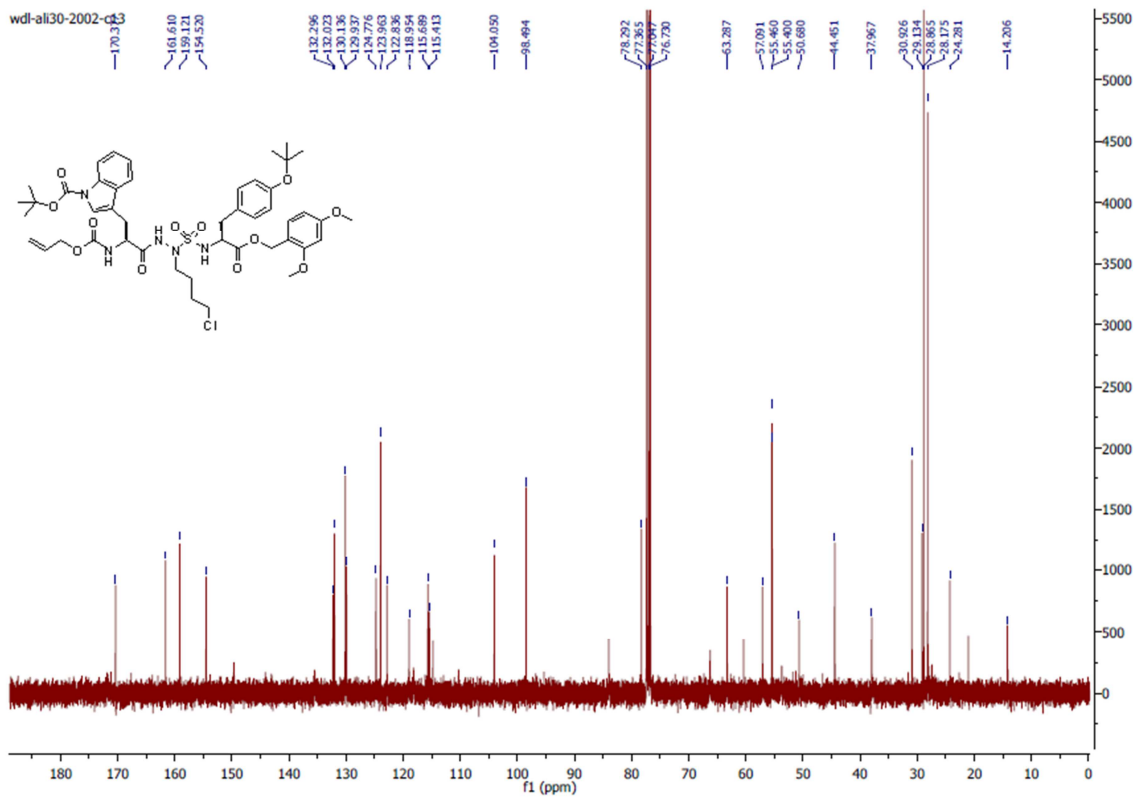
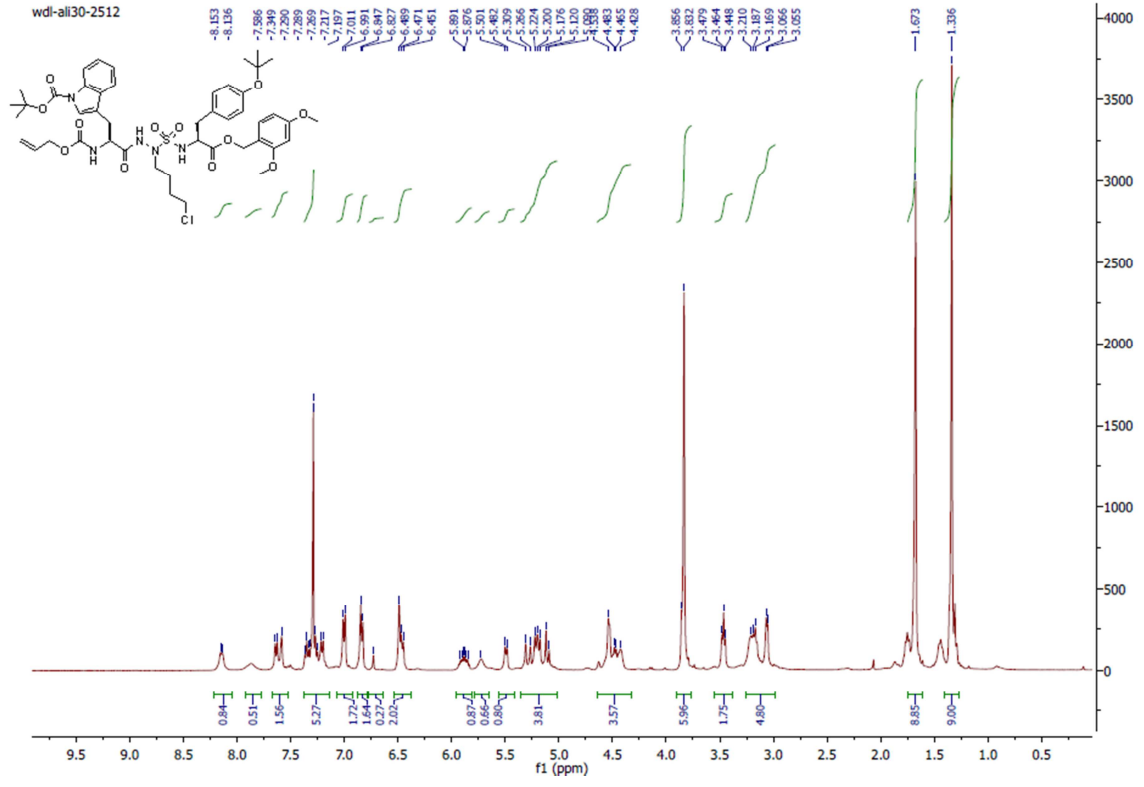


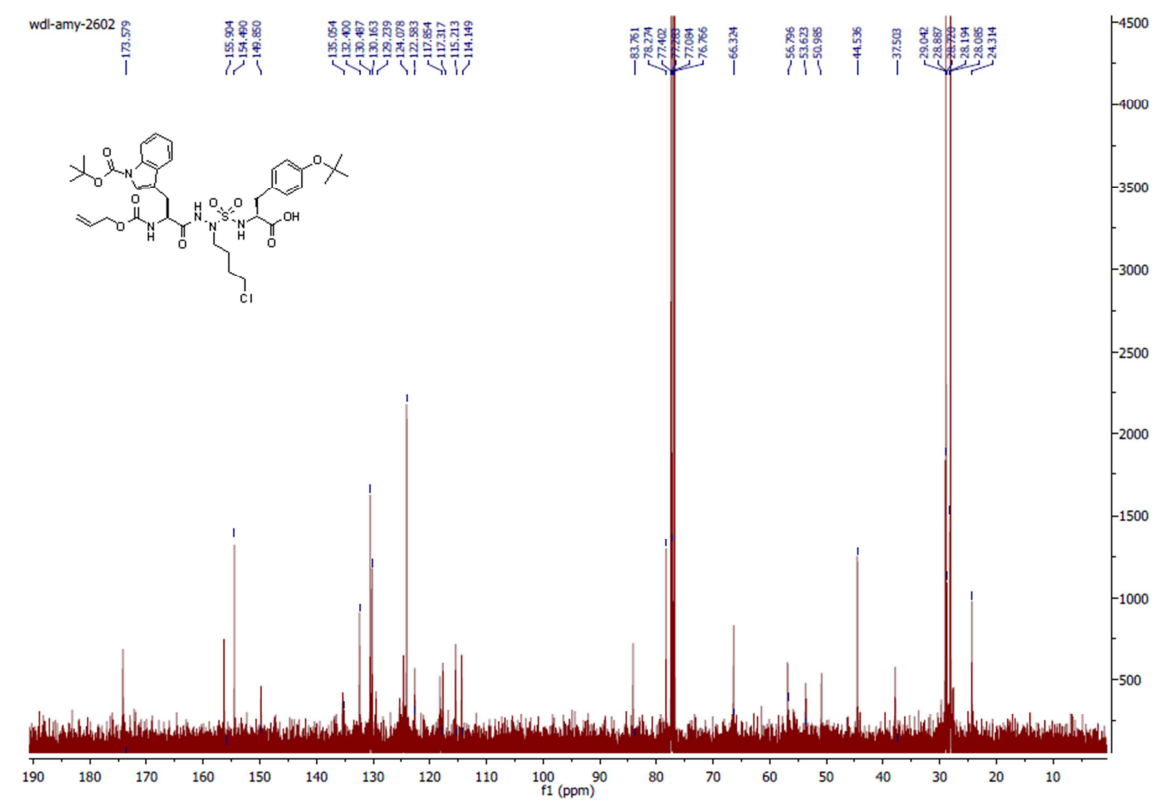
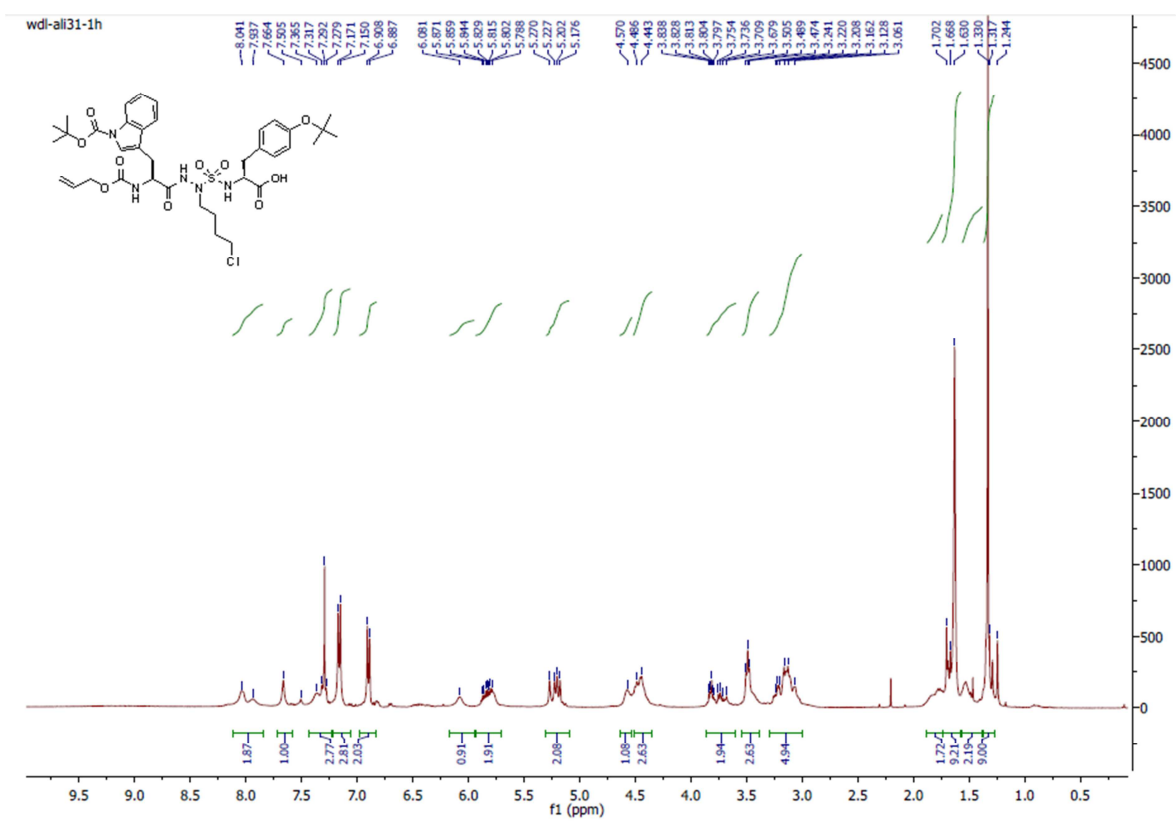
wdi-all27-2801-c13



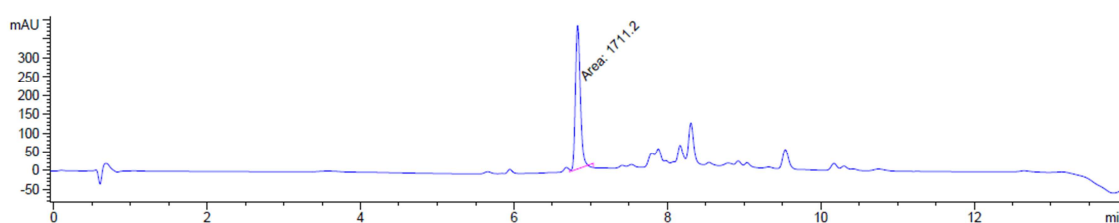




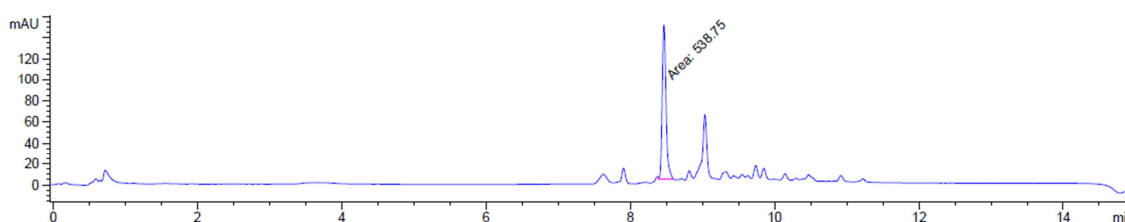




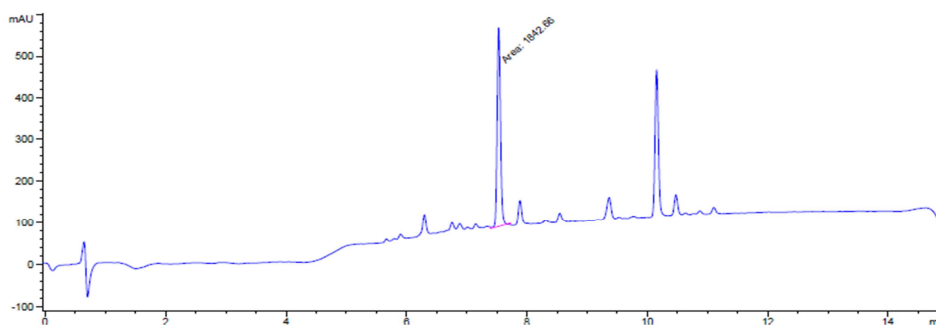
LC-MS Spectra



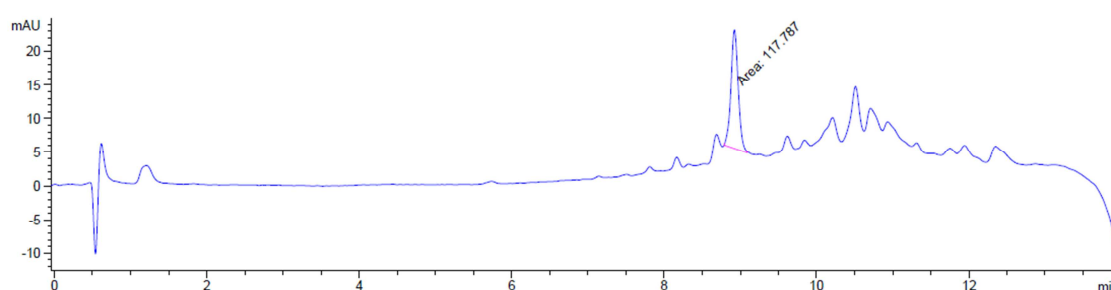
Compound 50(coupling tripeptide on resin): LCMS chromatogram (20-90% MeOH, 14 min, R.T. = 7.5 min), on a Sunfire C18 analytical column (100Å, 3.5 µm, 4.6 mm X 100 mm).



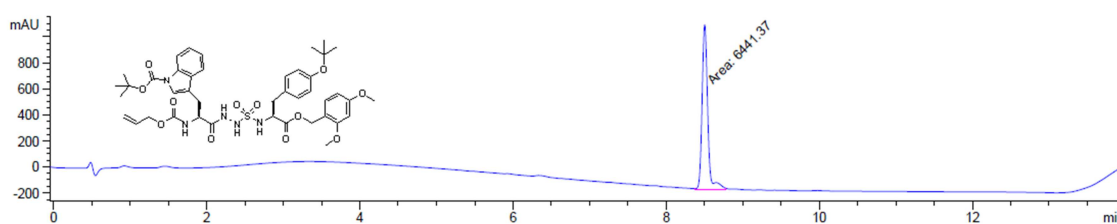
Compound 51(chloride to azide on resin): LCMS chromatogram (20-90% MeOH, 14 min, R.T. = 7.3 min), on a Sunfire C18 analytical column (100Å, 3.5 µm, 4.6 mm X 100 mm).



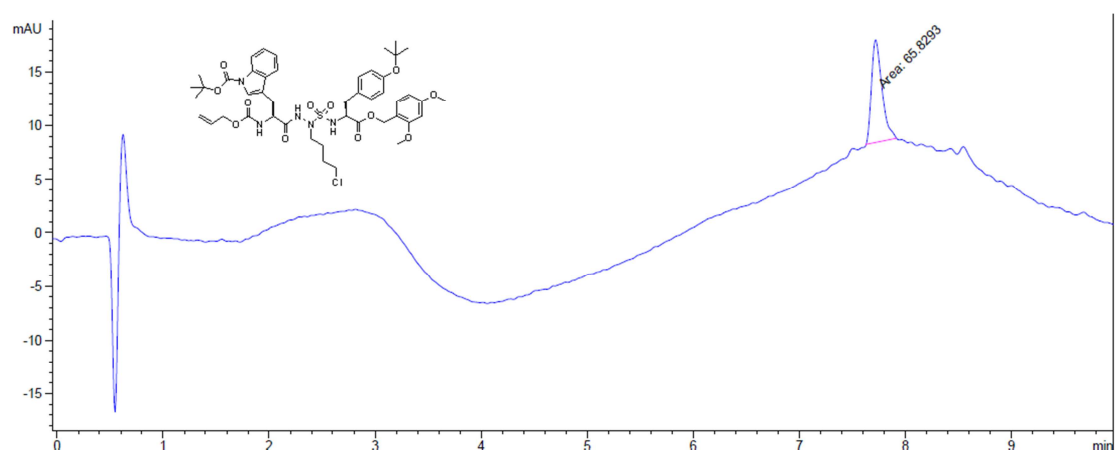
Compound 54(azide to primary amine on resin): LCMS chromatogram (10-90% MeOH, 15 min, R.T.= 7.6 min), on a Sunfire C18 analytical column (100Å, 3.5 µm, 4.6 mm X 100 mm).



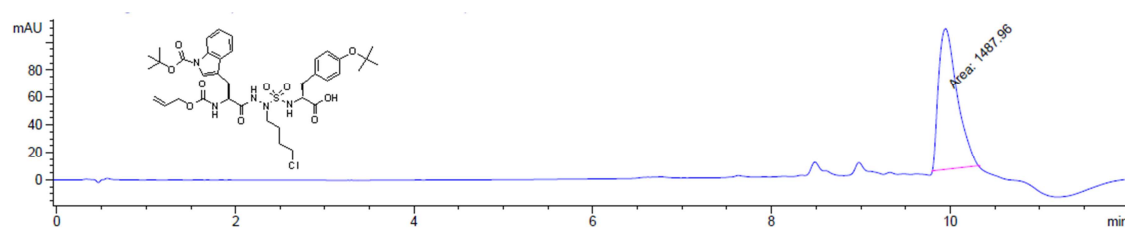
Compound 56(chloride to NMe₂ on resin): LCMS chromatogram (10-90% MeOH, 14 min, R.T. = 9.1 min), on a Sunfire C18 analytical column (100Å, 3.5 µm, 4.6 mm X 100 mm).



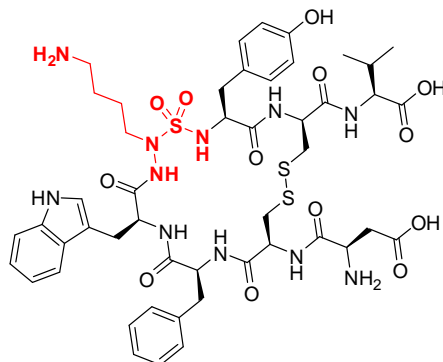
Compound 46: LCMS chromatogram (40-90% MeOH, 14 min, R.T. = 8.5 min), purified on a Sunfire C18 analytical column (100Å, 3.5 μm, 4.6 mm X 100 mm).



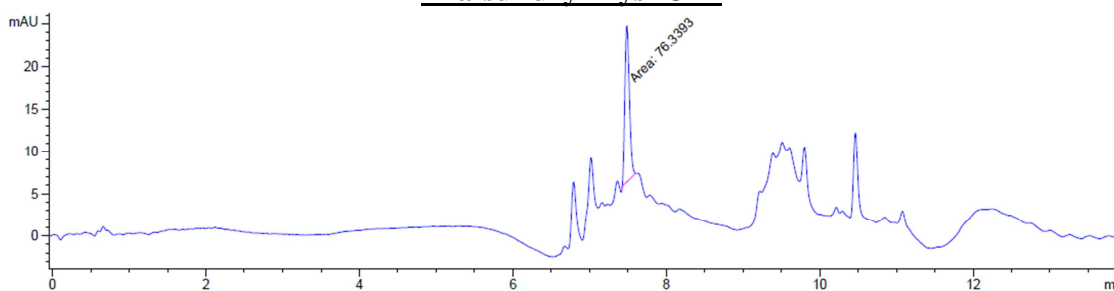
Compound 47: LCMS chromatogram (40-90% MeOH, 14 min, R.T. = 7.8 min), purified on a Sunfire C18 analytical column (100Å, 3.5 μm, 4.6 mm X 100 mm).



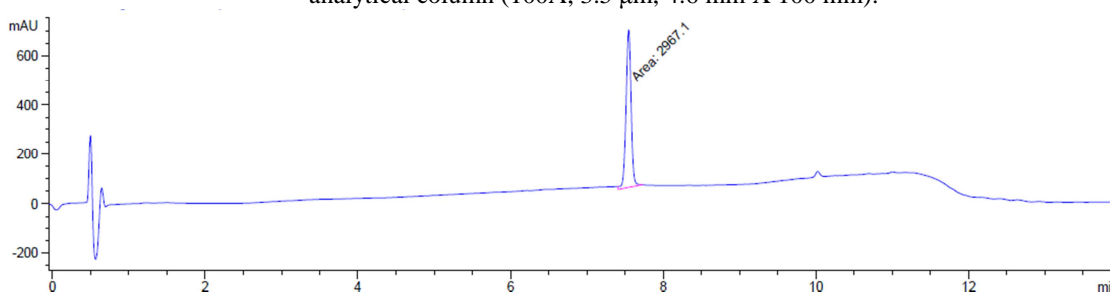
Compound 48: LCMS chromatogram (20-90% MeOH, 14 min, R.T. = 10.0 min), crude on a Sunfire C18 analytical column (100Å, 3.5 μm, 4.6 mm X 100 mm).



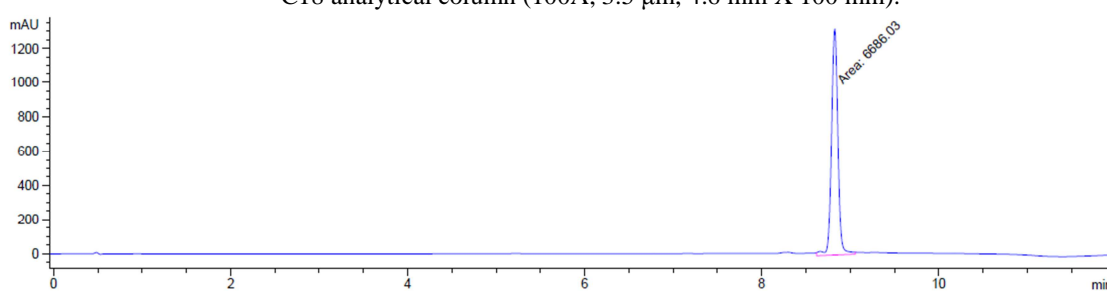
Aza-sulfuryl-Lys⁸ U-II



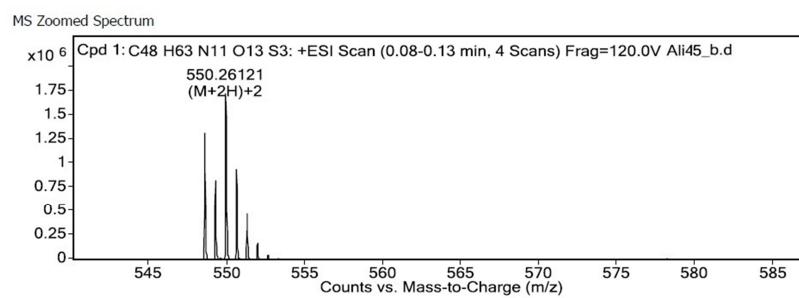
Aza-sulfuryl-Lys U-II: LCMS chromatogram (10-90% MeOH, 14 min, R.T. = 7.6 min), crude on a Sunfire C18 analytical column (100Å, 3.5 µm, 4.6 mm X 100 mm).



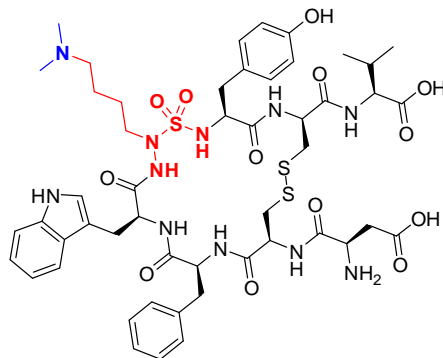
Aza-sulfuryl-Lys U-II: LCMS chromatogram (10-90% MeCN, 14 min, R.T. = 7.5 min), purified on a Sunfire C18 analytical column (100Å, 3.5 µm, 4.6 mm X 100 mm).



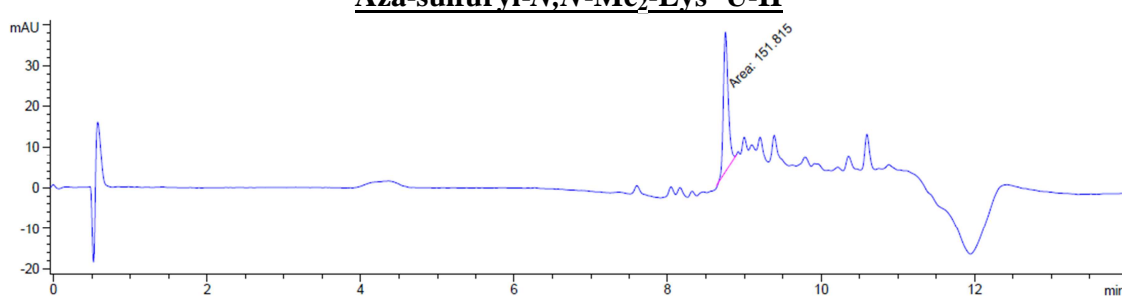
Aza-sulfuryl-Lys U-II: LCMS chromatogram (10-90% MeOH, 14 min, R.T. = 8.7 min), purified on a Sunfire C18 analytical column (100Å, 3.5 µm, 4.6 mm X 100 mm).



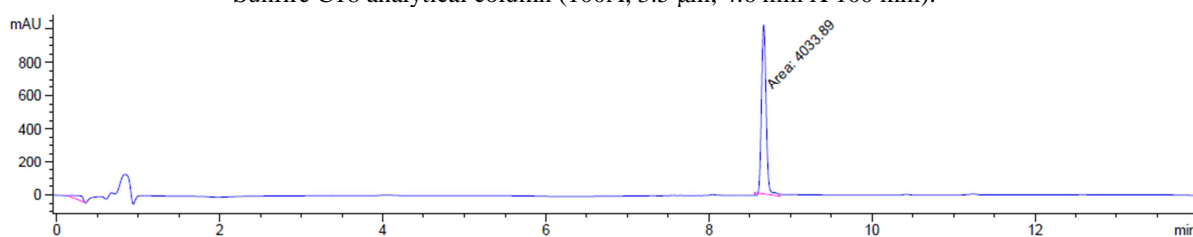
HRMS for chemical formula: C₄₈H₆₃N₁₁O₁₃S₃, calculated mass [M+2H]²⁺: 550.6172, found: 550.6153.



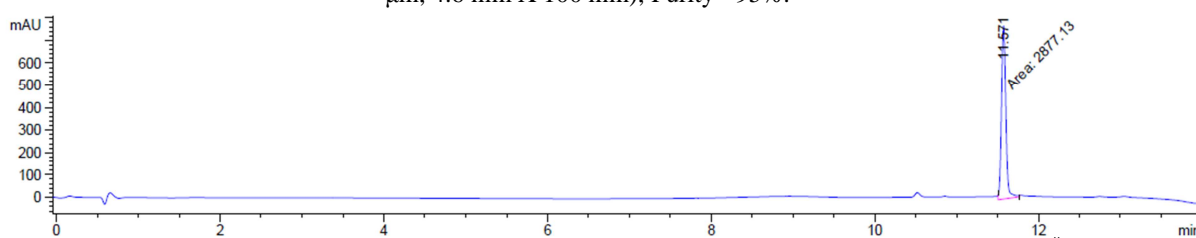
Aza-sulfuryl-*N,N*-Me₂-Lys⁸ U-II



Aza-sulfuryl-*N,N*-Me₂-Lys⁸ U-II: LCMS chromatogram (10-90% MeCN, 14 min, R.T. = 8.7 min), crude on a Sunfire C18 analytical column (100Å, 3.5 μm, 4.6 mm X 100 mm).

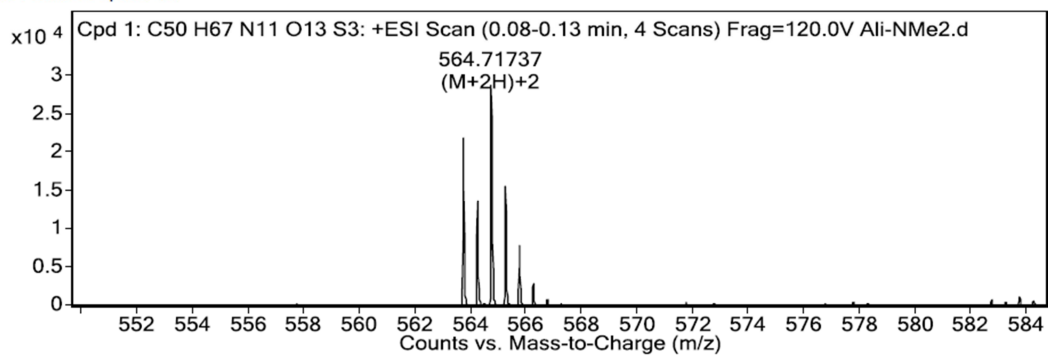


LCMS (0-80% MeCN, 14 min, R.T. = 8.7 min, purity =), purified on a Sunfire C18 analytical column (100Å, 3.5 μm, 4.6 mm X 100 mm); Purity >95%.



LCMS (0-80% MeOH, 14 min, R.T. = 11.6 min), purified on a Sunfire C18 analytical column (100Å, 3.5 μm, 4.6 mm X 100 mm); Purity >95%.

MS Zoomed Spectrum



HRMS for chemical formula: C₅₀H₆₇N₁₁O₁₃S₃, calculated mass [M+2H]²⁺; 564.7192, found: 564.7173.